DEVELOPMENT OF OSTEOINDUCTIVE, HIGH POROSITY POLYHIPES AS INJECTABLE BONE GRAFTS

A Dissertation

by

JENNIFER LINDSEY ROBINSON

Submitted to the Office of Graduate and Professional Studies of
Texas A&M University
in partial fulfillment of the requirements for the degree of

DOCTOR OF PHILOSOPHY

Chair of Committee,	Elizabeth Cosgriff-Hernàndez
Committee Members,	Duncan Maitland
	Harry Hogan
	Brian Saunders
Head of Department,	Gerard Coté

December 2014

Major Subject: Biomedical Engineering

ABSTRACT

Injectable bone grafts are space-filling materials that integrate with native bone to repair large defects from congenital deformities, trauma, and tumor resection. However, current injectable bone grafts limit healing due to lack of biodegradability, high temperatures during hardening, reduced porosity, and brittle compressive properties.

In this work, polymerized high internal phase emulsions (polyHIPEs) were developed as high porosity scaffolds for injectable bone grafting applications. Methods to modulate polyHIPE pore architecture, compressive properties, and degradation rates were established. Injectable polyHIPEs with pore sizes ranging from 1- 200 μm, compressive properties comparable to human cancellous bone, and degradation profiles spanning days to months were fabricated by altering compositional parameters (i.e. organic phase composition including macromers and surfactant, addition of an electrolyte in aqueous phase, and the phase in which initiator is soluble) and processing parameters (i.e. mixing speed, and cure and storage conditions). Cytocompatibility of all HIPE components was first verified and human mesenchymal stem cell (hMSC) adhesion and morphology was then assessed on polyHIPE sections. In order to confer an osteoinductive character to the bone grafts, calcium phosphate nanoparticles and demineralized bone matrix were incorporated into the polyHIPEs. PolyHIPE pore size and compressive properties were negligibly altered with the incorporation of particles. Alkaline phosphatase activity, a marker of osteoblast differentiation, was elevated from hMSCs on polyHIPE sections with osteoinductive particles. Finally, hMSC viability post

encapsulation in the polyHIPE was investigated to demonstrate the potential use as a cell carrier and viable cells were observed at 3 hours post encapsulation.

Overall, these studies highlight the potential of injectable polyHIPEs as improved bone grafts that can deliver and retain autologous hMSCs at the defect site while also inducing osteogenic differentiation for enhanced bone regeneration. Elucidation of key structure-property relationships in emulsion templated scaffolds can be used in future studies to further modulate cell-material interactions.

DEDICATION

To all who believed in me when I didn't and had full faith that I could do anything I put my mind to.

ACKNOWLEDGEMENTS

In writing this, I realize how surreal this moment is. If you asked me how I felt about graduate school at the end of my junior year in college, I would have said you were crazy. I was convinced only "brilliant" people obtained PhDs, and I definitely did not fall in that group. However, throughout this period of my life, I have realized that graduate school is a place for life-long learners and those who desire to find the answers and mechanisms to all the intricate processes in this life. I have truly enjoyed this state of constant learning.

I have to thank my advisor, Dr. Elizabeth Cosgriff-Hernandez, for offering me a spot in her lab after putting up with me when I was a naïve sophomore in college. She has always had confidence in me, even when I didn't, and constantly pushed me to reach my potential, as we always have room to grow. Also, I have learned that hard work is not always the most efficient or accurate, and at the end of the day, the job needs to be done correctly. I am extremely grateful for all of the time and effort she put forth to help me build my skills scientifically, professionally, and personally.

I also need to thank my committee members for providing outside expertise and perspective. Dr. Duncan Maitland and I had many entertaining conversations, and I will always appreciate the importance he places on commercializing novel technologies. Dr. Harry Hogan for entertaining me at ORS annual meetings and providing a smiling face on days I needed it. I am grateful Dr. Brian Saunders finally made it on my committee to provide the clinical expertise and discuss concerns from the veterinary science side. His contributions to this project definitely enhanced the work in our laboratory.

I am forever indebted to my wonderful lab mates who helped me through the good and the bad with their constant support, quirkiness, and laughs (especially on long nights or early mornings). I have had some of the most stimulating conversations while in the lab, and I would not trade any of that for the world. In no particular order I would like to thank Mary Beth Browning for her mentorship in and out of the lab and the importance she placed on work/life balance – oh and her wonderful hostess skills. Roya Nezarati who started and finished with me and definitely helped me remain sane these four year. These two girls have become two of my best friends, and I am so grateful I got to spend my graduate school time with them. Dave Dempsey for staying late with me and venting about our "hardships". Bobby Moglia for saying ridiculous comments that brightened my day and being a brilliant sound board and co-worker on the polyHIPE project. Nick Sears for always telling me I was doing a good job when I needed to hear it. Tyler Touchet for helping discuss and troubleshoot polymer synthesis issues and making sure the lab hung out after work. Alysha Kishan for giving me confidence and support even though she only knew me for a year. Mike Whitely for saving me as I was trying to finish my dissertation by running a majority of the experiments. Furthermore, I have learned many lessons from the undergraduates and master students I have trained. I would not have defended after 4 years if it were not for each of their help. Plus, I got to mentor some cool girls: Dawn Harrison, Shelby Buffington, Madison McEnery, Melissa Stuebben, and Hannah Pearce. I am also grateful for the entire Grunlan lab for sharing an office with us and not kicking us out!

My parents have been a constant support in my life and never once doubted me. I am especially grateful for their ability to let me pursue my own goals and find my niche, even if it did not fit what they initially thought would be best. I love you both and would not be who I am without you. To my grandparents, aunts, uncles, cousins, and distant relatives who have always acted interested in what I am pursuing and let me ramble on about tissue engineering and stem cells. I am blessed to have such a great support system.

Last, but surely not least, I must thank my amazing husband, the goofiest best friend, for being my number one supporter. I know I wouldn't have made it to this point without his hugs, love, laughter, crazy dancing study breaks, dinners, chores around the house….this list could go on forever. Most importantly, thanks for going on this crazy adventure of life with me.

NOMENCLATURE

AIBN	Azobisisobutyronitrile
BDMA	1,4 Butane Diol Dimethacrylate
BMP	Bone Morphogenetic Protein
BPO	Benzoyl Peroxide
EGDMA	Ethylene Glycol Dimethacrylate
FBS	Fetal Bovine Serum
HA	Hydroxyapatite
hMSC	Human Mesenchymal Stem Cell
PCL	Polycaprolactone
PDGF	Platelet Derived Growth Factor
PDMS	Polydimethylsiloxane
PEG	Poly(ethylene glycol)
PFDMA	Propylene Fumarate Dimethacrylate
PGPR	Polyglycerol polyricinoleate
PMMA	Poly(methyl methacrylate)
PolyHIPE	Polymerized High Internal Phase Emulsion
RGD	Arginine-Glycine-Aspartic Acid
SMP	Shape Memory Polymer
TMA	4, N,N - Trimethylaniline
VEGF	Vascular Endothelial Growth Factor

TABLE OF CONTENTS

Page

LIST OF FIGURES

Page

LIST OF TABLES

Page

CHAPTER I

INTRODUCTION AND LITERATURE REVIEW

1.1 Clinical Need: Repair of Non-Union Bone Defects

Musculoskeletal diseases and injuries result in over $250 billion spent in treatment and repair annually in the United States. Due to the range of conditions, the American Academy of Orthopedic Surgeons has characterized musculoskeletal diseases as the number one reason patients visit a doctor.[1] Specifically, bone fractures comprise a majority of these disorders; however, there is a need for improved healing as 5-10% of the roughly 6.2 million bone fractures reported in the United States are associated with impaired healing.[2] These defects result from traumatic injury, congenital deformities, and tumor resection. In general, bone has the ability to remodel and heal without scarring in smaller defects. However, at a critical size, defects are no longer able to heal naturally requiring reconstructive surgery to repair the defect. Key's Hypothesis states in skeletally mature dogs that a segmental long bone defect that exceeds 1.5X the diaphyseal diameter surpasses the regenerative capacity and is termed a critical size defect.[3, 4] Therefore, critical size defects are utilized as experimental models to test the efficacy of bone graft materials.

Bone functions to provide support for the body, structure for muscle contraction, acts as a reservoir for minerals, a site of hematopoiesis (bone marrow), and protects internal organs.[5] Bone is the primary calcium reservoir for the body and is responsible for the timely exchange of ions with the extracellular environment.[6] Native bone is comprised of two distinct tissue architectures: cortical and trabecular (cancellous) bone. Cortical

bone is relatively non-porous (~10% porosity) and comprised of extracellular matrix components (mainly calcium phosphate) that dictate the high compressive strength and modulus of bone (E=10-20 GPa).[7] Cortical bone makes up ~80% of the skeleton and constitutes long bones, short bones, and flat bones. Trabecular, or spongy, bone constitutes ~20% of the skeleton and is porous (50-90%) resulting in compressive modulus values much lower than cortical bone (E=20-500 MPa)[7]. Trabecular bone is typically found in the metaphysis of long bones and has a honeycomb-like pore structure. The periosteum is a thin membrane surrounding the outer surface of bones containing progenitor cells. The reparative nature of bone involves a dynamic relationship between osteoblasts, which produce and lay down supportive extracellular matrix, and osteoclasts, which resorb old or damaged tissue to make space for new matrix and healthy tissue. Osteocytes are mature osteoblasts that control the extracellular calcium and phosphorus concentrations and direct osteogenesis and resorption depending on the environment conditions via cell-cell interactions.[8] When the equilibrium of the bone cells is off, bone loss occurs which greatly affects the quality of life for the patient. Bone extracellular matrix, which provides much of the stellar qualities that bone encompasses, is comprised of hydroxyapatite, a mineral component, and an organic component. Hydroxyapatite composes 65-70% of the bone matrix and the organic constituents (glycoproteins, proteoglycans, and sialoproteins) make up the remainder.[9] Stimulating the natural repair process of bone in critical size defects is crucial in reestablishing support and quality of life to patients plagued with critical size bone fractures.

1.1.1 Natural Bone Healing

Unlike most tissues in which healing includes the formation of scar tissue, bone heals efficiently resulting in healthy new bone produced.[6] Bone tissue is in a constant state of rejuvenation – end-stage differentiated cells such as osteoblasts are replaced by newly differentiated osteoblasts geared for forming new bone. These young osteoblasts arise from multipotent progenitor cells known as mesenchymal stem cells (MSCs) which circulate in the bone marrow.[8, 10] Thus, these MSCs have a vital role in serving as the depot center for bone healing and repair.

1.1.1.1 Inflammatory Stage

During this first stage of bone healing, a hematoma forms and inflammatory cells and fibroblasts move into the fracture site resulting in granulation tissue formation, ingrowth of vascular tissue, and migration of mesenchymal stem cells.[8, 11] Platelets release transforming growth factor beta (TGF-β) and platelet-derived growth factor (PDGF) which induce angiogenesis as well as MSC migration and proliferation. BMPs are released from underlying bone matrix as well as secreted by recruited MSCs.[12]

1.1.1.2 Repair Stage

During the period of fibrocartilaginous callus formation, fibroblasts lay down a collagen matrix as vascular ingrowth occurs and chondroblasts produce fibrocartilage which is stronger to bridge the gap of the defect. Vascular ingrowth is controlled by fibroblast growth factor (FGF), vascular endothelial growth factor (VEGF), angiopoietin 1 and 2.[13, 14] Osteoblasts secrete osteoid, the unmineralized matrix composed of Type 1 collagen and proteoglycans, which is mineralized over time into a soft callus during the

bony callus formation period. The ossification of the soft callus to bridge the broken bones happens in 4 to 6 weeks if the bone is properly immobilized. New bone formation occurs via intramembranous or endochondral ossification which is dictated by the mechanical nature of the break – mechanically stable fractures heal by direct bone matrix formation void of cartilage whereas unstable fractures heal via the endochondral process in which cartilage is generated and remodeled as bone tissue.[15, 16] Mineralization refers to the general process of depositing mineral salts via calcification or ossification. Calcification is the deposition of calcium in tissues and occurs when the solubility of calcium in the interstitial fluid of specific tissues is exceeded. Ossification is the specific and organized deposition of calcium salts onto the collagen matrix that constitutes the osteoid and is specific to bone mineralization.[6]

1.1.1.3 Late Remodeling Stage

In this final stage of bone healing, remodeling occurs to ensure the neotissue is of adequate shape, structure, and strength. This process is dictated by mechanical loading as stated in Wolff's Law and can take months to years.[17] Adequate strength is commonly achieved in 3 – 6 months.

1.1.1.4 Role of Mesenchymal Stem Cells and the Trophic Effect

Marrow-derived mesenchymal stem cells are undifferentiated cells capable of differentiating into cells of mesenchymal tissue including bone, cartilage, connective tissue (tendons and ligaments), muscle, and fat.[18, 19] MSCs located within the periosteum and the marrow serve as the generals of the musculoskeletal healing army and are constantly surveying for damage and ready to signal for repair. In 2006, Arnold Caplan

and colleagues proposed with supporting evidence that MSCs were not necessarily differentiating into specific cells but rather releasing cytokines and growth factors to achieve a therapeutic effect, termed a trophic effect.[20] Multiple studies investigating treatment of cardiac ischemia, osteoarthritis, and stroke illustrated tissue repair after the delivery of MSCs to the defect site. However, in each of these studies, the MSCs did not differentiate into the specific cells required for new tissue formation. Instead, they acted as leaders recruiting and directing nearby cells to repair the damaged tissue via biochemical signals. Caplan determined five processes in which MSCs exhibit this trophic effect: they reduce apoptosis, limit fibrosis and scar formation, promote angiogenesis and blood vessel formation to enhance healing, stimulate the mitosis of tissue-specific progenitor cells, and release immunomodulatory chemicals that block T-cell surveillance suggesting the successful use of allogenic and xenogenic cells.[21] Recent work exemplifies these trophic properties in MSCs aiding in cardiac repair and the viable delivery and function of transplanted islets, chondrocytes, and Schwann cells to name a few of the cells being tested.[22-27] Researchers have shown MSCs may play a role in tumor suppression further illustrating the vitality of MSC delivery in tissue engineering and regenerative medicine.[28] The continuous increase in knowledge of bone biology, physiology, and fracture healing processes is advantageous in designing treatment options that best capitalize on the necessary tools to aid in long-term healing and reduce scarring.

1.2 Current Treatment Options

Annually, over 1 million patients with bone defects require grafts to provide complete union.[29] Even though bone grafting procedures have been performed for the past two centuries to provide a template for new growth, healing is still limited in large defects. For adequate healing, the overall goal of bone grafts is to capitalize on the body's natural ability to lay down new bone matrix and calcify under the mechanical stresses of the body. Therefore, the actual graft must provide initial mechanical integrity, promote osteogenesis and calcified matrix production, and degrade (including resorption and clearance by the body) once new tissue is formed.[6] Bone grafts are classified by the extent to which they promote osteogenesis. Osteoconductive grafts guide bone healing in the presence of all other necessary cues.[30] These materials promote infiltration of neovasculature and ingrowth of precursor cells. Osteoinductive materials can promote the osteogenic differentiation of stem cells into mature osteoblasts which can lay down new extracellular matrix. Biochemical promoters of osteogenesis such as bone morphogenetic proteins are examples of osteoinductive components.

1.2.1 Autografts

Autologous grafts are the gold standard for repair due to their osseointegration (ability of material to integrate with host bone), osteoinductivity, (ability to provide cues for the differentiation of stem cells to osteoblasts) and the lack of immune rejection. Commonly, bone harvested from the patient's iliac crest of the hip, rib, tibia, mandible, or skull is used to treat segmental defects or shaved and packed into smaller injury sites.[31] Success rates are generally high, between 70-100% in vertebral fusions which is

one of the most common uses for autografts.[32] Unfortunately, retrieval of tissue from the patient is limited due to anatomical availability and leads to donor site pain and morbidity.[32-34]

1.2.2 Allografts

Allograft bone is harvested from the same species and is typically obtained from cadaveric tissue in bone banks or commercial vendors.[35] This type of treatment is often used because of the increased availability relative to autografts. For the repair of segmental defects, cadaveric bone is decellularized to reduce immune rejection and the remaining matrix is used for repair. Depending on the defect geometry, it may be difficult to adequately fit allograft material into the defect site. Alternatively, cadaveric tissue can be demineralized and used as a paste to pack into the stabilized defect. However, the demineralization process reduces the loading ability of the graft. Allografts are typically osteoconductive due to the decellularization and demineralization procedures. Allograft particles can be added to a polymeric matrix for delivery and enhanced mechanical properties. Dumas *et al.* fabricated injectable polyurethane/allograft composites with a range of properties, degradation rates, and compressive properties on the low end of cancellous bone illustrating the ability to combine allograft particles with synthetic materials to increase mechanical integrity.[36] In general, autografts and allografts suffer from variability (quality of tissue from patient to patient) and limited availability necessitating the need for a reliable and viable bone graft option.

1.2.3 Poly(methyl methacrylate) Bone Cement

Poly(methyl methacrylate) (PMMA) bone cement is the most commonly utilized synthetic formulation in bone repair. In segmental defect repair, PMMA cement is used in fracture fixation to secure the metal implants into the native bone. In smaller applications such as vertebroplasties, cement is used to fill the defect site and withstand part of the load. Since the 1960s, surgeons have used this injectable cement formulation because of its viscosity, rheological, and cure properties.[37] Injectable PMMA cement is sold as two components: PMMA polymer powder with a radical initiator, benzoyl peroxide, and methyl methacrylate monomer. Upon mixing of the two phases, a paste/putty results and is easily applied to the defect. However, the exothermic temperature reached during PMMA polymerization exceeds 100ºC and has caused tissue necrosis and required revision surgery.[38, 39] PMMA bone cement is also not porous limiting cell migration, nutrient and waste transport, and tissue ingrowth. Furthermore, PMMA is not biodegradable resulting in residual material in the body which could impede bone healing.

1.2.4 Injectable Materials

Bone cements that flow at room temperature and harden once injected into the body are commonly utilized to heal non-union defects because they can fill irregularly shaped defects and harden without an additional stimulus. The availability, tunability, and mechanical properties of synthetic materials address inherent issues with autografts and allografts.

1.2.4.1 Calcium Phosphate Cements

Calcium phosphate cements have been used for bone grafting procedures since the 1980s due to their excellent biocompatibility and osteoconductivity.[1] Various formulations and fabrication techniques have been investigated resulting in

Table 1.1. Selected calcium phosphate cement formulations and properties[40]

Origin	***Material***	***Pore Size (μm)***	***Compressive Strength (MPa)***
Bovine	HA	100-1500	4.2-5.6
Bovine	60% HA/40% H2O	390-1360	1.0-20.0
Coral	HA	28-770	-
Synthetic	β-TCP	100-400	-
Synthetic	β-TCP	1-1000	-
Synthetic	80% TCP/20% HA	300-500	-
Synthetic	TTCP/DCP	2-50	6.3-34
Synthetic	62.5% α-TCP 26.8% DCPA 8.9% CaCO3 1.8% HA	<1	35-55
Synthetic	60% HA/40% β-TCP	-	-
Synthetic	73% β-TCP 21% MCP-H2O 5% MHPT	-	-
Synthetic	TTCP/DCP/TSC	-	14-24
Synthetic	α-TCP/CaCO3/ MCP-H2O	-	23-55

commercialization of many products illustrated in **Table 1.1**. In general, these pastes consist of two or more calcium phosphate compositions mixed with an aqueous solution with hardening occurring after mixing due to dissolution and precipitation.[41] Altering processing parameters, particle size, cement compositions, and additives are ways to tune cement set times. In general, CaP cements exhibit low fracture toughness and mechanical reliability as determined by the Weibull modulus which determines the probability of failure of brittle materials.[42]

1.3 Tissue Engineered Bone Grafts

Tissue engineering strategies combine the osseointegration and osteoinductivity of autografts with the availability and tunability of synthetic grafts to avoid complications.[43, 44] Tissue engineering strategies focus on harnessing the body's natural healing potential by providing 3-dimensional (3D) scaffolds embedded with instructive cues and human cells which promote new tissue formation. Tissue engineering constructs promote bone regeneration by instructing endogenous or seeded cells with appropriate bioactive cues to aid in cell differentiation and tissue growth.[45] Utilizing tissue engineering to regenerate bone requires the development of an osteoconductive matrix that promotes osteogenesis of encapsulated or endogenous osteoprogenitor cells via an osteoinductive factor.

1.3.1 Requirements for 3D Scaffolds

1.3.1.1 Pore Size

The collection of research conducted on the effect of pore size on osteogenesis and fully vascularized new bone indicates pore sizes greater than 300 μm is necessary

for bone ingrowth and capillary formation.[46] In polyHIPE literature, Akay *et al.* illustrated enhanced bone nodule formation from osteoblasts seeded on scaffolds with 100 μm pore sizes compared to smaller pores.[47] Work from the Mikos lab illustrated enhanced alkaline phosphatase activity, an early indicator of osteogenesis, of osteoblasts seeded on porous PLGA scaffolds with 500 – 700 μm pores.[48]

1.3.1.2 Interconnected Pore Architecture

It is well regarded in tissue engineering the importance of the pore size and interconnects between pores for ingrowth and proliferation of cells and the transport of nutrients and waste to maintain cell viability. The importance of interconnectivity on maintenance of cell viability in constructs with relatively small pore size has been recorded. Specifically, human embryonic stem cell-derived cardiomyocytes seeded on bimodal porogen-leached scaffolds with interconnected pores 30-40 μm remained viability for at least 2 weeks at a depth of 300 μm.[49] Additional work by Marcacci *et al.* demonstrated the critical importance of interconnected porosity on vascularization and full healing in a long bone segmental defect clinical trial.[50]

1.3.1.3 Adequate Mechanical Strength

For bone tissue engineering, the biomaterial must be able to withstand loading imparted while the defect is immobilized. Additionally, Wolff's law highlights the importance of compressive stress on the biomechanics of osteogenesis and resorption.[17] The maximum compressive forces loading on human bones has been estimated at 20-51 MPa.[51] Although bulk polymers could be designed to withstand these stresses, it is difficult to design highly porous scaffolds able to support this magnitude of load.

Fortunately, it is accepted that materials with compressive properties similar to cancellous bone (modulus = 30-100 MPa and strength = 2-10 MPa) are adequate to promote full bone healing.[46, 52, 53]

1.3.1.4 Degradation Rate Matching In Vivo Healing

Tissue engineered materials are designed to provide the necessary physiological matrix and cues to stimulate growth. To this end, 3D scaffolds are designed and tuned to degrade once new, stable tissue has been formed. Work conducted by Dr. Guelcher sheds new light on the necessary scaffold mechanical properties for healing in a rabbit femoral defect illustrating enhanced healing at later time points when polyurethane/allograft scaffold degradation rates closely matched those of new bone formation.[54] Designing and fabricating scaffolds with tunable degradation rates is advantageous as the healing environment (enzymes, pH, etc.) differs from patient to patient and for various applications.

1.3.1.5 Injectability

A relatively new push has been on the design of materials that harden and mold to the desired shape *in vivo* to reduce the time and cost required to fabricate scaffolds via a 3D reconstruction of a defect based on a computer-aided design model. Furthermore, these injectable materials can completely space-fill any irregularly shaped defect without a gap and are less invasive methods to heal tissue.[35] This is important to promote native cell infiltration and migration and eliminate any micromotion from occurring which could result in inflammation and scar tissue formation. For the delivery of cells and

growth factors, aqueous based systems such as hydrogels are advantageous in promoting viability and maintaining bioactivity of encapsulated biologics.

1.3.2 3D Scaffold Fabrication Techniques

Material scientists have developed a multitude of 3D porous scaffold fabrication techniques for use in various applications. The most common techniques used to generate highly porous scaffolds for tissue engineering applications include electrospinning, gas foaming, porogen leaching, thermally induced phase separations, and hydrogels. Specifically, these techniques paired with the macromer/polymer chemistries used result in constructs with tunable properties for use in soft and hard tissue applications. A particular difficult design problem is generating highly porous scaffolds that retain good mechanical properties.

1.3.2.1 Electrospinning

Electrospinning is a method utilized to produce fibrous meshes with tunable pore sizes, large surface area to volume ratios, and fibers of nano- to micron-sized diameters.[55, 56] Altering system parameters (accelerating voltage, distance to the collector, spinning time, collector geometry, and environmental humidity) and polymer solution parameters (viscosity, hydrophobicity, and dielectric constant of the solvent) result in widely tunable fiber diameters and alignments.[57] However, the resulting meshes are typically 2D limiting this technique for use in space-filling an irregularly shaped defect in the surgical suite.

1.3.2.2 Gas Foaming

Generating gas, typically CO2, utilizing chemical or physical processes is utilized to produce pores.[58, 59] Overall porosity of 94% with pore sizes from 100-500 μm can be achieved in this manner. This process is advantageous because it can be performed without the use of toxic solvents; however, a non-porous skin layer typically forms on the surface of the scaffold which must be removed prior to implantation.[58] Furthermore, this fabrication technique generally utilizes high temperatures and pressures limiting their formation *in situ*.

1.3.2.3 Porogen Leaching

In this technique, porogens, traditionally salts, are dispersed in a polymer solution and leached out after the network is formed to create pores.[60, 61] Interconnected pores are formed by the fusing together of the porogens.[62] Biodegradability and injectability are achieved depending on the polymer and porogen utilized.[49, 63, 64] Pore sizes and shapes are dictated by the size and shape of the porogen. Thus, often the pores are irregularly shaped causing stress concentrators and decreasing the overall mechanical properties and the ability to dictate these properties.[61, 65-68]

1.3.2.4 Thermally Induced Phase Separation

Porous scaffolds are fabricated by inducing phase separation in a polymer solution to create polymer-rich and polymer-poor regions. The solvent is then removed via sublimation, similar to the removal of water in freeze-drying processes, resulting in a porous scaffold. The polymers, temperatures, and procedures used to sublimate the solvent modulate the tunable pore architecture ranging from long, aligned to spherical

pores.[69, 70] However, this procedure requires solvents and cold temperatures reducing the ability to use this as an injectable system for the delivery of cells.

1.3.2.5 Shape Memory Foams

The term shape memory polymers (SMPs) have been utilized to describe systems that capitalize on inherent polymer thermal properties to tune network properties. These systems have garnered interest for medical applications due to their ability to be designed in an original shape, molded into a temporary shape for delivery through a catheter or small vehicle, and expanded to the original shape once an energy stimulus such as heat or UV light are applied.[71] SMPs have been fabricated into foams which exhibit increased permeability and volume expansion relative to neat SMPs. Ultra low density, highly crosslinked SMP foams incorporating polyurethane chemistry have been widely studied for multiple biomedical applications including embolic devices for cerebrovascular aneurysms, thrombectomy retrieval, and stents.[72, 73] Altering polymer chemistries allows for modulation of the transition temperatures and rate of recovery. Singhal *et al.* reports the ability to control the polyurethane SMP foam actuation rate which naturally exhibits a passive shape memory behavior due to plasticization in water.[74] Furthermore, the 3D scaffold fabrication technique employed provides further ability to modulate properties and delivery method. Zhang *et al.* have illustrated the bone grafting potential of polycaprolactone (PCL) – polydimethylsiloxane (PDMS) block copolymer SMPs fabricated via an altered particulate leaching process with polydopamine coating.[62] The authors illustrated the ability to tune pore size, porosity, compressive modulus, and degradation rate by altering the length of the PDMS chains.[75]

SMPs have been utilized in the organic phase of high internal phase emulsions resulting in highly porous foams with good shape memory behavior.[76] Currently, it is unclear whether encapsulated cells could remain viable under shape programming conditions including non-physiological temperatures and large shear forces. Also, their ability to integrate with native tissue on the nanoscopic scale remains to be shown. Furthermore, irregularities in the expansion may result in heterogeneous, unexpected properties. Much of this work employs shape memory behavior at temperatures exceeding 37ºC reducing the ability to use them as materials that set at physiological temperature.

1.3.2.6 Hydrogels

Hydrogels are polymer networks that swell in water to 1000X their dry weight. These gels are advantageous for tissue engineering and drug delivery applications due to their similar properties to soft tissue, ability to incorporate biomolecules without solubility constraints, and encapsulate human cells and maintain their viability.[49, 63, 77-81] Commonly natural polymers (collagen, gelatin, fibrin, glycosaminoglycans, alginate, and agarose) and synthetic polymers such as poly(ethylene glycol) (PEG) modified with integrin binding sites are utilized for tissue engineering applications.[82-84] Many groups have shown bone regeneration *in vivo* with engineered hydrogels.[84] However, these materials will not be able to withstand physiological loading without additional fixation which may cause stress shielding and reduced healing in some applications.

1.3.3 Polymerized High Internal Phase Emulsions (PolyHIPEs)

The template polymerization of a high internal phase emulsion results in highly porous scaffolds that have the potential to match the properties of cancellous bone as

seen in **Figure 1.1**. High internal phase emulsions are dictated by the internal phase composing ≥ 74% of the total volume. For the past 25 years, researchers have investigated the use of polyHIPEs as tissue engineered scaffolds. **Table 1.2** depicts the range of polyHIPE compositions utilized, their respective pore and interconnect sizes, and compressive properties achieved.

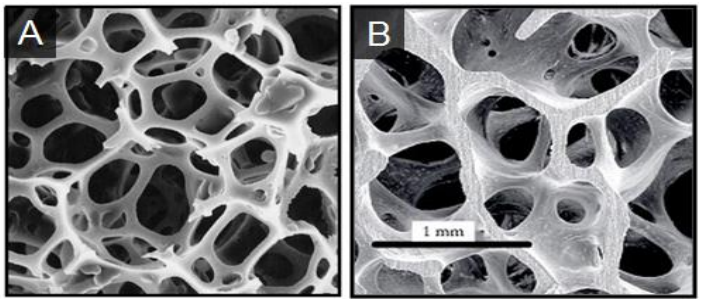

Figure 1.1. Scanning electron micrograph of representative polyHIPE scaffold[47] (A) compared to image of cancellous bone micro-architecture[85] (B)

A specific class of emulsions known as pickering emulsions are stabilized by solid particles which adsorb to the oil-water interface rather than a molecular surfactant.[86] Multiple groups have successfully fabricated and characterized water-in-oil (w/o) pickering polyHIPEs utilizing both titania and silica nanoparticles.[87-90] In reference to polyHIPEs for bone regeneration, the preferential location of self-assembled particles at the pore wall in direct contact with encapsulated MSCs is beneficial for providing a bioactive component that could be utilized for osteoblast differentiation. Recently, hydroxyapatite nanoparticles have been utilized to stabilize o/w and w/o/w emulsions as

a method to coat polymeric microspheres.[90] Therefore, it's possible to utilize osteoinductive particles which self-assemble at the organic-aqueous interface to signal differentiation of encapsulated hMSCs. Recently a styrene-based polyHIPE

Table 1.2. Selected polyHIPE compositions and respective pore diameter, interconnect size and compressive properties

Materials	Surfactant	Pore Diameter (μm)	Interconnect Size (μm)	Compressive Properties (MPa)	Ref
PS, DVB	Span 80	73-90 40-100 20-45 5-100	16-26 15-30 1-16 NR	NA NA 0.007-12 3-110	91 47 92 93
PS, DVB, THF	Span 80	5-100 35-104	1-5 11-26	NA NA	94 95
PS, DVB, Toluene	Span 80	10	NR	NA	96
DVB, EVB	Span 80	20-30	0.65-2.55	NA	97
PS, PMMA, PLA	Span 80 Span 85 Tween 85 Synperonic PE L121	5-20	NR	NA	98
PCL-vinyl	Span 80 Span 85 Tween 80 Synperonic PE L121	5-100	NR	NA	99
PCL, tBA, DVB	Span 80	5-3000	0.2-2	0.012-0.56	100
PCL-triol, HDI, THF	PGPR 4125	5-100, CO_2=1000	0.1-10	0.012-0.5	101
HA polyHIPE	NR	NR	NR	NA	102
PPF, PFDA, Toluene	Span 80	10-400, >500	2-5	NA	103
Hydrogel—polyHIPE Hydroxyapatite	Span 80	100	NR	NA	104

system (Alvetex®) has been commercialized for use as a routine 3D cell culture substrate illustrating the capability of polyHIPEs to promote cell viability and proliferation.[105]

1.3.3.1 Tailoring PolyHIPE Pore Architecture

Extensive research has focused on the effects of specific compositional and processing variables on polyHIPE pore size and interconnectivity. Emulsion stability at the gel point dictates the pore size. Thus, all factors affecting emulsion stability contribute to the resulting polyHIPE pore architecture. Williams illustrated the importance of surfactant concentration on pore size.[106] Since the early work by Williams, many other studies have further emphasized surfactant concentration as the variable having the largest affect on pore size. Interconnected pore architecture is achieved by the tearing of the thin wall between adjacent droplets and is therefore modulated by the wall thickness and densification forces during crosslinking.[107-110] This process that occurs during curing is advantageous over other techniques in which post-fabrication reticulation must be performed to create interconnected porosity.[74]

1.3.3.2 Modulating PolyHIPE Degradation Rate

Traditionally, polyHIPE systems have been fabricated with styrene incorporating divinyl benzene as a crosslinker. Although these polyHIPEs exhibit excellent interconnected architecture, these monomers are non-biodegradable limiting their use as tissue engineered scaffolds. Biodegradability was introduced via polyurethanes and unsaturated polyesters.[101, 103] Furthermore, a recent push in the biomaterials community has illustrated enhanced hydrolytic degradation rates by the incorporation of thiols in

acrylate and methacrylate systems. Recently, a couple of research groups have fabricated thiol-ene polyHIPEs[111, 112] and illustrated the ability of these biodegradable scaffolds to support human keratinocyte growth.[113]

1.3.3.3 Bioactive PolyHIPEs

Recent work on developing polyHIPEs with enhanced bioactivity has focused on the use of biopolymers and/or covalently attaching bioactive peptides post-fabrication.[114, 115] Oil-in-water (O/W) HIPEs were fabricated utilizing the polysaccharides dextran and pullulan and resulted in excellent interconnected scaffolds which promoted retinal cell adhesion.[114] Polypeptide-grafted styrene-based polyHIPEs were fabricated illustrating the potential to surface modify monoliths with any growth factor or signaling peptide of interest.[115] Although, these systems produce well interconnected scaffolds with tunable pore sizes and bioactivity, all post-fabrication techniques eliminate the potential as an injectable material able to space-fill any irregularly shaped defect. Furthermore, biopolymeric scaffolds generally exhibit inferior mechanically properties relative to highly crosslinked synthetic networks thus the importance for utilizing synthetic polymers in HIPE systems.

1.4 Bioactive Factors to Enhance Bone Regeneration

1.4.1 Calcium Phosphate Particles

Calcium and phosphate ions are essential for bone mineralization and important for the signaling processes that occur for healing. In this manner, incorporating calcium phosphate-based particles into biomaterials is a means of providing cells cues to promote osteogenesis. Depending on the temperature, number of impurities, and presence of

water, calcium phosphates can occur in multiple different phases.[116] A range of bioactivities and degradation rates exist for calcium phosphates depending on the Ca/P ratio, crystallinity, and phase purity. **Table 1.3** displays a selection of calcium phosphate formulations and their respective calcium/phosphate molar ratios and solubility in physiological pH (~7.4). The size, shape, and resulting dissolution rate dictates the

Table 1.3. Range of calcium phosphate formulations and properties achieved by using calcium phosphate particles with different Ca/P ratios[1]

Calcium Phosphate Formulation	***Ca/P Molar Ratio***	***Solubility Product***
Monocalcium phosphate (MCP)	0.5	7.2×10^{-2}
Amorphous calcium phosphate (ACP)	1.2-2.2	varies due to metastable nature
β-Tricalcium phosphate (β-TCP)	1.5	1.25×10^{-29}
Hydroxyapatite	1.67	2.35×10^{-59}

ability of cells to engulf ions and respond with matrix formation.[117] Davison *et al.* discuss importance of calcium phosphate submicrostructure on inflammatory response *in vivo.*[118]

1.4.2 Demineralized Bone Matrix (DBM)

In the early 19th century, it was hypothesized that de-calcified bone could be utilized to provide antimicrobial healing in bone defects. Urist and colleagues in 1965 published initial work showing matrix-induced bone formation after implanting bone

matrix in muscle.[119] This work confirmed the hypothesis that by providing decalcified bone matrix, the tissue will heal via an autoinduction mechanism initiated by histiocytes (multinucleate macrophages) that detect degraded bone in the implant site and signal differentiation and repair. Furthermore, the collagenous DBM matrix sequesters important growth factors for MSC differentiation including bone morphogenetic proteins (BMPs).[120] Similar to any matrix component, the amount and presentation of biological agents dictates certain physiological results. Zhang *et al.* illustrated the effects of DBM particle size on osteoinductivity indicating particles ranging from 500 – 710 μm resulted in maximum calcium deposition in an ectopic bone growth mouse model.[121] Additionally, they determined the effect of various levels of matrix decalcification and found that partially decalcified matrix elicited the highest increase in osteogenesis using alkaline phosphatase activity as the marker suggesting that too much calcified matrix hinders the signaling for and/or new mineralization. Smaller amounts of residual calcium nodules provide nucleation sites for new mineralization when implanted. Furthermore, the ability of calcium ions to block the release of proteins such as BMPs suggests that a threshold value of residual calcium exists in which to promote new matrix formation while allowing for the release of growth factors such as BMPs to signal for osteogenic differentiation and new bone formation.[121]

1.5 Benefit of MSC Delivery in Bone Regeneration

The advancements in stem cell biology and effective protocols for culturing multipotent cells have provided the opportunity for testing and analyzing the advantages of delivering autologous stem cells to injured sites via 3D tissue engineered scaffolds.

Recent studies have illustrated enhanced bone regeneration with the delivery of bone marrow derived mesenchymal stem cells.[122-125] Petite *et al.* showed complete bridging of a sheep segmental defect with the delivery of MSCs compared to fresh bone marrow and the blank coral scaffold.[123] In accordance with the tissue engineering paradigm, the incorporation of mesenchymal stem cells which are equipped to promote osteogenesis into a biodegradable, porous bone graft will increase the regeneration rate by imitating the body's natural healing process.

1.5.1 Autologous Stem Cell Delivery in a Rigid Bone Graft

The knowledge and techniques developed by stem cell biologists has greatly increased the ability to extract, expand in *in vitro* culture to acquire enough cells, and deliver viable autologous adult stem cells. The FDA has cleared multiple indications for the use of adult stem cells for treatment of multiple sclerosis, multiple ischemia pathologies, motor neuron disease, and blood and immune disorders including certain cancers.[126, 127] Unfortunately, these cells often flow or migrate away from the application site too quickly and do not remain for the time necessary for treatment or healing to occur, therefore necessitating a biomaterial delivery system for these cells to remain viable and available for direct healing at the defect site. The earliest work on cell encapsulation employed natural polymer-based (collagen, fibrin, agarose, and alginate) hydrogels to provide an extracellular-like matrix to promote cell adhesion and proliferation.[83, 84, 128] Burdick *et al.* illustrated the ability to stimulate bone growth and matrix formation of osteoblasts cultured in PEG hydrogels with covalently attached RGD adhesive peptides covalently incorporated.[84] Although these systems can be

engineered to have specific integrin binding sites and easily serve as encapsulation vehicles for the delivery of viable cells, they lack the requisite mechanical properties to support bone regeneration. Furthermore, a rigid, 3D scaffold that promotes MSC viability, proliferation, and osteogenic differentiation has the potential to enhance bone regeneration by providing a network that can withstand physiological loading known to stimulate osteogenesis.

1.6 Summary and Approach

Although autografts and allografts provide the necessary cues to promote osteogenesis, the high variability and reduced availability of healthy tissue justify the need for a reproducible, highly available graft. Calcium phosphate bone fillers provide the necessary mineral components to drive osteogenic differentiation but lack the porosity and compressive toughness to promote long term viability at the defect. Utilizing a synthetic approach to fabricate highly tunable tissue engineered scaffolds addresses the issue of poor availability and reliability. Furthermore, the ability to incorporate bioactive components and stem cells facilitates a system that promotes osteogenesis similar to native tissue. The template polymerization of high internal phase emulsions provides a highly tunable technique to produce injectable bone grafts with compressive properties comparable to cancellous bone with the added benefit of autologous stem cell encapsulation to promote regeneration directly at the defect site.

CHAPTER II

MODULATING INJECTABLE POLYHIPE PORE AND INTERCONNECT SIZE*

2.1 Introduction

For decades, tissue engineers have illustrated the importance of 3D biomaterial scaffolds in healing by providing a matrix to direct tissue regeneration. These scaffolds stimulate neotissue formation by sequestering vital growth and transcription factors, providing an interconnected network to facilitate nutrient and waste transport, exhibiting compressive properties matching native tissue, and demonstrating a degradation profile that mirrors the healing rate *in vivo*. Polymerized high internal phase emulsions (polyHIPEs) are a unique fabrication technique that is currently being studied for their utility as tissue engineered scaffolds. High internal phase emulsions are dictated by an internal phase volume fraction greater than 74%. Polymerization of the continuous phase of a high internal phase emulsion (polyHIPE) results in a highly porous, interconnected foam. Multiple compositional and processing variables have been determined to affect emulsion stability which dictates the resulting pore architecture and consequent mechanical properties. Through manipulation of these variables, a range of pore sizes, porosities, compressive properties, and rheological properties can be achieved,

---

* Reprinted with permission from "Injectable PolyHIPEs as High-Porosity Bone Grafts," by Robert S. Moglia, Jennifer L. Holm, Nicholas A. Sears, Caitlin J. Wilson, Dawn M. Harrison, and Elizabeth Cosgriff-Hernandez, Biomacromolecules 2011, 12 (10), 3621-3628. Copyright (2011) American Chemical Society.
Reprinted with permission from "Achieving Interconnected Pore Architecture in Injectable PolyHIPEs for Bone Tissue Engineering," by Jennifer L. Robinson, Robert S. Moglia, Melissa C. Stuebben, et al, Tissue Engineering Part A 2014, 20 (5-6), 1103-1112. Copyright (2014) Mary Ann Liebert, Inc.

illustrating the utility of polyHIPEs for hard and soft tissue repair.[47, 91-99, 101-104, 106, 114, 129-137]

A unique characteristic of the polyHIPE system as a tissue engineered graft is its mayonnaise-like viscosity prior to cure which is suitable for injection and retention at the defect site. An injectable scaffold that fills irregularly-shaped defects and integrates with host tissue can enhance healing and reduce inflammation.[138] Initially, styrene-based polyHIPE systems were studied due to the established control of the interconnected pore architecture. Bioactive components were successfully introduced into styrene-based polyHIPEs to provide substrates that promoted osteoblast and neuronal cell adhesion and proliferation.[47, 94, 139] Although these polyHIPEs are valuable as 3D cell culture substrates, these materials are not biodegradable or injectable which limits their use as tissue engineered scaffolds. Biodegradability was introduced into polyHIPEs by the substitution of unsaturated polyesters into systems that still contained non-biodegradable crosslinkers or diluents.[92, 99, 140] Subsequently, fully biodegradable systems were achieved by eliminating styrene and utilizing polyurethane and fumarate chemistries.[103, 141] Although these compositions were biodegradable, the necessity of a toxic diluent and cure temperatures at or above 60°C rendered them non-injectable. An injectable polyHIPE system requires low viscosity macromers for HIPE formation without the need for a toxic diluent and reaction kinetics permitting crosslinking *in situ.*

Our lab has developed the first biodegradable and injectable HIPE system based on propylene fumarate dimethacrylate (PFDMA) macromers.[142] These polyHIPEs were fabricated without a toxic diluent and successfully cured at 37°C. Traditionally, selection

of HIPE surfactants has been based on trial and error and historical precedence. Rational design was utilized to determine effective surfactants to stabilize PFDMA HIPEs based on structural features and predictors. The fabrication of these injectable polyHIPEs was a great advancement for bone tissue engineered scaffolds; however, the ability to tune pore architecture must be illustrated. PolyHIPE pore size is dictated by the internal phase droplet size at the gel point. The 3D pore architecture largely affects the compressive properties of the monolith indicating the importance of developing a system with tunable, homogenous pore sizes. This work demonstrates the ability to utilize surfactant concentration and mixing speed to modulate injectable HIPE emulsion stability and thereby tune pore sizes.

Interconnected porosity is vital in tissue engineered scaffolds to promote the transport of essential nutrients to cells. Recent work by Madden *et al.* highlighted the importance of interconnectivity for cell migration and nutrient/waste transport in scaffolds with small pore sizes. Human embryonic stem cell-derived cardiomyocytes seeded on bimodal scaffolds with interconnected pores ranging from 30 – 40 μm were viable for at least two weeks to a depth of 300 μm into the construct.[49] Marcacci *et al.* reported that porosity and interconnectivity was also of critical importance in the vascularization and healing of a bone segmental defect clinical trial.[143] Therefore, interconnectivity is a key design criterion in the development of an injectable polyHIPE system to support full healing *in vivo.*

In the polyHIPE system, interconnects, or windows between discrete pores, form at the gel point from rupture of the thin walls between droplets.[144] This phenomenon is

dependent on both wall thickness and macromer densification forces from volume contraction during conversion of monomer to polymer. Varying the wall thickness and densification forces can result in film breakage if the contractile forces are large enough to strain the film to failure. Diluents and monomers utilized in the majority of past polyHIPE systems most likely enhanced the interconnectivity by decreasing wall thickness and increasing the magnitude of densification forces, respectively. Recently, the Silverstein group published studies describing the effect of the locus of initiation on pore architecture and properties.[87, 109, 110, 145] The authors proposed that organic-phase initiation resulted in larger, spherical, interconnected pores and an increased loss modulus relative to aqueous-phase initiation.[110] However, a mechanistic description of the effect of locus of initiation on the resulting macromer densification forces and the corollary effect on interconnect formation was not described.

To this end, we have developed a biodegradable and injectable polyHIPE system with readily tunable pore sizes, interconnected pore architecture, compressive properties, injection parameters, and stable storage capabilities for use an off-the-shelf bone graft. The majority of the work is based on propylene fumarate dimethacrylate (PFDMA) macromers which have a suitable viscosity for HIPE formation and reactive methacrylate end groups which enable *in situ* crosslinking into rigid monoliths at 37˚C. Furthermore, fumarate-based polymers have shown great promise as bone grafts with established osteoconductivity in vivo.[146-148] The ability to synthesize a fully biodegradable polyHIPE without a toxic diluent that can also cure at physiological temperatures is an important adaptation of emulsion templating. Parameters such as

surfactant concentration, mixing speed, and the phase in which initiation occurs were utilized to generate closed vs. open-pore scaffolds with pores ranging from 2 – 29 μm. A model system using ethylene glycol dimethacrylate macromers illustrated the potential of a hydrophilic polymer to promote Ostwald ripening and increase pore sizes from 50 – 200 μm. The potential of injectable PFDMA polyHIPEs to be stored at reduced temperatures and then thawed before implementation as a bone graft was evaluated. Additionally, the effects of precure, storage, and injection on polyHIPE pore architecture, work time, and set time were also characterized. Finally, the resulting compressive moduli and strength values were evaluated over the course of two weeks. Overall, these studies highlight the ability to use multiple compositional variables and processing techniques to generate injectable and biodegradable PFDMA polyHIPEs with a usable range of pore sizes, compressive properties, cure times, and deployment options. This fundamental understanding of mechanisms that dictate HIPE stability and resulting properties is vital in rationally designing monoliths to guide mesenchymal stem cell proliferation and differentiation into functional osteoblasts to lay down healthy bone matrix and stimulate full healing in bone defects.

2.2 Materials and Methods

2.2.1 Materials

Polyglycerol polyricinoleate (PGPR 4125) was donated by Palsgaard (Morris Plains, NJ). All other chemicals were purchased and used as received from Sigma Aldrich (Milwaukee, WI) unless otherwise noted.

2.2.2 PFDMA Synthesis

PFDMA was synthesized in a two-step process adapted from Timmer et al.[149] Briefly, propylene oxide was added dropwise to a solution of fumaric acid and pyridine in 2-butanone (2.3:1.0:0.033 mol) and refluxed at 80°C for 16-18 hours. Residual propylene oxide and 2-butanone were removed by distillation, residual acidic byproducts and water were removed with washing, and the product was dried under vacuum. The diester bis(1,2 hydroxypropyl) fumarate product was then end-capped with methacrylate groups in an addition process with triethylamine (TEA) and methacryloyl chloride (MAC). The molar ratios of the diester, MAC, TEA were 1:2.1:2.1, respectively. Hydroquinone was added at a molar ratio of 0.008:1 to diester to inhibit crosslinking during the synthesis. The reaction was maintained below -10˚C to reduce undesirable side reactions and stirred vigorously overnight under a nitrogen blanket. The product was washed overnight in 2 M potassium carbonate to neutralize methacryloyl chloride after which the PFDMA was passed through a chromatography column loaded with alumina at a 9:1 molar ratio alumina:TEA to remove any residual TEA and methacrylic acid. The product was then washed in deionized water to remove any alumina and subjected to a brine wash and stirred over anhydrous sodium sulfate to remove water. The PFDMA product was dried under vacuum and the structure confirmed using H NMR (300 MHz, $CdCl_3$) δ 1.33 (dd, 3H, CH3), 1.92 (s, 3H, CH3), 4.20 (m, 2H, -CH2-), 5.30 (m, 1H, -CH-), 5.58 (s, 1H, -C=CH2), 6.10 (s, 1H, -C=CH2), 6.84 (m, 2H, -CH=CH-). The integration ratio of methacrylate protons to fumarate protons in the ^{1}H

NMR spectra was used to confirm > 90% functionalization for all macromers prior to polyHIPE fabrication.

2.2.3 EGDMA Inhibitor Removal

The EGDMA was passed through a column containing alumina oxide using high air pressure to remove the monomethyl ether hydroquinone inhibitor and collected in a round bottom flask.

2.2.4 PolyHIPE Fabrication

HIPEs were prepared using the FlackTek Speedmixer DAC 150 FVZ-K. Briefly, PFDMA was mixed with the surfactant PGPR in the Speedmixer cup prior to emulsification. The PGPR concentrations used in this study were 5, 10, 15, and 20 wt%. For studies investigating the effects of surfactant concentration and mixing conditions, the aqueous solution of calcium chloride (1% v/v), ammonium persulfate (5 wt %) and deionized water was then added to the organic phase in the speedmixer cup. The calcium chloride was used to prevent Ostwald ripening while the ammonium persulfate initiated radical crosslinking of the macromer chains. HIPEs were then transferred to a 37°C aluminum bead bath for 12 hours to facilitate cross-linking. The resulting polyHIPE foams were placed under vacuum for 24 hrs to remove water prior to characterization.

The polyHIPE fabrication process is illustrated in **Figure 2.1**. For the studies looking at the effect of poly(ethylene glycol) molecular weight and concentration and temperature effects, both PFDMA and EGDMA HIPEs were made to elucidate the effects within HIPEs of differing viscosities. The aqueous phase was comprised of water and 3 w/v% PEG with one of the following molecular weights: 200, 300, 400, 2k, 6k,

10k, or 35k. Calcium chloride was not added to the aqueous phase as this electrolyte is utilized to hinder Ostwald ripening and could therefore negate any effect from the PEG. For studies looking at the effect of the locus of initiation on pore architecture, PFDMA

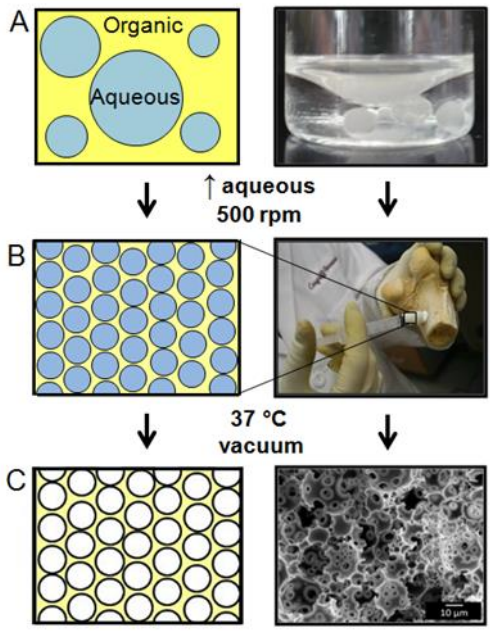

Figure 2.1 Schematic of the process to fabricate a polymerized high internal phase emulsion. A) The emulsion is comprised of a hydrophobic organic phase and an aqueous phase. B) HIPE is defined by the aqueous volume phase greater than 74% and exhibits a whipped, mayonnaise consistency prior to cure. C) PFDMA crosslinks at 37°C locking in the emulsion geometry creating a polyHIPE with high porosity.

was first mixed with 5 wt% of the organic-phase soluble initiator, benzoyl peroxide (BPO), and 5 wt% PGPR prior to emulsification. Once thoroughly mixed, the aqueous solution of calcium chloride (1 wt%) and deionized water was then added to the organic

phase (75% v) in six additions and mixed at 500 rpm for 2.5 minutes each. HIPEs were transferred to a 37°C aluminum bead bath to facilitate crosslinking overnight. To evaluate the effects of locus of initiation on pore architecture, polyHIPEs were also fabricated with 5 wt% ammonium persulfate (APS), the aqueous-phase soluble initiator, added to the aqueous solution prior to emulsification with the organic phase. Initiator concentrations were calculated based on the organic phase weight and kept constant between the two systems. This results in a relatively higher initiator concentration in the organic phase (5 wt% BPO to total organic phase) compared to initiator concentration in the aqueous phase (1.66 wt% APS to total aqueous phase).

2.2.5 Pore and Interconnect Size Characterization

SEM (JEOL 6500) was utilized to image all polyHIPEs and determine average pore and interconnect size for pre-treatment and storage studies. PolyHIPEs were subjected to vacuum drying for 72 hours to remove water prior to pore architecture characterization. Circular specimens from three separate polyHIPE specimens were sectioned into quarters, fractured at the center, coated with gold, and imaged in a rastor pattern yielding five images. Pore size measurements were completed on the first ten pores that crossed the median of each 1000X magnification micrograph. Average pore sizes for each polyHIPE composition are reported (n=150). A statistical correction was calculated to account for non-perfect spherical pores, $h^2 = R^2 - r^2$, where R is the void diameter's equatorial value, r is the diameter value measured from the micrograph, and h is the distance from the center. The average diameter values were multiplied by this correction factor resulting in a more accurate description of pore diameter.[95] To calculate

interconnect sizes, three median lines were drawn on each image, and the first ten interconnects located in pores crossing each of these lines was counted. Average interconnect sizes for each polyHIPE composition are reported (n=150).

2.2.6 Compressive Testing

The change in polyHIPE compressive properties over time was investigated to determine the maximum values for a 5 wt% BPO polyHIPE. The PFDMA HIPE was split into five centrifuge tubes and cured at 37°C for 1, 3, 7, 10, and 14 days prior to mechanical testing. ASTM D1621-04a was utilized to determine the compressive modulus and strength of the polyHIPEs.[150] Each polyHIPE specimen was sectioned into three disks with a 3:1 diameter to height ratio using an Isomet® saw (Buehler) and compressed using an Instron 3300 at a strain rate of 50 μm/s. The compressive modulus was calculated from the slope of the linear region after correcting for zero strain and the compressive strength was identified as the stress at the yield point or 10% strain, whichever point occurred first. Reported moduli and strength data were averages of the three disks for each time point tested (n=15).

2.2.7 Pre-treatment and Storage Studies

The potential of injectable PFDMA polyHIPEs to be stored at reduced temperatures and then thawed prior to implementation as a bone graft was evaluated. HIPEs fabricated with 5 wt% BPO were split into six 5 ml syringes and subjected to either 20°C or 37°C, stored for one week at 4°C, injected, and cured. HIPEs were also subjected to pre-treatment heat conditions prior to storage in order to promote crosslinking and reduce cure time *in vivo*. The duration of pre-treatment time was

investigated for 1, 2, and 6 hours at 20°C and 37°C. Time points for the pre-treatment studies were determined as the hourly times that allowed for initial crosslinking before the gel point was reached. The specific storage and pretreatment conditions are detailed in the table found on page 51. This study was repeated for a total of three polyHIPE specimens in each condition.

2.2.8 Statistical Analysis

The data are displayed as mean ± standard deviation for each composition. A Student's t-test was performed on the compressive data to determine any statistically significant differences between compositions. Tests for set time and compressive properties were carried out at a 90% ($p < 90\%$) and 95% confidence interval ($P<0.05$), respectively.

2.3 Results and Discussion

2.3.1 PFDMA Synthesis and Analysis

PFDMA was synthesized by the two-step reaction described previously. The first step produced a diester intermediate, bis-(1,2-hydroxypropyl) fumarate, which was then functionalized with methacrylate endgroups, **Figure 2.2**. Following purification, the structure of the resulting PFDMA product was confirmed with 1H NMR. The integration ratio of methacryloyl protons to fumarate protons in the 1H NMR spectra, **Figure 2.3**, confirmed the structure of PFDMA as a single fumarate unit with two terminal methacrylate groups. The average functionalization was calculated to be ~83%. The methacrylate and fumarate groups provided sites for radical crosslinking of the macromer to permit cure of the HIPE at physiological temperatures. Furthermore,

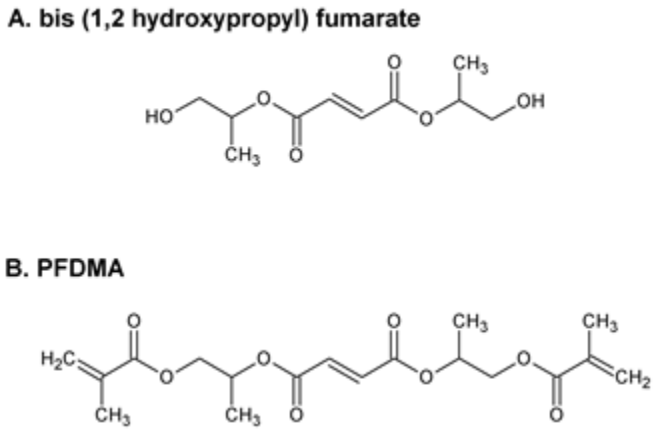

Figure 2.2. Molecular structure of (A) bis (1,2 hydroxypropyl) fumarate and (B) PFDMA.

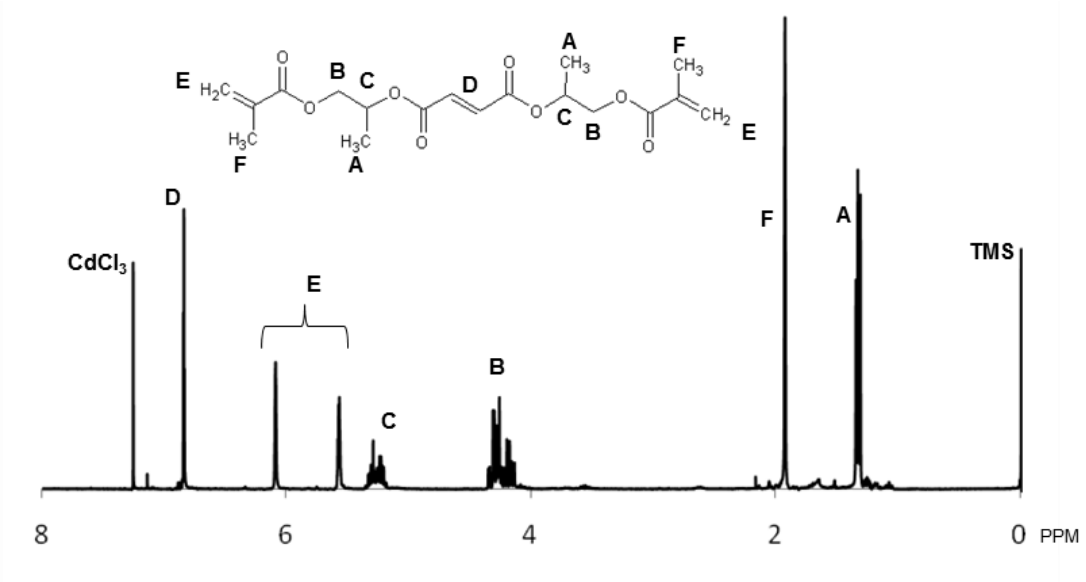

Figure 2.3. Nuclear magnetic resonance spectrum of PFDMA.

fumarate-based bone grafts have shown promising osteoconductivity results in vivo.[146-148] The resulting macromer had a sufficiently low viscosity (0.125 Pa·s) and hydrophobicity to permit HIPE formation.

2.3.2 Injectable Porous Scaffolds

Stable PFDMA HIPEs were incubated at 37°C to initiate radical crosslinking of the unsaturated double bond of the methacrylate groups. The resulting polyHIPE monoliths exhibited ~75% porosity and an average compressive modulus and strength of 33 and 5 MPa, respectively. SEM analysis was utilized to determine pore size and morphology. Polymerization of the continuous phase of the HIPE locked in the emulsion geometry resulting in a high-porosity foam with a closed-pore morphology and average pore size ranging from 4 – 29 µm. These studies represent an important milestone in the development of an injectable bone graft. Specifically, these polyHIPEs utilize a biodegradable and osteoconductive polymer, have a suitable pre-cure viscosity for injection; and cure at physiological temperatures to a rigid, high-porosity monolith. The potential utility of this new polyHIPE system as an injectable bone graft is illustrated in **Figure 2.4**.

Figure 2.4. Injectable PFDMA polyHIPEs can be used in situ to space fill complex defects without the need for expensive CAD software.

2.3.3 Effect of PGPR Concentration on Pore Architecture

Given that the polyHIPE architecture is dictated by the emulsion geometry prior to cure, modulation of emulsion stability may be used to tune the resulting polyHIPE architecture. This requires a brief review of the thermodynamics involved in both emulsion formation and phase separation. The increase in surface energy of an emulsion compared to the non-emulsified components (Δ W) is a product of both the interfacial energy (σ) and the change in surface area (Δ A) upon emulsification.

$$\Delta W = \sigma \cdot \Delta A$$

ΔW is the free energy of the interface and corresponds to the reversible work brought into the system during emulsification. The magnitude of ΔW can be considered a measure of the thermodynamic instability of the emulsion and drives phase separation as a means to decrease ΔA. From this relationship, it is evident that ultimate stability against coalescence processes is only achieved if σ approaches zero. The surfactant's role during emulsification is to reduce this interfacial tension and form a barrier between the two phases.

Two relationships relevant to polyHIPE architecture can be inferred from this discussion: 1) an increase in interfacial tension ($\uparrow\sigma$) will increase the rate of droplet coalescence due to an increase in ΔW; 2) an increase in interfacial tension ($\uparrow\sigma$) will correspond to larger initial droplet sizes ($\downarrow$ ΔA) for a given ΔW. It follows that the surfactant which directly impacts interfacial tension can be used to tune pore sizes by changing the initial droplet size and/or the rate of droplet coalescence prior to cure. To this end, Williams et al. studied the effect of surfactant concentration on both pore size

and wall thickness between droplets.[93] It was reported that a reduction in surfactant concentration could be used to increase pore size by destabilizing the HIPE. In addition, an increase in surfactant concentration was found to decrease wall thickness and induce pore opening upon polymerization. We hypothesized that HIPE stability could be modulated by changing the surfactant concentration to achieve a range of polyHIPE pore sizes and an open-pore morphology. PGPR concentrations from 5 to 40 wt% were utilized to investigate the effect of surfactant concentration on polyHIPE pore architecture. SEM analysis of polyHIPE monoliths was conducted to quantify pore and interconnect size using the 10.7 pixels/μm ratio at 1000x, **Table 2.1**. Decreasing the concentration of PGPR from 20 to 5 wt% was found to increase average pore diameter in PFDMA polyHIPEs (6 to 29 μm), **Figure 2.5**. A narrowing of pore size distributions with increasing surfactant concentration was also observed, **Figure 2.6**.

Table 2.1. The effect of surfactant concentration on polyHIPE architecture

Surfactant (wt%)	Porosity (%)	Average Pore Diameter (μm)
5	75.1 ± 0.4	29 ± 19
10	75.1 ± 0.3	21 ± 11
15	75.1 ± 0.1	14 ± 8
20	74.1 ± 0.1	4 ± 2

Gravimetric porosity, N = 3, average ± standard deviation. Average pore measurements from image analysis of scanning electron micrographs, N = 150, average ± standard deviation.

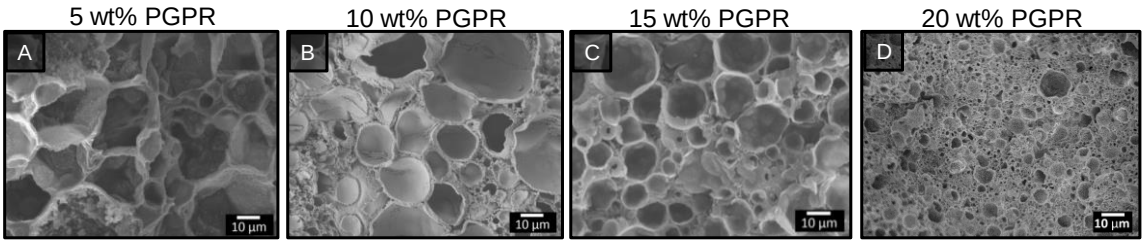

Figure 2.5. Scanning electron micrographs (A,B,C,D) of PFDMA polyHIPEs with increasing surfactant concentrations. It can be seen that pore sizes decrease as PGPR concentration increases from 5-20 wt%.

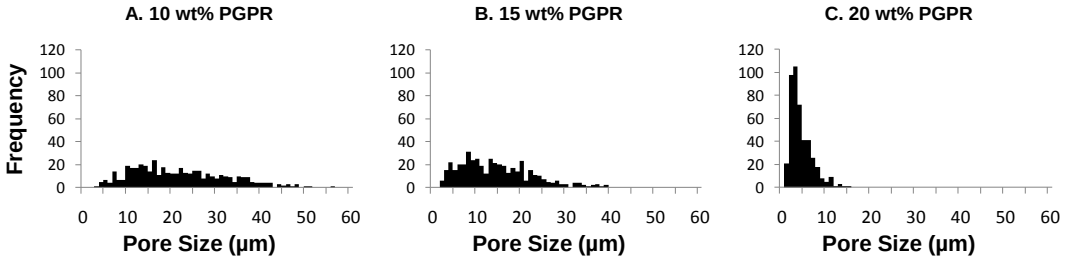

Figure 2.6. Distribution of pore sizes for 75/25 polyHIPEs with varied PGPR concentrations, mixed at 500 rpm. (A) 10 wt%, (B) 15 wt%, and (C) 20 wt%. Pore sizes become more uniform as PGPR content increases.

The decreased pore size observed at higher surfactant concentration was attributed to a decrease in interfacial tension with a corollary decrease in droplet size, as discussed above. Assuming conservation of organic phase volume, this increase in surface area also decreases the film thickness between droplets;[151] however, this wall thinning was insufficient to lead to pore opening in this system. Based on these preliminary results, it was hypothesized that increased densification in combination with decreasing film thickness would be needed to generate open-pore polyHIPEs. This is the subject of current investigation using alternative fumarate-based macromers. A

narrowing of the pore size histograms also indicated that a higher surfactant concentration resulted in a more uniform pore size, **Figure 2.6**. Williams *et al.* reported that increased pore size homogeneity was observed with increased surfactant due to a reduction in droplet coalescence.[93] However, the droplet coalescence observed in these studies was characterized by a few large pores surrounded by many smaller pores. As illustrated in **Figure 2.6**, there was a continuum of pore sizes observed rather than the more bimodal distribution reported by Williams et al.[93] Ostwald ripening has also been reported to increase the pore size distribution of polyHIPEs. In this process, diffusion of water from smaller droplets to larger droplets causes a more gradual broadening of the pore size distribution.[95] Both of these processes are affected by the nature and concentration of surfactant; however, it is unclear whether droplet coalescence or Ostwald ripening is responsible for the observed difference in pore size distribution. Based on the histograms alone, it appears that Ostwald ripening may be more significant; however, additional studies are needed to make a stronger claim on this front.

2.3.4 Effect of Mixing Speed on Pore Architecture

Processing parameters such as mixing speed can also be utilized to tune the pore architecture through manipulation of the emulsion geometry prior to cure. Revisiting the thermodynamic stability of the system yields mechanistic answers for the effect altered mixing speed has on pore size and homogeneity. Varying the mixing speed directly affects the difference in surface energy of the emulsion relative to the non-emulsified components. By adding mechanical energy into the system through mixing, the surface

energy of the emulsion is increased yielding a larger change relative to the non-emulsified components (ΔW). This causes an increase in the surface area (ΔA) of the droplets upon emulsification, assuming low interfacial tension due to surfactant (σ). This increase in surface area corresponds with decreased droplet sizes. We hypothesized that pore size and homogeneity can be modulated by altering the free energy of the system resulting in decreased pore diameters and increased homogeneity with an increase in mixing speed.

Mixing speeds of 500, 1000, and 2000 rpm on the FlackTek Speedmixer™ were tested to investigate the effect on pore architecture. Initially, HIPEs with 20 wt% PGPR were utilized resulting in minimal change in pore size with an increase in mixing speed as seen in **Table 2.2**. We hypothesized that destabilizing the emulsion with a lower concentration of PGPR would result in a larger pore size distribution, thereby clearly illustrating the effect of mixing speed. Scanning electron micrographs of both 10 and 20 wt% PGPR compositions at varying mixing speeds are found in **Figure 2.7**. A decrease in pore size was observed with both 10 and 20 wt% PGPR specimens as mixing speed was increased (500 to 2000 rpm). As discussed, the trend was more evident with the 10 wt% PGPR specimens, **Table 2.2**, and further illustrates the effect of surfactant on emulsion stability and pore architecture. The narrowing of the histograms in **Figure 2.8** from 500 to 2000 rpm indicates a more homogeneous pore size distribution which is illustrated in the SEM images. As stated previously, increased surfactant produced an increase in pore homogeneity due to decreased surface energy. Combining both mixing speed and surfactant had a large effect on pore size homogeneity as observed in **Figure**

Table 2.2. The effect of mixing speed on polyHIPE pore structure with a constant volume fraction (75/25) and varied surfactant concentration (10 and 20 wt% PGPR)

Mixing Speed (rpm)	[PGPR]	Average Pore Diameter (µm)
500	10 wt%	21 ± 11
	20 wt%	4 ± 2
1000	10 wt%	8 ± 4
	20 wt%	3 ± 2
2000	10 wt%	4 ± 3
	20 wt%	2 ± 1

Average pore measurements from image analysis of scanning electron micrographs, N = 150, average ± standard deviation.

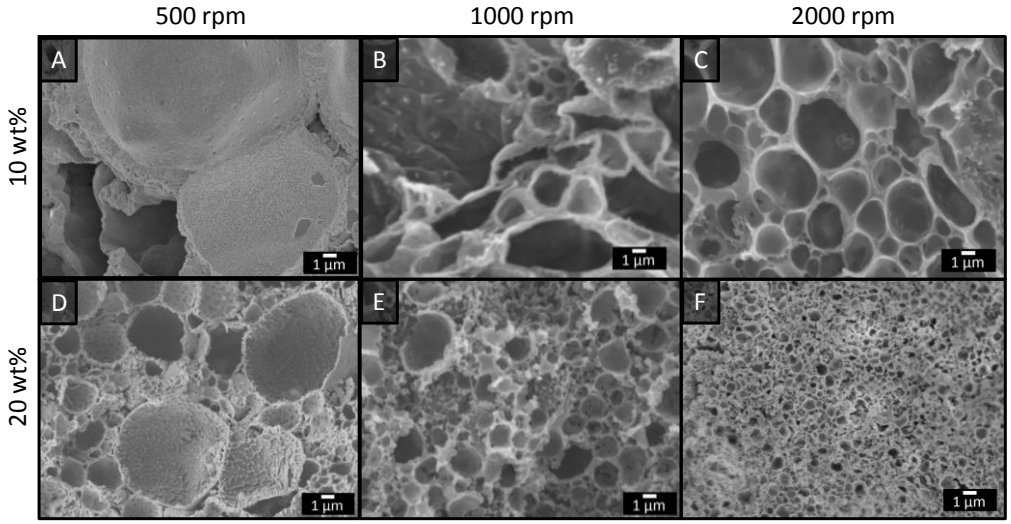

Figure 4. Scanning electron micrographs of PFDMA polyHIPEs fabricated at increasing mixing speeds: (A-C) 10 wt% PGPR (A) 500 rpm (B) 1000 rpm (C) 2000 rpm, (D-F) 20 wt% PGPR (D) 500 rpm (E) 1000 rpm (F) 2000 rpm

Figure 2.7. Scanning electron micrographs of PFDMA polyHIPEs fabricated at increasing mixing speeds. (A-C) 10 wt% PGPR (A) 500 rpm (B) 1000 rpm (C) 2000 rpm, (D-F) 20 wt% PGPR (D) 500 rpm (E) 1000 rpm (F) 2000 rpm. A decrease in pore size is seen with an increase in mixing speed.

2.8 by increasing the surface area of the emulsion and decreasing the interfacial energy of the droplets, respectively, to reduce droplet size and coalescence.

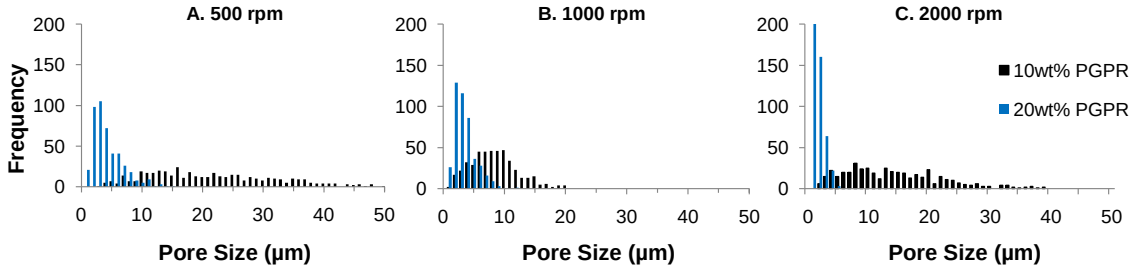

Figure 2.8. Distribution of pore sizes for 75/25 polyHIPEs fabricated with 10 (black) and 20 wt% PGPR (blue) at 500, 1000, and 2000 rpm.

2.3.5 Effect of Poly(ethylene glycol) on Pore Architecture

Work by Carnachan *et al.* illustrated the ability to modulate polyHIPE pore size via the incorporation of a hydrophilic polymer in the aqueous phase.[95] The addition of

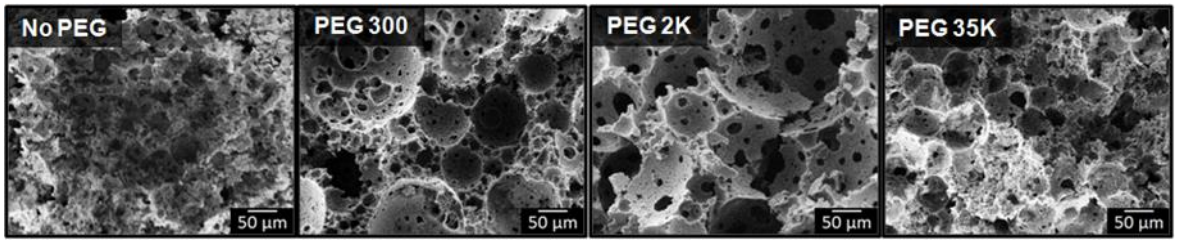

Figure 2.9. Scanning electron micrographs illustrating the effect of PEG molecular weight on aqueous phase Ostwald ripening and resulting pore architecture in EGDMA polyHIPEs

water-miscible poly(ethylene glycol) promotes increased diffusion of water droplets and results in Ostwald ripening. **Figure 2.9** displays the effect of PEG molecular weight on EGDMA polyHIPE pore architecture. An increase in pore size (50 – 200 µm) was

observed with an increase in PEG molecular weight with the largest effect at a molecular weight of 2k. At molecular weights higher than 2k, a negligible effect was seen which may be due to limited diffusion kinetics. No effect was observed in PFDMA polyHIPEs due to the increased viscosity of the organic phase providing a physical barrier for phase separation.

2.3.6 Locus of Initiation

Previous PFDMA polyHIPEs were initiated with the aqueous-phase soluble initiator APS and resulted in closed pore foams. Interconnectivity was achieved in this study by switching the locus of initiation from the aqueous to organic phase using BPO as the radical initiator. The BPO concentration was chosen as the lowest amount that produced cured monoliths in the range of 2-3 hours. Because the organic phase comprises a quarter of the total HIPE volume in these studies, the amount of BPO required to achieve roughly the same cure time among the two systems was one third the amount of APS utilized previously. This reduction in initiator concentration decreases the possibility that residual initiator leaches out of the material and has cytotoxic effect *in vivo.* The effect of the locus of initiation on interconnect formation is illustrated in **Figure 2.10.** Organic-phase initiation resulted in the formation of interconnects compared to the closed-pore morphology from aqueous-phase initiation in the PFDMA polyHIPE system. The effect of the locus of initiation on pore interconnectivity has been noted previously in the polyHIPE literature.[87, 109, 110, 145] However, a mechanistic understanding of the process has yet to be discussed. A probable description of

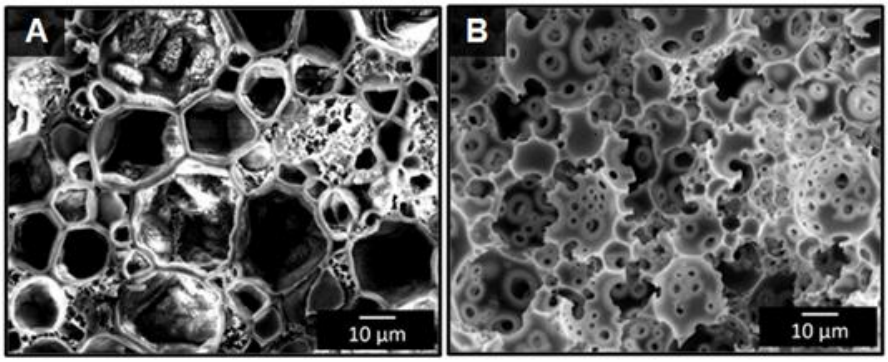

Figure 2.10. Scanning electron microscopy micrographs illustrate PFDMA polyHIPEs with (A) closed pore morphology from interfacial initiation and (B) open pore morphology from organic phase initiation.

interconnect formation based on the forces generated during the conversion from PFDMA macromer to crosslinked polymer is illustrated in **Figure 2.11**. The green gradient region illustrates the progression of crosslinking from initiation sites. It is proposed that the thin film between water droplets in the aqueous-phase initiation system is crosslinked resulting in a closed-pore architecture as evident by the location of the green region between pores. In organic-phase initiation, the green regions are located in the denser pockets where pores are not adjacent to each other. The force of densification upon conversion of macromer to polymer results in forces that pull and tear the thin film between the pores which is shown as the yellow regions in the figure. This tearing results in interconnects or windows between the pores. With this understanding, future tuning of interconnect size and frequency may be achieved. Current work is focused on increasing densification which is heavily dictated by the size/density of the

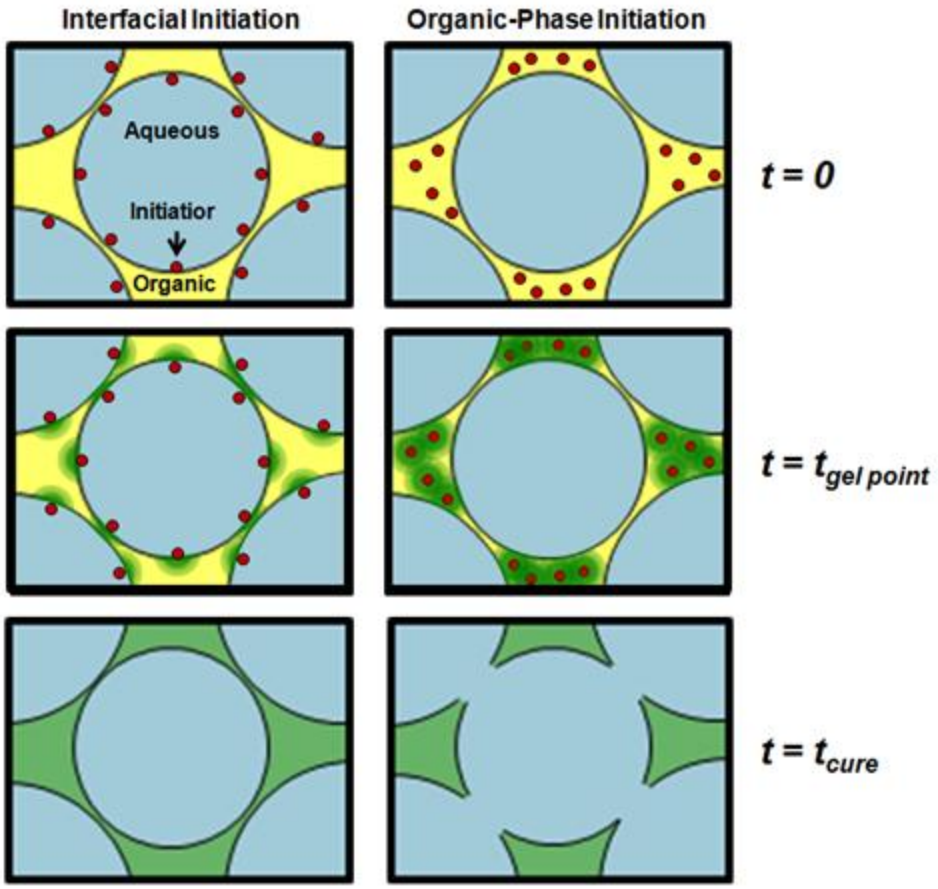

Figure 2.11. Schematic of the proposed mechanism for interconnect formation illustrating the effect of initiation loci on macromer densification forces during cure. Organic phase initiation results in sufficient densification forces as the macromer chains convert to polymer to tear the thin film between droplets and open pores. Red illustrates initiator, yellow illustrates macromer, and green illustrates the loci of initiation and regions where crosslinking is occurring.

monomer/macromer and altering crosslinking kinetics to further increase interconnect size.

2.3.7 Compressive Properties

Compressive modulus and strength values were determined using an Instron mechanical testing apparatus on polyHIPEs cured through two weeks. A representative stress/strain plot for specimens with a yield point prior to or after 10% strain is shown in **Figure 2.12.** PFDMA polyHIPEs initiated with 5 wt% BPO resulted in compressive modulus and strength values increasing through two weeks as illustrated in **Figure 2.13.** It is probable that crosslinking is continuing over time due to the relatively slow reaction kinetics at 37°C. Average values recorded at two weeks for compressive modulus and strength were 43 ± 12 MPa and 3 ± 0.2 MPa, respectively. These values approach those of human cancellous bone of 20-500 MPa[46, 152] for modulus and 2-30 MPa[153, 154] for strength. This data suggests that the compressive strength may continue to increase as

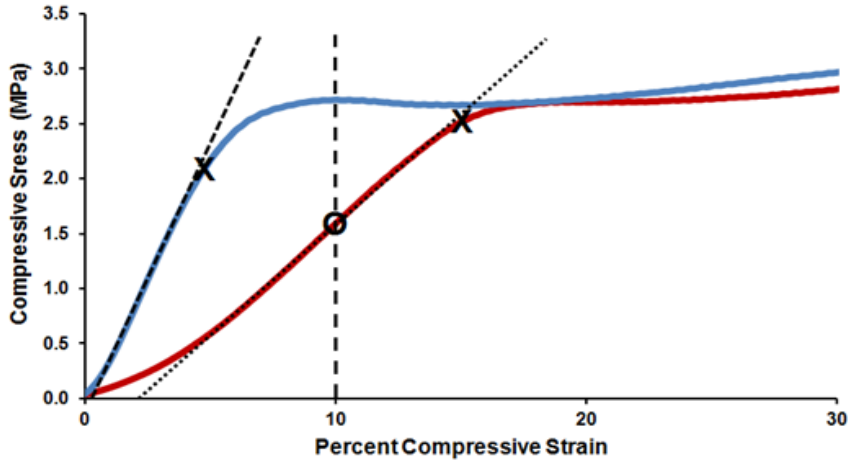

Figure 2.12. Stress/strain plot illustrating two representative specimens with yield points before or after 10% strain with "X" denoting the yield points taken for strain. The dotted line indicates 10% strain and the "O" denotes compressive stress taken at 10% strain for strength values.

indicated by the lack of a plateau in values. Analyzing the compressive properties of HIPEs stored for a year at 4°C illustrated maintenance of properties, namely a modulus of 47 MPa and strength of 2.2 MPa. ISO standard 5833 for bone cement states a requisite ≥ 70 MPa of compressive strength.[155] However, materials with compressive properties on the low end of human cancellous bone have been shown to encourage new tissue growth in animal models *in vivo*.[53, 156] Therefore, it may not be necessary to meet these high compressive properties of bone cement in a tissue engineered scaffold that will be remodeled to bone.

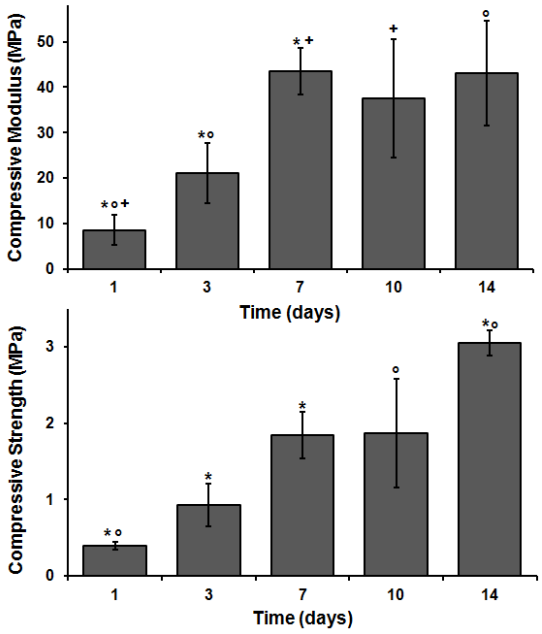

Figure 2.13. The effect of time on PFDMA polyHIPE compressive modulus and strength. *+° indicate statistically significant differences between respective samples $p < 0.05$

2.3.8 Pre-treatment Studies: Effect on Cure Time

HIPEs were subjected to pre-treatment conditions to promote crosslinking prior to injection for reduced cure time *in vivo* without the need to alter HIPE composition such as initiator concentration. Work time is the time available to a surgeon after the onset of mixing to manipulate the material without detriment to its properties.[157] The work time can be determined by the gel point in which the crosslinking in the system is sufficient to resist flow.[158] The intersection of loss and storage modulus is often utilized to determine this gel point of crosslinkable polymers.[159] However, in the HIPE system, the storage modulus was determined to be larger than the loss modulus throughout the duration of testing which was attributed to the HIPE's viscoelastic behavior. Therefore, the onset of the increase in storage modulus determined with DMA was utilized as the work time in this study. PolyHIPE set time, or the time required for the material to cure to a solid monolith, was approximated using tack-free time as defined in the methods. Work and set time values as a function of pre-treatment conditions are located in **Table 2.3.** Pre-treatment for one hour at 37°C decreased the work time but not statistically significantly compared to the storage control. However, the set time was statistically significantly decreased by pre-treating at 37°C for one hour as seen in **Figure 2.14.** In these studies, pre-treating at 20°C and 37°C had a modest effect on set time. BPO has an average 10 hour half life at 70°C in benzene.[149] Therefore, at 37°C only a fraction of BPO is dissociating into radicals, reducing the number of chains able to propagate which results in a longer set time. Increasing the reaction kinetics in the system via aqueous phase temperatures during HIPE formation and cure temperatures is expected to increase the

Table 2.3 The effect of storage and injection on polyHIPE microarchitecture, work time, and set time. Work time was only determined for the storage control and pre-treatment at 37°C composition to estimate the range of time the HIPE could be manipulated before injection.

Storage Conditions	Injection Conditions	Pre-treatment Time (hrs)	Pore Size (μm)	Interconnect Size (μm)	Work Time (hrs)	Set Time (hrs)
No storage	Not injected	-	12 ± 10	3 ± 2	-	3.5 ± 0.5
	Injected	-	12 ± 9	3 ± 2	-	3.00 ± 0.5
1 week 4°C	Injected	-	12 ± 9	3 ± 2	2.25 ± 0.25	3.00 ± 0.75
		1 @ 20°C	12 ± 8	3 ± 2	-	2.25 ± 0.5
		2 @ 20°C	11 ± 8	3 ± 2	-	2.25 ± 0.25
		1 @ 37°C	12 ± 11	3 ± 2	2.00 ± 0.25	2.00 ± 0.75

rate of BPO dissociation thereby increasing the number of propagating chains and decrease set time. Studies are currently underway to increase the aqueous phase temperature upon addition to the organic phase and pre-treatment temperature to further

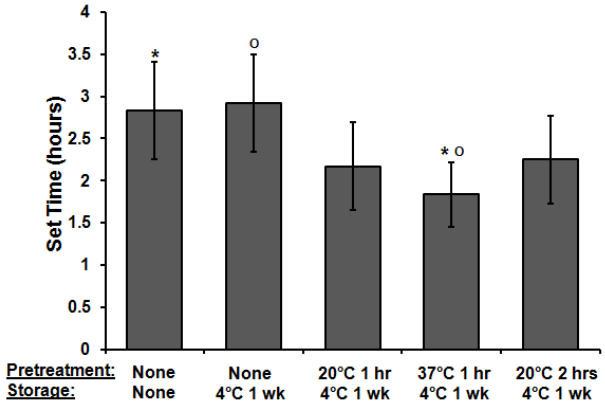

Figure 2.14. The effect of pre-treatment on polyHIPE set time. The specific pre-treatment and storage conditions are listed in the first and second rows of the axis title, respectively. *° indicates statistically significant differences between respective samples $p < 0.10$

decrease cure time *in vivo*. An additional benefit with increased pre-treatment temperatures is the ability to decrease initiator concentration without the concern of an increased set time. Decreased initiator concentrations may be advantageous to avoid negative cytotoxic effects of the radical initiator.

2.3.9 Storage Studies: Effect on HIPE Stability

Storage studies were employed to investigate the use of PFDMA polyHIPEs as off-the-shelf bone grafts. The envisioned deployment method includes: HIPE fabrication and transfer to a sterile syringe, pre-treatment to produce desired properties post injection, storage at reduced temperatures, and injection after thawing in the surgical suite. To this end, it was essential to determine the effect of storage conditions on emulsion stability and resulting pore architecture. Storing PFDMA polyHIPEs at 4°C for

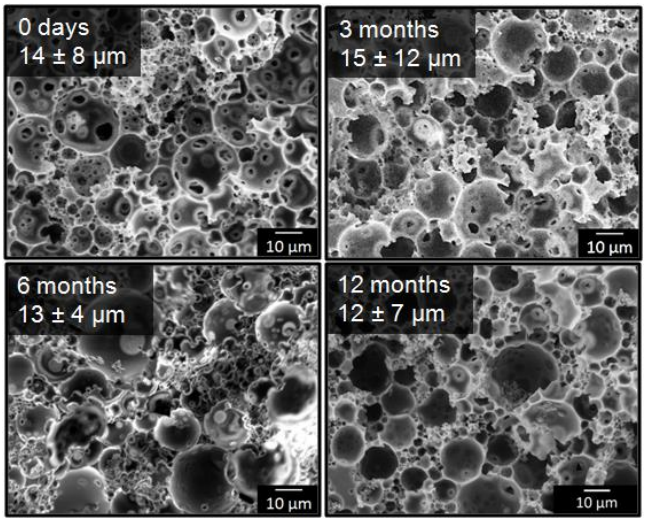

Figure 2.15. Representative SEMs of PFDMA polyHIPEs after storing unpolymerized HIPEs at 4 °C for up to 6 months

one year had a negligible effect on the pore and interconnect size as seen in **Figure 2.15** indicating the potential of PFDMA polyHIPEs as off-the-shelf bone grafts. Additionally, all pre-treatment conditions resulted in no statistically significant change in pore and interconnect sizes again noting the ability to pre-treat, store, and inject these scaffolds without affecting the determined pore architecture. It is probable that the current pore sizes of injectable PFDMA polyHIPEs are too small for full bone healing *in vivo*. Previous work with ceramic and polymer scaffolds indicated a range of pore sizes from 75 – 400 μm was necessary for osteogenesis and increased bone formation.[160-162] Previous polyHIPE studies by other investigators have shown a significant increase in pore size by heating the aqueous phase to temperatures ranging from 40°C to 80°C prior to addition to the organic phase.[47, 95] We have recently replicated these results by increasing both aqueous phase and pre-treatment temperature and are pursuing ways to homogenize the pore size. Future work will focus on fabricating lower viscosity polyHIPEs with EGDMA and butanediol dimethacrylate macromers added to the organic phase and have preliminary data illustrated increased pore sizes.

2.4 Conclusions

The application of emulsion templating in the development of tissue engineering scaffolds is a relatively new area of orthopedic research. In this work, polyHIPEs were fabricated without toxic solvents or monomers at cure temperatures appropriate for in situ deployment. These new polyHIPEs have potential application as an injectable, tissue engineered bone graft. Injectable grafts that are also biodegradable and porous offer unique advantages over current alternatives in terms of deployment and tissue

integration. The focus of this work was to develop *injectable* polyHIPEs with tunable pore size and interconnectivity. The potential for these scaffolds to be utilized as tissue engineered bone grafts was then evaluated by examining injection parameters, compressive properties, and stability during storage. By modulating compositional parameters (e.g. surfactant concentration, polyethylene glycol molecular weight, aqueous vs. organic-phase initiation) and processing parameters (e.g. mixing speed, conditions prior to cure, and storage environment) polyHIPEs with a range of pore architectures, compressive properties, and set times were produced. In PFDMA polyHIPEs, the pore size was increased by decreasing surfactant concentration and the mixing speed during fabrication. Adding higher molecular weight PEG to increase Ostwald ripening and resulting pore size was demonstrated in EGDMA polyHIPEs indicating the potential to use this tool in lower viscosity HIPEs. Interconnectivity was introduced to these biodegradable, injectable porous scaffolds by altering the phase in which radical initiation occurs. Organic-phase initiation resulted in macromer densification forces that facilitated pore opening. In addition to facilitating bone ingrowth, this interconnected porosity will also enable the PFDMA polyHIPEs to be pursued as rigid cell carriers through the encapsulation of human mesenchymal stem cells (hMSCs). Pre-treatment of the materials prior to injection allowed for tuning of both work and set times. Finally, storage of the polyHIPEs for one year at 4°C had a negligible effect on pore architecture providing an initial indication of the ability of these materials to be utilized as off-the-shelf grafts. With the understanding of how these phenomena affect emulsion stability and resulting pore architecture, polyHIPE

monoliths can be rationally designed to have a wide range of properties and flexible deployment options. Overall, this work highlights the potential of interconnected PFDMA polyHIPEs as injectable scaffolds for bone tissue engineering.

CHAPTER III

MODULATING INJECTABLE POLYHIPE DEGRADATION RATE

3.1 Introduction

Traditionally, polyHIPEs have been fabricated utilizing styrene and divinylbenzene monomers to create highly crosslinked networks within the polymerized organic phase.[93, 106, 151] While these scaffolds have excellent interconnected pore architectures, these monomers are not susceptible to hydrolysis, designating them non-biodegradable. Biodegradability was introduced into polyHIPEs by the substitution of unsaturated polyesters into systems that still contained non-biodegradable cross-linkers or diluents.[92, 98, 99] Subsequently, fully biodegradable systems were achieved by eliminating styrene and utilizing polyurethane and fumarate chemistries.[103, 141] The introduction of hydrolytically-labile ester and urethane groups in the network allows for degradation; however, these degradation profiles are potentially too slow to match that of tissue healing. Therefore, introducing β-thioesters into the organic phase of HIPEs provides the ability to modulate the hydrolytic degradation rate to better match physiological healing rates.

Recently, work in the Hubbell lab illustrated the highly tunable nature of hydrolysis dependent on the proximity of a sulfide group to a hydrolytically labile ester. In this work, they illustrated the ability to tune the degradation rate of PEG-based hydrogels from days to weeks solely by increasing the distance from the sulfide to the ester by a single methylene unit.[163] This phenomenon was attributed to the change in atomic charge on the carbonyl group. As the number of methylenes between the sulfide

and the ester decreases, the atomic charge on the carbon atom becomes more positive due to the electronegativity of the thiol resulting in increases susceptibility to hydrolytic attack. Also, the increase in hydrophilicity with the removal of one methylene may also increase hydrolytic degradation rate. This ability to finely tune the hydrolytic degradation rate of a synthetic polymer network could be advantageous in injectable polyHIPEs for bone tissue engineering.

Many researchers have probed Michael addition-type reactions to create ideal, step-growth crosslinked networks that further modulate hydrolytic degradation rate.[163, 164] Specifically, thiol-ene chemistry, defined as the radical, step-growth polymerization involving multifunctional thiols and multivinyl monomers, has been pursued as a means to achieve homogeneous, predictable crosslinked networks that have a quick gelation rate.[165-168] In contrast to the traditional free-radical polymerization of unsaturated vinyls, thiol-ene polymerization proceeds in a unique step-growth addition mechanism that is facilitated by a free-radical chain transfer process.[112, 168] Specifically, the reaction of acrylates and methacrylates with thiols has been investigated as a mixed-mode polymerization encompassing both the traditional radical polymerization of these reactive groups and step-growth of the thiol radical with the unsaturated vinyl.[169] This specific mixed-mode polymerization allows for the ability to spatiotemporally control the crosslinking reactions while maintaining the predictable step-growth polymerization mechanisms and tunable degradation rate.[169] Additionally, the thiol-vinyl reaction is less susceptible to oxygen inhibition resulting in efficient polymerizations in physiological environments.[169, 170] Translation of this chemistry into biocompatible polymeric network

systems has been a focus of Anseth's and Bowman's research. Specifically, they have investigated the relative reactivities of multifunctional thiols with acrylates and the effects on 3D network formation noting the contributions of both the radical polymerization of the acrylates and the step-growth reaction of the vinyl with the thiol.[165, 169, 171-176] Rydholm *et al.* probed the effect of the concentration of a tetrafunctional thiol on network formation, degradation rate, and mechanical properties, illustrating an increase in degradation rate due to a decreased network chain length from increased chain transfer with thiol.[169] Furthermore, they illustrated the ability to use this mixed-mode polymerization to achieve fast gelation times without the need for any added initiator indicating the potential for enhanced bioactivity and viability of encapsulated proteins/biomolecules and cells, respectively.[177] This work revolutionized the biomaterials field by illustrating the facile nature of creating thiol-acrylate networks without the use of solvent and harsh crosslinking conditions.

In the past four years, multiple groups have fabricated thiol-ene polyHIPEs and investigated the effect of acrylate and thiol molecular weights and the number of functional groups (i.e. tri vs. tetrafunctionalized) on crosslinking efficiency, elastic modulus, and degradation rate.[111-113, 178] Furthermore, these thiol-ene polyHIPEs have been illustrated as suitable tissue engineering scaffolds that promote human keratinocyte growth and proliferation.[113] The majority of these past thiol polyHIPE systems were initiated via photoinitiation and require an external energy source, commonly ultraviolet light. Although photoinitiation is a quick and extremely efficient process to generate crosslinked networks, thermal initiation at physiological temperatures increases the

translation of HIPEs as off-the-shelf bone grafts. Cook and colleagues have pursued the thiol-ene polymerization of a tetrafunctional thiol and divinyl ether via thermal initiation investigating the effects of initiator type on gelation time and cure kinetics illustrating the ability to generate thiol-ene polymerization via thermal initiation.[179] Furthermore, Sergent *et al.* have fabricated thiol-ene polyHIPEs crosslinked with a thermal initiator.[112] Although this additional work illustrates the ability to thermal cure thiol-ene materials, the cure temperatures exceed 37°C, eliminating the utility in an injectable system. Additionally, the utilization of a toxic diluent in these other systems limits their use as an injectable graft option. Currently, thermal polymerization to produce thiol-ene chemistries has not been pursued as a means to decrease hydrolytic degradation rate in an injectable polyHIPE system.

To this end, we further developed our injectable polyHIPE system to exhibit a tunable hydrolytic degradation rate based on the concentration of a tetrafunctional thiol, pentaerythritol tetrakis(3-mercaptoproprionate (tetrathiol). Mass loss under accelerated conditions was determined as a means to measure the hydrolytic degradation rate. Cytocompatibility of the degradation products was assessed after accelerated degradation in water at 80ºC via an adapted extraction dilution viability assay based on ISO 10993-5. The effect of a range of tetrathiol concentrations on crosslinking efficiency was investigated to probe the contributions of the thiol as a chain transfer agent on network properties. Specifically, we monitored rheological properties and determined the work and set time in response to thiol incorporation as well as the resulting compressive properties. With this work, we have illustrated the utility of β-thioesters as a

moiety to increase the degradation rate in polyHIPEs and decrease the need for large amounts of initiator potentially increasing the viability of encapsulated cells. This work further exhibits the exciting potential of PFDMA polyHIPEs as quick-curing injectable bone grafts.

3.2 Materials and Methods

3.2.1 Materials

Polyglycerol polyricinoleate (PGPR 4125) was donated by Palsgaard. All other chemicals were purchased and used as received from Sigma–Aldrich, unless otherwise noted. Human mesenchymal stem cells were provided by the Texas A&M Health Science Center College of Medicine Institute for Regenerative Medicine at Scott & White.

3.2.2 PFDMA Synthesis and Purification

Propylene fumarate dimethacrylate (PFDMA) was synthesized in a two-step process adapted from Timmer et al.[149] Briefly, propylene oxide was added dropwise to a solution of fumaric acid and pyridine in 2-butanone (2.3:1.0:0.033 mol) and refluxed at 80°C for 16-18 hours. Residual propylene oxide and 2-butanone were removed by distillation, residual acidic byproducts and water were removed with washing, and the product was dried under vacuum. The diester bis(1,2 hydroxypropyl) fumarate product was then end-capped with methacrylate groups in an addition process with triethylamine (TEA) and methacryloyl chloride (MAC). The molar ratios of the diester, MAC, TEA were 1:2.1:2.1, respectively. Hydroquinone was added at a molar ratio of 0.008:1 to diester to inhibit crosslinking during the synthesis. The reaction was maintained below

-10˚C to reduce undesirable side reactions and stirred vigorously overnight under a nitrogen blanket. The product was washed overnight in 2 M potassium carbonate to neutralize methacryloyl chloride after which the PFDMA was passed through a chromatography column loaded with alumina at a 9:1 molar ratio alumina:TEA to remove any residual TEA and methacrylic acid. The product was then washed in deionized water to remove any alumina and subjected to a brine wash and stirred over anhydrous sodium sulfate to remove water. The PFDMA product was dried under vacuum and the structure confirmed using H NMR (300 MHz, $CdCl_3$) δ 1.33 (dd, 3H, CH3), 1.92 (s, 3H, CH3), 4.20 (m, 2H, -CH2-), 5.30 (m, 1H, -CH-), 5.58 (s, 1H, -C=CH2), 6.10 (s, 1H, -C=CH2), 6.84 (m, 2H, -CH=CH-). The integration ratio of methacrylate protons to fumarate protons in the ^{1}H NMR spectra was used to confirm > 90% functionalization for all macromers prior to polyHIPE fabrication.

3.2.3 PolyHIPE Fabrication

HIPEs were prepared using a FlackTek Speedmixer DAC 150 FVZ-K according to a protocol adapted from Moglia et al.[180] Redox initiation was utilized to create a quick curing HIPE that resembles the work and set time of current PMMA bone cement. Molecular structures of PFDMA and pentaerythritol tetrakis(3-mercaptoproprionate) (tetrathiol) are shown in **Figure 3.1**. Two equal amounts of PFDMA were first mixed with 1 wt% of organic phase soluble initiators BPO or TMA in a speedmixer cup. Next 10 wt% surfactant, polyglycerol polyricenoleate (PGPR 4125), was added before emulsification. Tetrathiol was added at either 5 or 10 molar percent to the organic phase. Tetrathiol amounts were chosen as the maximum amount that could be incorporated

A) Propylene Fumarate Dimethacrylate *(PFDMA)*

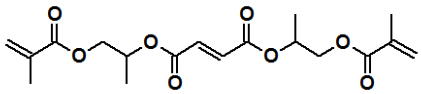

B) Pentaerythritol tetrakis(3-mercaptoproprionate) *(tetrathiol)*

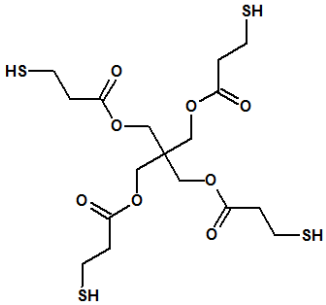

Figure 3.1. Molecular structure of A) propylene fumarate dimethacrylate (PFDMA) and B) pentaerythritol tetrakis(3-mercaptoproprionate) (tetrathiol)

without drastically reducing the resulting polyHIPE compressive properties. Once thoroughly mixed, the aqueous solution of calcium chloride (1 wt%) and deionized water was then added to the organic phase (75% v) in six additions and mixed at 500 rpm for 2.5 min each to promote emulsion formation. The two HIPEs (BPO and TMA) were mixed at 2500 rpm for 30 seconds in the Speedmixer to initiate crosslinking. HIPEs were transferred to either 2 mL microcentrifuge tubes or 15 mL centrifuge tubes and placed in a 37°C aluminum bead bath to facilitate crosslinking overnight.

3.2.4 Determining Pore Architecture

Scanning electron microscopy (SEM, Phenom Pro, Nanoscience Instruments) was utilized to qualitatively determine polyHIPE pore architecture. PolyHIPE sections were subjected to vacuum drying for 48 hours to remove water prior to imaging. Circular

specimens from three separate polyHIPE specimens were sectioned into quarters, fractured at the center, coated with gold, and imaged.

3.2.5 Work and Set Time

Work and set times of the polyHIPEs were characterized using an Anton Paar MCR 301 rheometer following a procedure adapted from Foudazi et al.[181] HIPEs were injected onto the plate heated to 37ºC through a mixing head to facilitate redox initiation. Storage and loss moduli were measured every 15 seconds using a parallel-plate configuration with a 1 mm gap and 0.5% strain. Work time is presented as the onset of increasing storage modulus and set time is presented as the tan δ minimum, which corresponds to storage modulus yielding. The data represents samples (n=3) from three different HIPEs for each composition.

3.2.6 Compressive Testing

The effect of thiol concentration on polyHIPE compressive modulus and strength was investigated following ASTM D1621-04a. PolyHIPEs cured in 15 mL centrifuge tubes were sectioned into disks with a 3:1 diameter to height ratio using an Isomet saw (Buehler) and compressed using an Instron 3300 at a strain rate of 50 mm/s. The compressive modulus was calculated from the slope of the linear region and the compressive strength was identified, after correcting to zero strain, as the stress at the yield point or 10% strain, whichever point occurred first. Reported moduli and strength data were averages of the disks for each polyHIPE composition (n=9).

3.2.7 Accelerated Degradation In Vitro

PolyHIPEs cured in a 15 mL centrifuge tube were sectioned using an Isomet saw (Buehler) into 1 mm thick sections. Specimens were vacuum dried for 48 hours after which dry weights were recorded. Accelerated degradation was carried out at a ratio of 1 g specimen to 20 mL in 0.25 and 0.5 M NaOH for four weeks. Samples were secured with Teflon weights in the solution and placed on a shaker table at 37°C. The solutions were changed every 2-3 days with time points every week for four weeks. At each time point, n=3 specimens were washed twice with RO water, incubated for 1 hr with 1 mL RO water to remove any salts, and dried for 48 hours before weighing.

3.2.8 Gel Fraction

PolyHIPEs cured in a 15 mL centrifuge tube were sectioned 1 mm thick using an Isomet saw (Buehler) vacuum dried for 48 hours. Weighed specimens were suspended in dichloromethane (DCM) at a ratio of 1 mL DCM to 10 mg of sample to facilitate dissolution of uncrosslinked macromer. Sections in DCM were placed on a shaker table at room temperature for 48 hours. After incubation period, DCM was removed and specimens were vacuum dried for 48 hours. The gel fraction was determined as the fraction of mass loss over original dry mass (n=6). PGPR was accounted for in all calculations so that the gel fraction reflected all macromer that was crosslinked into the network.

3.2.9 Statistical Analysis

The data are displayed as mean ± standard deviation for each composition. A Student's t-test was performed to determine any statistically significant differences

between compositions. All tests were carried out at a 95% confidence interval ($P<0.05$).

3.3 Results and Discussion

The focus of this work was to fabricate quick-curing, injectable polyHIPE bone grafts with degradation rates that can be tuned to match new tissue growth. The reaction of a thiol with the vinyl of an acrylate or methacrylate has been shown to enhance the hydrolytic degradation rate due to an increase in atomic charge of the ester carbonyl from the electron pull of the sulfide. Thiol polyHIPEs fabricated in the past utilized toxic solvents and were cured with UV radiation. Here we expand on our injectable PFDMA polyHIPE system to fabricate highly interconnected monoliths with tunable degradation. Given that successful HIPE fabrication is dependent on characteristics such as monomer/macromer hydrophobicity and viscosity, it was important to first assess HIPE formation and emulsion stability. The tetrathiol has a logP of 1.0 and a viscosity of 0.41 Pa·s compared to PFDMA with a logP of 3.4 and 0.13 Pa·s viscosity. Despite these differences in molecular hydrophobicity, all compositions formed stable HIPEs and cured to rigid, interconnected monoliths, as illustrated in **Figure 3.2**. Likely, the low concentration of tetrathiol in the organic phase and rapid cure of the PFDMA HIPE limited any effects on polyHIPE architecture. This understanding is beneficial for future work in fabricating HIPEs with tunable degradation rates for range of physiological degradation rates.

It is well established that thiols behave as chain transfer agents during the polymerization of vinyls.[171, 172, 182-184] Thiols are often utilized as chain transfer agents in acrylic polymerizations to control the molecular weight and polydispersity of the

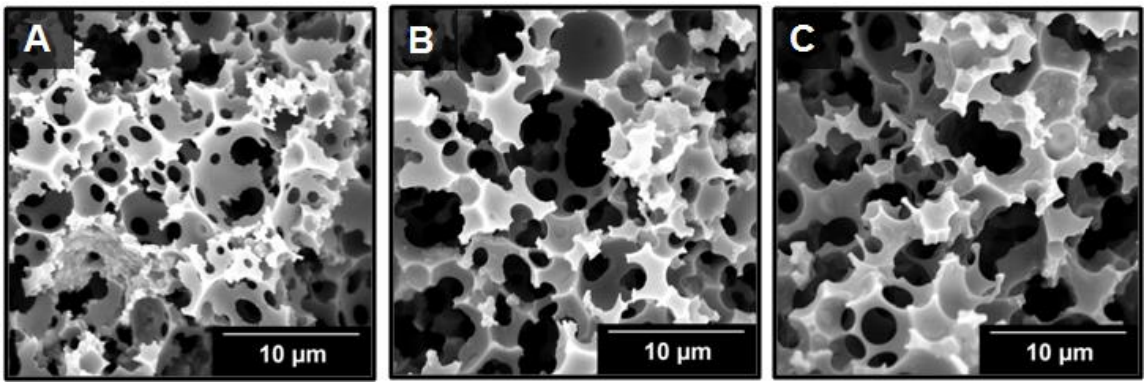

Figure 3.2. Scanning electron micrographs of PFDMA/tetrathiol polyHIPEs A) PFDMA control B) 5 mol% tetrathiol C) 10 mol% tetrathiol

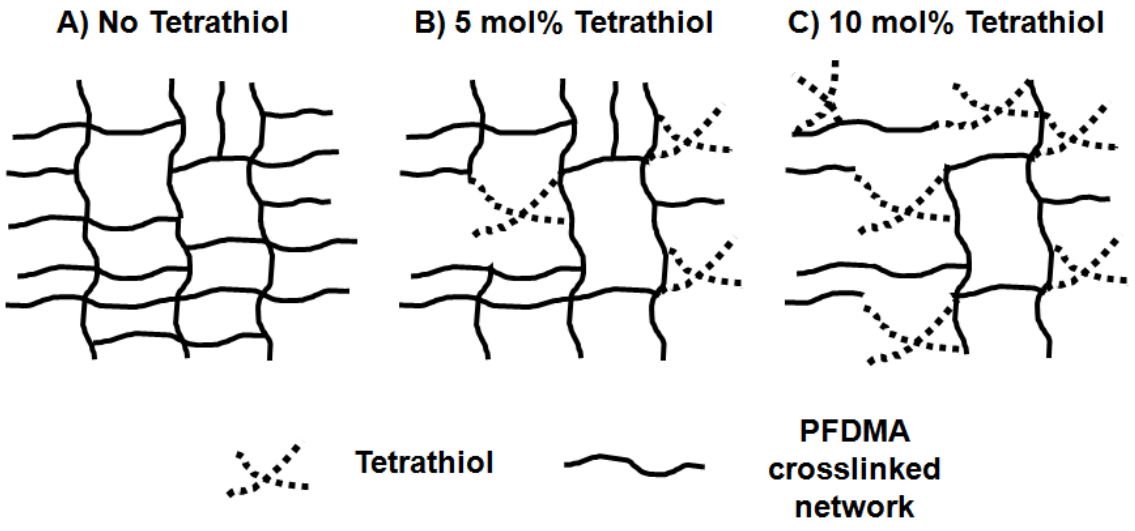

Figure 3.3. Effect of tetrathiol acting as a chain transfer agent on PFDMA network formation A) No tetrathiol B) 5 mol% tetrathiol C) 10 mol% tetrathiol

products.[182, 183] During the propagation step of the PFDMA polymerization, two reactions can occur at the methacrylic radical: addition of another PFDMA chain or hydrogen abstraction/chain transfer of the radical to the thiol.[171] A schematic of network formation with increasing molar ratio of tetrathiol is shown in **Figure 3.3**.The effect of this reaction on resulting polyHIPE properties was then characterized.

3.3.1 Effect of Tetrathiol on Work and Set Time

Work time, as defined in Chapter II, is essentially the time at which a physician can manipulate and inject the graft without altering any material properties. The set time is the point at which the material has reached its gelation point and the network is set. These two properties were determined utilizing rheology as a method to generate reproducible, quantitative data. PFDMA polyHIPE work and set time decreased with the addition of tetrathiol as seen in **Figure 3.4**. The ~1.5 minute work time of PFDMA was reduced to 15 seconds with the addition of either 5 or 10 mol% tetrathiol. Similar trends were observed with the set time of these polyHIPEs. No significant difference in work and set times was observed between thiol concentrations utilizing this method. The addition of the thiol radical coupled with the traditional chain growth propagation of radical polymerization is hypothesized to result in increased reaction rates and decreased work and set times. Furthermore, the thiol-methacrylate reaction is not inhibited by oxygen, resulting in the maintenance of quick cure times in aerobic environments.[170] Quick-curing HIPE formulations can be advantageous as well to reduce the time in which phase separation can occur before the emulsion geometry is set, thereby ensuring

more homogenous pore architectures.[113] According to ISO 5833, acrylic based cements should have a set time of 10-15 minutes. Although the presented set times are approximately 10X faster than these standard values, the cure times can be readily increased by decreasing redox initiator concentration, initiator ratios, and chemistries as has been shown previously in PFDMA polyHIPEs.[180] Currently ferrocene is being scouted as a reducing agent to potentially increase cytocompatibility and reduce the amount of initiator required to maintain quick cure times.

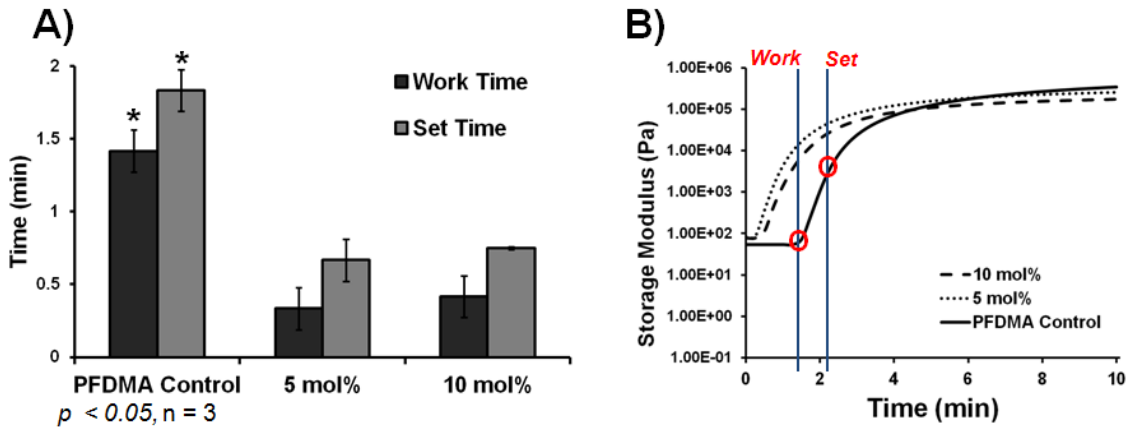

Figure 3.4. Effect of tetrathiol concentration on rheological properties A) Work and set time decrease with the addition of tetrathiol B) Representative plot of storage modulus illustrates the increase of work time (onset of storage modulus) and set time (yielding of storage modulus) with tetrathiol

3.3.2 Effect of Tetrathiol Concentration on PolyHIPE Compressive Properties

PFDMA/tetrathiol polyHIPE compressive modulus and strength were assessed to ensure the incorporation of thiol did not drastically reduce mechanical integrity. A

decrease in compressive modulus and strength was observed with an increase in tetrathiol concentration as seen in **Figure 3.5**. PFDMA polyHIPEs fabricated with greater than 10 mol% tetrathiol were much weaker and had properties similar to soft tissue and were not further characterized. PFDMA polyHIPEs with 10 mol% tetrathiol resulted in an average compressive modulus of 15 MPa and strength of 0.7 MPa. While this is lower than the average values for human trabecular bone, *in vivo* studies in animal models illustrated bone healing with materials exhibiting compressive properties on the low end of trabecular bone.[53, 156] The hypothesized mechanism for this trend is the result of the thiol as a chain transfer agent. When the thiol abstracts the radical this reduces chain propagation and length thereby decreasing crosslink density and results in a decrease in compressive properties. A similar decrease in compressive modulus with increasing amount of trithiol was observed by Rydholm *et al.* in poly(ethylene glycol)-based hydrogels.[169] Recent work is focused on incorporating additional methacrylate-functionalized monomers into the HIPE organic phase to further modulate viscosity for cell encapsulation. PolyHIPEs fabricated from these monomers alone have increased crosslink density and therefore increased compressive properties. As a result, it is probable that modulating the molar ratio of PFDMA:methacyrylated-monomer will result in an increase in compressive properties relative to standard PFDMA polyHIPEs.

3.3.3 Effect of Tetrathiol on Gel Fraction

Gel fraction was used to assess crosslinking efficiency to further determine the effect of the tetrathiol on network formation. Overall gel fraction increased with the increase in tetrathiol concentration as displayed in **Figure 3.6.** The data displayed is after

accounting for the loss of PGPR during swelling in DCM which does not attribute to the crosslinked network. The gel fraction values were as follows: PFDMA control polyHIPEs exhibited 85%, 5 mol% tetrathiol showed 87%, and 10 mol% tetrathiol

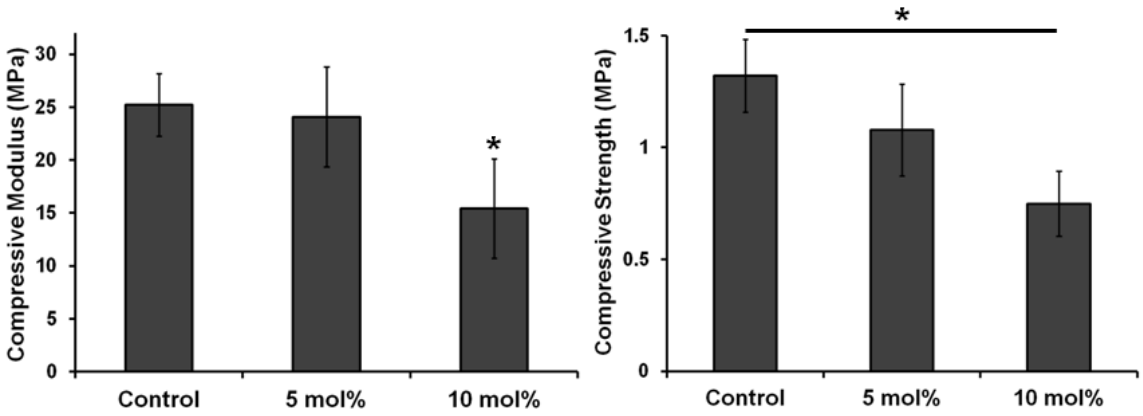

Figure 3.5. Effect of tetrathiol concentration on PFDMA polyHIPE compressive modulus and strength

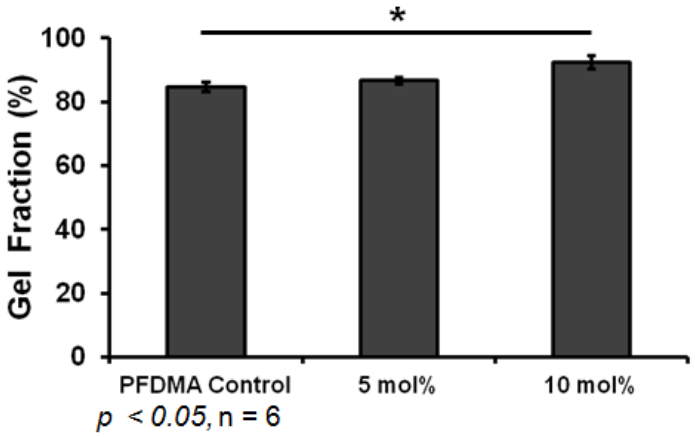

Figure 3.6. Effect of tetrathiol concentration on crosslinking efficiency of PFDMA polyHIPEs

resulted in 92%. As was seen with the effect of work and set times, the addition of the thiol radical increased number of reactive sites within the network and most likely attributed to the increase in gel fraction. In the PFDMA control polyHIPEs, it is hypothesized that reduced radical diffusion and steric hindrances due to PFDMA and tetrathiol organic phase viscosity resulted in reduced crosslinking efficiency and remaining unreacted macromer. The increase in crosslinking efficiency with the addition of the tetrathiol can be attributed to the reaction kinetics that are uninhibited by oxygen, and the thiol acting as a chain transfer agent. These mechanisms decrease the propagation of long chains thereby reducing any problems the effect of steric hindrance has on hindering reactive radical ends from finding unreacted methacrylates. Similar studies with lower molecular weight monomers illustrated gel fractions near 100%.[180] Therefore, reducing PFDMA/tetrathiol organic phase viscosity with these methacrylated-monomers is hypothesized to further increase gel fraction of resulting monoliths.

3.3.4 Degradation Rate

The overall goal of fabricating thiol-methacrylate polyHIPEs was to generate scaffolds with a tunable degradation profile for future matching with *in vivo* neotissue formation. The use of β-thioesters to decrease the electronegativity of the carbonyl of the ester and thereby increase the hydrolytic degradation rate has been explored.[163] Schoenmaker *et al.* demonstrated an increase in atomic charge on the carbon atom of the carbonyl of an ester the closer the sulfur atom was positioned to the ester. The electron pull from the sulfur increases the positive charge on the carbonyl rendering it more

susceptible to hydrolytic attack. Accelerated degradation scouting studies were conducted at a range of sodium hydroxide concentrations to determine what conditions would be effective in illustrating the effect of tetrathiol on PFDMA polyHIPE degradation. The 0.25 and 0.5 M NaOH solutions were utilized to differentiate the effect of increasing tetrathiol incorporation on hydrolytic degradation. Values reported reflect mass loss after accounting for the theoretical mass of the surfactant, PGPR. To this end, an increase in mass loss was observed with an increase in tetrathiol concentration when assessed in basic, accelerated conditions as seen in **Figure 3.7**. All PFDMA/tetrathiol polyHIPEs exhibited complete loss of integrity by 3 weeks whereas the PFDMA control

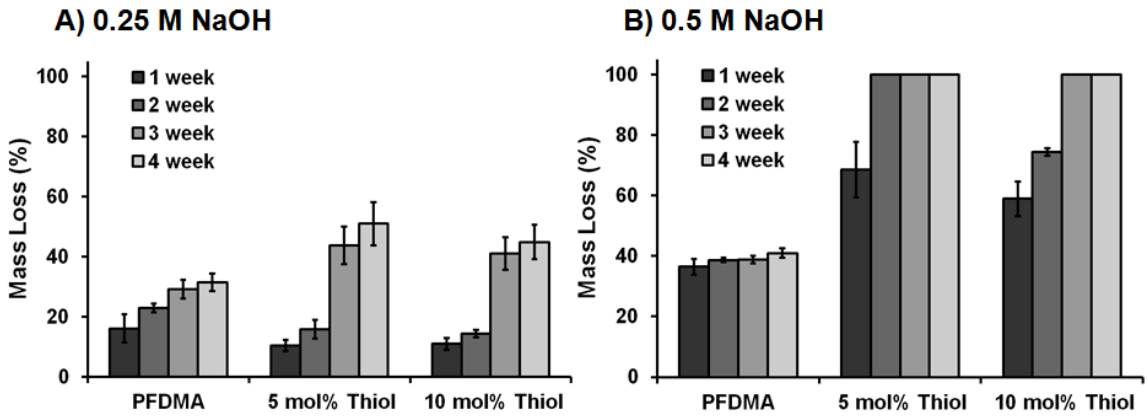

Figure 3.7. PFDMA/tetrathiol polyHIPE degradation in accelerated conditions at 37°C A) 0.25 M NaOH and B) 0.5 M NaOH

loss of integrity by 3 weeks whereas the PFDMA control polyHIPE maintained ~35% mass loss after the initial mass loss at 1 week. Initial PFDMA mass loss at one week can be attributed to the removal of unreacted macromer which can be further supported with the lower gel fraction of PFDMA control polyHIPEs. PFDMA polyHIPEs exhibit a gel fraction of 85% and FTIR analysis of DCM solutions post swelling illustrates residual methacrylated-macromer. Another explanation is the formation of microgels, which are intramolecularly crosslinked macromolecules with low molecular weights, which would degrade at a much faster rate than the fully crosslinked network.[185] The two week specimens for the 10 mol% thiol polyHIPEs in the 0.5 M NaOH condition did not behave similarly to the three and four week specimens under the same conditions. These specimens used for later time points had lost integrity by two weeks. Therefore, two week data for the 10 mol% thiol polyHIPEs is most likely an outlier. Overall, this work illustrates the ability to alter the organic phase chemistry to increase hydrolytic degradation rate without drastically affecting pore architecture or compressive properties.

Previously, polyHIPEs fabricated using multi-arm acrylates and trithiols exhibited ~15-35% mass loss in 0.1 M NaOH, 37°C accelerated conditions comparable to the results observed in the 0.1 M NaOH initial scoutings.[113] Although an increase in degradation rate was observed *in vitro,* the *in vivo* degradation rate of these specific polyHIPE formulations is unknown and would need to be explored in an animal model. However, multiple studies illustrate evidence of *in vivo* degradation of poly(propylene fumarate) injectable cements with a similar chemical structure as PFDMA in rat models

at 5-6 weeks thus indicating promise for the tunable *in vivo* degradation of PFDMA/tetrathiol polyHIPEs from months to a year.[186, 187]

3.4 Conclusions

Tissue engineered scaffolds are designed to degrade at a rate comparable to neotissue growth to provide space for cells to proliferate and lay down new extracellular matrix and reduce any long-term complications from material remaining in the body. In this work, PFDMA polyHIPEs were fabricated with a tetrathiol to increase hydrolytic susceptibility of the ester and finely tune the hydrolytic degradation rate for future use in bone grafting applications. Resulting network formation efficiency, cure properties, compressive modulus and strength, and *in vitro* degradation rate were assessed. The role of the thiol as a chain transfer agent in the radical polymerization of PFDMA resulted in decreased work and set times, increased crosslinking efficiencies, and decreased compressive properties. Accelerated degradation studies demonstrated a complete loss of integrity of PFDMA/tetrathiol polyHIPEs at 3 weeks with the PFDMA control stabilizing at 40% mass loss over 4 weeks. The rate of healing in bone differs widely due to physiology of the defect, health of the patient, and severity of injury. Therefore, understanding how to modulate polyHIPE chemistries and pore architecture to dictate *in vivo* healing rate is advantageous in addressing large bone defects. Current studies are underway to investigate the effect of reducing organic-phase viscosity with small monomers and the resulting effect on network formation, compressive properties, and degradation rate. The results from this work provide additional tools for use in modulating polyHIPE rheological and compressive properties while increasing the rate

of degradation for improved design of injectable bone grafts to address healing rates in a range of defect physiologies and with patients of various ages and health conditions.

CHAPTER IV

EVALUATION OF HUMAN MESENCHYMAL STEM CELL BEHAVIOR AND BONE INTEGRATION*

4.1 Introduction

Tissue engineers focus on harnessing the body's innate ability to regenerate and heal. One key facet of the tissue engineering paradigm is the fabrication of a 3D scaffold that not only provides the mechanical support and degradation profile to match neotissue formation but also provides a cell niche to stimulate adhesion, proliferation, and extracellular matrix production. The template polymerization of high internal phase emulsions produces highly porous and interconnected monoliths with tunable properties, as discussed in Chapters II and III, for use in injectable bone grafting applications. However, further tuning and design must be done to ensure these injectable polyHIPEs are cytocompatible and promote desired cellular processes.

Injectable systems that have the viscosity to mix with a cell suspension and integrate with native tissue to provide site-targeted cell delivery have gained interest in the biomaterials field. Specifically, aqueous-phase soluble materials such as hydrogels are advantageous due to the ease of incorporating cells and bioactive agents without killing or denaturing any components. Although hydrogels can be functionalized with cell-responsive peptides or fabricated with natural polymers to achieve superior

---

* Reprinted with permission from "Achieving Interconnected Pore Architecture in Injectable PolyHIPEs for Bone Tissue Engineering," by Jennifer L. Robinson, Robert S. Moglia, Melissa C. Stuebben, et al, Tissue Engineering Part A 2014, 20 (5-6), 1103-1112. Copyright (2014) Mary Ann Liebert, Inc.

bioactivity, the compressive properties are limited to soft tissue applications. Therefore, a rigid polyHIPE graft that promotes hMSC viability and proliferation while providing appropriate mechanical properties is desired.

The use of polyHIPE monoliths to support cell viability and proliferation has been pursued by multiple groups. Akay and colleagues initially illustrated the potential of styrene-divinylbenzene based emulsion-templated monoliths to support osteoblast growth and proliferation.[47] Post-fabrication processing techniques including coating procedures and covalent functionalization have been used to attach bioactive components onto these porous polyHIPE scaffolds. Traditional styrene-divinylbenzene polyHIPEs have been coated with laminin and poly-D-lysine, functionalized with galactose, and grafted with a range of proteins for enhanced bioactivity.[94, 115, 130, 188] Furthermore, efforts have focused on fabricating polyHIPEs with natural polymers to confer bioactivity for enhanced cellular interactions. Barbetta *et al.* translated HIPE fabrication technology to oil-in-water emulsions with dextran, pullulan, and gelatin with excellent interconnected pore morphology and support of mouse retinal neural cells.[114] Bokhari and colleagues illustrated the ability of styrene-divinylbenzene-hydroxyapatite polyHIPEs fabricated with a hydrogel containing a self-assembling peptide to enhance osteoblast ingrowth and support osteogenesis.[104] The work by Viswanathan *et al.* utilized the intrinsic phase separation properties of amphiphilic block copolymers within a styrene-divinylbenzene polyHIPE system to modulate surface hydrophobicity and thereby control protein adsorption on the surface, further tuning cellular adhesion and interactions.[189] PolyHIPE technology has been further commercialized as a system for

3D cell culture sold as Alvetex®, illustrating the ability of these scaffolds to support cell viability and proliferation in a 3D environment.[105] Although this work resulted in scaffolds which enhanced 3D cell proliferation and performance, all of these polyHIPEs were fabricated with solvent and cured at temperatures greater than physiological temperature, limiting the ability to encapsulate and maintain viable stem cells prior to curing for injection into the defect site.

Cytocompatibility of all polyHIPE components in an injectable system is crucial as post-fabrication techniques to remove cytotoxic components are impossible. For materials that are prefabricated and cured *ex vivo*, the scaffold is typically washed and any cytotoxic components are extracted prior to implantation; however, for materials that cure *in vivo*, additional testing and characterization must be conducted to ensure all components, any heat generated, and/or products created during the hardening process are cytocompatible. Additionally, the increased production of radicals during the initiation and propagation steps of the polymerization reaction must be considered in regard to cell viability. Bryant *et al*. investigated the cytocompatibility of commonly used photoinitiators and the concentrations at which these small molecules could be used without eliciting a cytotoxic effects.[190] This work illustrated good cell viability at low initiator concentrations (< 0.01 w/w%); however, common thermally cured systems require initiator concentrations ~100X greater when cured at physiological temperatures due to the high decomposition temperature of the initiator. Finally, the cytocompatibility of uncured macromer is an important parameter to assess. This requires ensuring that all reactants, solvents, and side products created during the synthesis of the macromer have

been removed prior to HIPE formation. These numerous additional cytocompatibility concerns in an injectable system highlight the importance of *in vitro* characterization and scaffold development to promote cell adhesion and viability.

This work details the development of a cytocompatible, injectable polyHIPE which retains the pore architecture, cure times, compressive properties, and degradation rates detailed in earlier chapters. Viability of hMSCs in contact with initiators, the surfactant PGPR, and PFDMA, BDMA, and tetrathiol macromers was determined using both direct and indirect cell culturing methods. The effect of culture conditions including overnight serum concentration and hMSC seeding density on resulting cell morphology was evaluated. Subsequently, the ability of the polyHIPEs to inject into irregular defects and integrate with bone was investigated. A porcine femur model was utilized to determine the integration and retention of the injected polyHIPE in a defect site. Furthermore, the ability to maintain hMSC viability post-encapsulation in PFDMA/BDMA HIPE was assessed. The studies presented and discussed encompass the iterative process in ensuring that the injectable polyHIPE graft is cytocompatible throughout injection, cure, and remodeling.

4.2 Materials and Methods

4.2.1 Materials

Polyglycerol polyricinoleate (PGPR 4125) was donated by Palsgaard (Morris Plains, NJ). Human mesenchymal stem cells were provided by the Texas A&M Health Science Center College of Medicine Institute for Regenerative Medicine at Scott & White. KRGDS peptide was purchased from CelTek Biosciences. All other chemicals

were purchased and used as received from Sigma Aldrich (Milwaukee, WI) unless otherwise noted.

4.2.2 BDMA Inhibitor Removal

Butanediol dimethacrylate (BDMA) was passed through a column containing alumina oxide using high air pressure to remove the monomethyl ether hydroquinone inhibitor and collected in a round bottom flask.

4.2.3 PolyHIPE Fabrication

HIPEs were prepared using the FlackTek Speedmixer DAC 150 FVZ-K. Briefly, PFDMA was mixed with 10 wt% surfactant (PGPR) in the Speedmixer cup prior to emulsification. For bone integration studies, 5 wt% BPO was added to the organic phase to initiate radical crosslinking. In later studies evaluating hMSC viability and behavior on quick-curing polyHIPEs, two separate HIPEs were made each with either the oxidizing redox initiator (BPO) or reducing initiator (TMA or Ferrocene) added to the organic phase. Tetrathiol was added to the organic phase at 5 and 10 mol% to investigate the effect of macromer on hMSC cytocompatibility. Once thoroughly mixed, the aqueous solution of calcium chloride (1 wt%) and deionized water was then added to the organic phase (75% v) in six additions and mixed at 500 rpm for 2.5 min each to promote emulsion formation. For redox-initiated polyHIPEs, the two HIPEs (BPO and TMA) were mixed at 2500 rpm for 30 seconds in the Speedmixer to initiate crosslinking. HIPEs were transferred to either 2 ml microcentrifuge tubes or 15 ml centrifuge tubes and placed in a 37°C aluminum bead bath to facilitate crosslinking overnight.

4.2.4 Cytocompatibility of Individual HIPE Components

4.2.4.1 Initiator and Surfactant Cytocompatibility

The cytocompatibility of individual HIPE components was assessed initially to ensure all components were individually cytocompatible. Initiator cytocompatibility was evaluated at concentrations that encapsulated cells would experience following a protocol adapted from Bryant *et al.*[190] Briefly, the initiators benzoyl peroxide (BPO) and 4, N,N – trimethylaniline (TMA) were dissolved in a 6 vol% ethanol solution and added to media for a final concentration of 0.03 wt% ensuring the amount of solvent in the media was 0.6 vol%. Control wells exposed solely to 0.6 vol% of each solvent were tested simultaneously to ensure no effect from the solvents on viability. PGPR cytocompatibility was assessed at concentrations that reflect what could leach out and affect encapsulated cells. PGPR was added to media at 0.1, 1.0, and 5.0 wt% after determining that cells would see 0.2 wt% in a 10 wt% PGPR polyHIPE. Bone marrow-derived human mesenchymal stem cells (hMSCs) were obtained as Passage 1 in a cryovial from the Center for the Preparation and Distribution of Adult Stem Cells. Cells were cultured in growth media containing 16.5% fetal bovine serum (FBS, Atlanta Biologicals), 1% L-glutamine (Life Technologies) and Minimum Essential Media α (MEM α, Life Technologies) to 80% confluency and utilized at Passages 5 and 6. Cells were seeded directly on tissue culture polystyrene in the media containing initiator or surfactant at a density of 2000 cells/cm^2. A Live/Dead® assay was utilized to determine the viability of hMSCs in contact with dissolved initiators at 3, 24, and 72 hours. Rastor

imaging (5 images per specimen) was conducted on four specimens per time point (n=20) utilizing a fluorescent microscope (Nikon Eclipse TE2000-S).

4.2.4.2 Macromer Cytocompatibility

Further investigation of organic phase (initiator and macromer) cytocompatibility was performed prior to seeding cells directly on polyHIPE sections to ensure any macromer or radicals that diffuse out are cytocompatible. The *in vitro* cytocompatibility of PFDMA and PFDMA with redox initiators (0.5 wt% BPO/ 2.5 wt% TMA and 0.5 wt% BPO/ 2.5 wt% Ferrocene) was assessed using a modified ISO 10993-5 extraction dilution test. Cells were trypsinized with 0.25% Trypsin-EDTA (Life Technologies) and seeded at a density of 40,000 cells/cm^2 in a 96 well plate and allowed to adhere for 24 hours. On the following day, 100 µl of each PFDMA/initiator organic phase was incubated in 300 µl growth media supplemented with 1 vol% Penicillin-Streptomycin (Life Technologies) in a 48 well plate to mimic the ratio of organic to aqueous phase in the HIPE. After 10 minute incubation at 37°C, 5 % CO_2, the supernatant above the macromers was aspirated and diluted to 10 and 100X solutions. This time frame was selected based on the cure rates determined previously for these systems and therefore the results are based on the maximum time for extraction of unreacted macromer prior to cure. Extracted and diluted media (1, 10, and 100X) was then added to cells and cultured for an additional 24 hours. Viability was assessed utilizing the Live/Dead® assay kit (Molecular Probes). Analysis was completed using a plate reader (Tecan Infinite M200Pro) with excitation/emission wavelengths of 485/528 and 528/620 for the calcein-AM and ethidium homodimer-1 dyes, respectively. Viability was normalized to cells on

tissue culture polystyrene. Further studies with the PFDMA macromer investigated the effect of washing with DI water at a 1:100 volume ratio and/or vacuum drying for 24 hours to further purify the macromer before any cell work. The same procedure was followed for all extraction dilution viability assays.

4.2.5 Indirect Cytocompatibility of PFDMA PolyHIPEs

To ensure all components were cytocompatible in the HIPE system during cure, a indirect Transwell® (Corning) well plate system with polycarbonate membrane inserts was utilized to access cytocompatibility of any macromer or radicals that could diffuse out while the HIPE was hardening. HIPEs were fabricated as stated above utilizing a range of redox initiator combinations: 0.5 wt% BPO/2.5 wt% TMA, 0.5 wt% BPO/2.5 wt% Ferrocene, or 1 wt% BPO/5 wt% TMA. These compositions were chosen based on the range of set times, namely 3, 4, and 8 minutes. Cells were trypsinized with 0.25% Trypsin-EDTA (Life Technologies) and seeded at a density of 10,000 cells/cm^2 onto the polystyrene well plate. HIPEs were injected into the respective inserts and plates put in incubator. Viability at 3 hours was assessed utilizing the Live/Dead assay kit (Molecular Probes). Cells were washed with PBS, stained with 2 μM Calcein and 2 μM ethidium homodimer-1 for 30 minutes in 37°C. Intensity of stains was completed using a plate reader (Tecan Infinite M200Pro) with excitation/emission wavelengths of 485/528 and 528/620 for the calcein-AM and ethidium homodimer-1 dyes, respectively. Following this assessment, the same Transwell® system was utilized to ensure any leachables from the cured polyHIPE monolith were cytocompatible. PFDMA HIPEs were fabricated with either 5 wt% AIBN or 5 wt% BPO as stated previously, subjected to sterilization and

wetting ladder, and loaded into inserts. hMSC seeding and analysis was performed as stated previously in this section.

4.2.6 Direct Cytocompatibility of PolyHIPEs

4.2.6.1 Effect of Serum Concentration and Seeding Density on Morphology

The effect of *in vitro* hMSC culture techniques on PFDMA polyHIPEs was assessed to establish effective protocols for determining cell response to the monoliths. hMSCs stained with CellTracker™ Orange were utilized in initial studies to visibly assess morphology, adhesion, and spreading. PFDMA polyHIPEs fabricated with 5 wt% AIBN were utilized for two studies looking at the effect of overnight FBS concentration and seeding density on cell behavior. One day prior to seeding, cells were stained with 10μM CellTracker™ Orange (Molecular Probes) for 45 minutes in 37°C, 5% CO_2 and replenished with growth media overnight. Specimens were sectioned and sterilized as stated previously and subjected to a wetting ladder and progressive solvent extraction with PBS. Wafers were incubated overnight with growth media supplemented with FBS to increase the amount of protein adsorption to provide increased integrin binding sites. To investigate the effect of overnight FBS concentration on cell adhesion and morphology, polyHIPE sections were soaked overnight in 10, 40, or 70 wt% FBS in αMEM. CellTracker™ Orange stained cells were seeded at 2,000 cells/scaffold and imaged at 6 hours. After determining 40 wt% resulted in enhanced adhesion and more spread cells, this concentration was utilized for the remaining studies. To determine the effect of seeding density on 72 hour cell adhesion and morphology, stained hMSCs were seeded at 2,000, 10,000, and 250,000 cells/ml (~ 60, 300, and 2000 cells/ml of

polyHIPE). Once it was determined that the higher seeding density resulted in a spread monolayer of cells on the polyHIPEs at 72 hours, cells were seeded at a density of 250,000 cells/ml (~7000 cells/ml of polyHIPE) for all other studies in this section. hMSC behavior was observed using a fluorescent microscope (Nikon Eclipse TE2000-S).

4.2.6.2 Effect of Initiator on Morphology after Direct Seeding

Initial cell work was conducted on PFDMA polyHIPEs initiated with AIBN. However, once the laboratory started fabricated quick-curing redox polyHIPEs with BPO, the majority of the remaining cell work was conducted with BPO/TMA initiated polyHIPEs. Evaluation of OCT-stained hMSC morphology on polyHIPEs crosslinked with either 5 wt% BPO or 5 wt% AIBN was completed to compare any effect from the two initiators. After observing a decrease in cell spreading on BPO-initiated polyHIPEs, additional studies focused on decreasing the BPO concentration while maintaining quick set times and compressive properties. Therefore, 24 and 72 hour viability was assessed on PFDMA and BDMA polyHIPEs initiated with 1 wt% redox (0.5 wt% BPO and 0.5 wt% TMA) following protocols detailed earlier.

4.2.6.3 Effect of Increased Gel Fraction on Cell Viability

Cell viability after 1 week was assessed on polyHIPEs made with 70:30 and 50:50 molar ratios of PFDMA:BDMA. These HIPE compositions have the reduced viscosity necessary to promote mixing with cell suspension that is the subject of encapsulation studies in Chapter V. It was also hypothesized that this composition had a

higher gel fraction than PFDMA polyHIPEs with a corollary improvement in cytocompatibility.

4.2.7 Cytocompatibility of PFDMA/Tetrathiol PolyHIPEs

A β-thioester was incorporated into PFDMA polyHIPEs to increase the electronegativity of the carbonyl for increased hydrolytic degradation rate. Investigation of hMSC viability and morphology was done to assess any effect of the tetrathiol on cell behavior compared to control PFDMA polyHIPEs. A macromer extraction dilution viability assay was conducted on PFDMA supplemented with 5 and 10 mol% tetrathiol and tetrathiol as a control. The extraction was done for 10 minutes and 10 and 100X dilutions were made. Viability was assessed as discussed previously. Following indirect viability analysis, hMSCs were seeded directly on PFDMA/tetrathiol specimens. PolyHIPEs were fabricated utilizing 0 or 10 mol% tetrathiol, cured in 2 ml microcentrifuge tubes, and sectioned into 500 μm thick wafers using the Isomet® saw. Specimens were sterilized for 3 hours in 70% ethanol, washed 4 times with PBS, and incubated overnight in basal media supplemented with 40 w/v% FBS at 5% CO_2, 37°C. Cells were utilized at Passages 4-6 and trypsinized with 0.25% Trypsin-EDTA (Life Technologies) and seeded at a density of 10,000 cells/cm^2 onto the polyHIPE sections. Viability at 24, 72 hours and 1 week was assessed utilizing the Live/Dead assay kit (Molecular Probes). Cells were washed with PBS, stained with 2 μM Calcein and 2 μM ethidium homodimer-1 for 30 minutes in 37°C, and replaced with PBS for imaging. Rastor imaging (5 images per specimen) was conducted on four specimens (n=20) utilizing a fluorescent microscope (Nikon Eclipse TE2000-S). After determining that

PFDMA/tetrathiol polyHIPEs exhibited poor gel fraction and resulting viability, gel fraction was increased by reducing the organic phase viscosity with BDMA. HIPEs were fabricated with PFDMA and BDMA at a 1:1 molar ratio and 10 mol% tetrathiol and utilized as discussed previously to determine hMSC viability. A Transwell™ extraction study was conducted on the 1:1 PFDMA:BDMA control and 10 mol% tetrathiol polyHIPE sections.

4.2.8 Gel Fraction

Gel fraction of polyHIPEs fabricated with low and high viscosity macromers and a range of initiator concentrations was done to determine any correlation with hMSC viability. PolyHIPEs cured in a 15 mL centrifuge tube were sectioned 1 mm thick using an Isomet saw (Buehler) vacuum dried for 48 hours. Weighed specimens were suspended in dichloromethane (DCM) at a ratio of 1 mL DCM to 10 mg of sample to facilitate dissolution of uncrosslinked macromer. Sections in DCM were placed on a RT shaker table for 48 hours. After incubation period, DCM was removed and specimens were vacuum dried for 48 hours. The gel fraction was determined as the fraction of mass loss over original dry mass. PGPR was accounted for in all calculations so that the gel fraction reflected all macromere that was crosslinked into the network.

4.2.9 Synthesis of Cell Adhesive Amphiphile

An amphiphile containing the integrin-binding sequence RGDS was rationally designed utilizing logP values to self-assemble at the pore wall thereby providing binding sites for hMSCs. RGDS is an amino acid sequence located in the extracellular matrix glycoprotein fibronectin which has been shown to promote cell interaction when

incorporated into synthetic polymer matrices.[84] Octadecyl isocyanate (OI), the largest fatty acid, was reacted with the primary amines on the lysine-terminated RGDS at a 2:1 molar ratio. Briefly, KRGDS was dissolved in dimethylsulfoxide (DMSO) and loaded into a syringe with a needle. Octadecyl isocyanate added to reaction vial was mixed and KRGDS added dropwise to the OI. Reaction proceeded for 24 hours at 40°C under anhydrous conditions. After reaction was completed, excess solvent was removed using high vacuum. Successful functionalization was determined using fourier transform infrared (FTIR) spectroscopy.

4.2.10 Rheology – Work and Cure Time for Encapsulation

The effect of initiator concentrations in media HIPEs on work and set time was determined for future encapsulation studies. Work and set times of the polyHIPEs were characterized using an Anton Paar MCR 301 rheometer following a procedure adapted from Foudazi et al.[181] HIPEs were injected onto the plate heated to 37ºC through a mixing head to facilitate redox initiation. Storage and loss moduli were measured every 15 seconds using a parallel-plate configuration with a 1 mm gap and 0.5% strain. Work time is presented as the onset of increasing storage modulus and set time is presented as the tan δ minimum, which corresponds to storage modulus yielding. The data represents three runs (n=3) from one HIPE of the encapsulation composition.

4.2.11 Compressive Testing for Encapsulation PolyHIPEs

The compressive modulus and strength of media PolyHIPEs crosslinked with lower ratios of the redox initiators BPO and Ferrocene were determined following ASTM D1621-04a. PolyHIPEs cured in 15 mL centrifuge tubes were sectioned into

disks with a 3:1 diameter to height ratio using an Isomet saw (Buehler) and compressed using an Instron 3300 at a strain rate of 50 mm/s. The compressive modulus was calculated from the slope of the linear region and the compressive strength was identified, after correcting to zero strain, as the stress at the yield point or 10% strain, whichever point occurred first. Reported moduli and strength data were averages of the disks (n=3).

4.2.12 Cell Behavior Post Encapsulation in Rigid HIPE

The ability to encapsulate and deliver viable hMSCs in a rigid foam to the defect site would address current limitations with hydrogel delivery systems which are mechanically weak. HIPEs were fabricated following the protocol in Chapter III using basal media (αMEM) as the aqueous phase. BDMA was mixed with 10 wt% PGPR and 0.25 wt% BPO/0.5 wt% Ferrocene. Once the HIPE was fabricated, it was loaded into the large side of a 10:1 double barrel syringe using a syringe and 16G needle. hMSCs at Passage 5 were trypsinized, counted, and loaded into the small side of the double barrel syringe. Cells were encapsulated at 0.3 million cells/mL HIPE. Mixing of the HIPE with cell suspension was achieved by injecting through a mixing head. HIPEs were cured in between microscope slides with a 500 µm gap held by spacers, transferred to a 48 well plate, and covered with 300 µl growth media. Viability was determined at 3 Live/Dead® viability assay. Cells were washed with PBS, stained with 2 µM Calcein and 2 µM ethidium homodimer-1 for 30 minutes in 37°C, and replaced with PBS for imaging. The effect of encapsulated cells on polyHIPE pore architecture was assessed using SEM on a respective control and experiment specimens (n=1).

4.2.13 PolyHIPE Injection and Integration with Bone

The space-filling ability of a 10 wt% PGPR HIPE was evaluated utilizing an *ex vivo* porcine femur model. Cylindrical voids 1 cm in diameter and 0.5 cm in depth were created with a Dremel rotary tool in the femur and injected with the HIPE. After curing in the bead bath, the bone with polyHIPE was sectioned utilizing a low speed Isomet® saw and imaged utilizing a scanning electron microscope (SEM) (JEOL 6500). The ability for injectable PFDMA polyHIPEs to fill the defect site without overflow or loss of material was evaluated utilizing an inverted porcine femur model. Three cylindrical voids with a diameter of 1 cm and depth of 0.5 cm were created with a Dremel rotary tool, injected with HIPE solution, and the bone with HIPE inverted in a 37°C water bath overnight. After overnight cure, each defect in the bone was cross-sectioned into three specimens utilizing a low speed Isomet® saw and imaged utilizing a scanning electron microscope (JEOL 6500, n=9). All bones utilized in these studies were donated by the Rosenthal Meat Science and Technology Center at Texas A&M University. The flow properties are important for an injectable bone graft to ensure the material will integrate with the defect and remain at the site prior to cure. The feasibility of utilizing PFDMA polyHIPE to evaluate the *in vivo* integration and healing was assessed in a non-load bearing rat cranial defect. A critical-size defect with a diameter of 8 mm was created in the rat cranium using a dental bur with an outer diameter of 6.9 mm. PFDMA HIPEs were fabricated and loaded in a double-barrel syringe with mixing head as discussed previously and injected into the cranial defect. Digital photographs were taken to document the procedure.

4.2.14 Statistical Analysis

The data are displayed as mean ± standard deviation for each composition. A two-tailed Student's t-test was performed to determine any statistically significant differences in all sets of data. All tests were carried out at a 95% ($p < 0.05$) except the gel fraction studies with PFDMA and BDMA which were done at a 99% confidence interval ($P<0.01$).

4.3 Results and Discussion

The work in this chapter details the progression of evaluating polyHIPE cytocompatibility. Initial work on macromers, surfactant and initiators was conducted separately before incorporating into the HIPE to ensure all components were cytocompatible prior to cure. Afterward, indirect viability assays on cured monoliths in which cells were not directly seeding on the polyHIPE sections were done to determine cytocompatibility of any leachables. Finally, the viability of cells directly seeded on polyHIPE sections determined any effects surface chemistry and hydrophobicity had on protein adsorption and cell adhesion. All of these studies were vital in developing a HIPE system which promotes hMSC viability and proliferation during and post cure for future encapsulation work.

4.3.1 Cytocompatibility of Individual HIPE Components

4.3.1.1 Initiator and Surfactant Cytocompatibility

Determining the cytocompatibility of new macromers, initiators, and other components is a critical step in designing and implementing novel biomaterials. To this end, the viability of hMSCs seeded with media containing either organic-phase soluble

BPO and TMA initiators or the surfactant PGPR was evaluated. Each component was dissolved in the media following a protocol adapted from Bryant *et al.*[190] **Figure 4.1** illustrates the resulting viability of hMSCs in media with varying concentrations of dissolved PGPR. In the HIPE systems with 10 wt% PGPR, the maximum concentration cells would experience was calculated at 0.2 wt% in the media. PGPR, which is commonly used in the fabrication of chocolate, was cytocompatible at all concentrations investigated providing evidence that any future cytotoxic effect was not due to the surfactant.

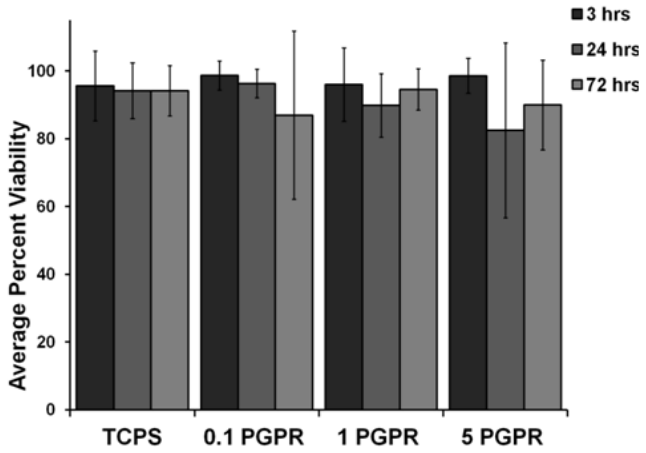

Figure 4.1. Viability of hMSCs in direct contact with PGPR at 3, 24, and 72 hours

Similar studies were run to investigate the cytocompatibility of BPO and TMA. However, no cells were adhered at 3 hours indicating these initiators at the concentrations tested affected hMSC adhesion. Furthermore, the media with a phenol red

pH indicator turned yellow when BPO was added indicating acidic pH. These results warranted future studies in initiator cytocompatibility under conditions mimicking the HIPE system with all components.

4.3.1.2 Macromer Cytocompatibility

An extraction dilution viability assay altered from ISO 10995-3 was done to determine the cytocompatibility of the organic phase without PGPR, which was shown to be cytocompatible. The initial extraction dilution was conducted on the organic phase with PFDMA and initiators (either 0.5 wt% BPO/2.5 wt% Ferrocene or 0.5 wt% BPO/2.5 wt% TMA) to investigate cytocompatibility of diffusible macromere during cure. All extractions in growth media were done for at a 1:3 volume ratio macromer: media to mimic the ratio of organic to aqueous phase in the HIPE. Extractions were done for 10 minutes as this is the maximum estimated cure time any for all potential redox HIPE compositions. This experiment indicated that the macromer alone was causing cell death (< 5% viability compared to polystyrene controls) as shown in **Figure 4.2.** PFDMA macromer was then purified further by washing at a 1:100 volume ratio with deionized water and/or subjecting to high vacuum for 24 hours followed by an additional extraction dilution viability assay. **Figure 4.2** illustrates an increase in hMSC viability when PFDMA is washed and placed under vacuum to remove any residual acid, base, or solvents not detectable using analytical techniques (NMR, FTIR). Future work will determine protocols to extensively purify PFDMA in large batches for *in vitro* and *in vivo* studies. Extensive studies in the Mikos group have illustrated *in vitro*

cytocompatibility and *in vivo* biocompatibility of poly(propylene fumarate) biomaterial systems.[61, 68, 146]

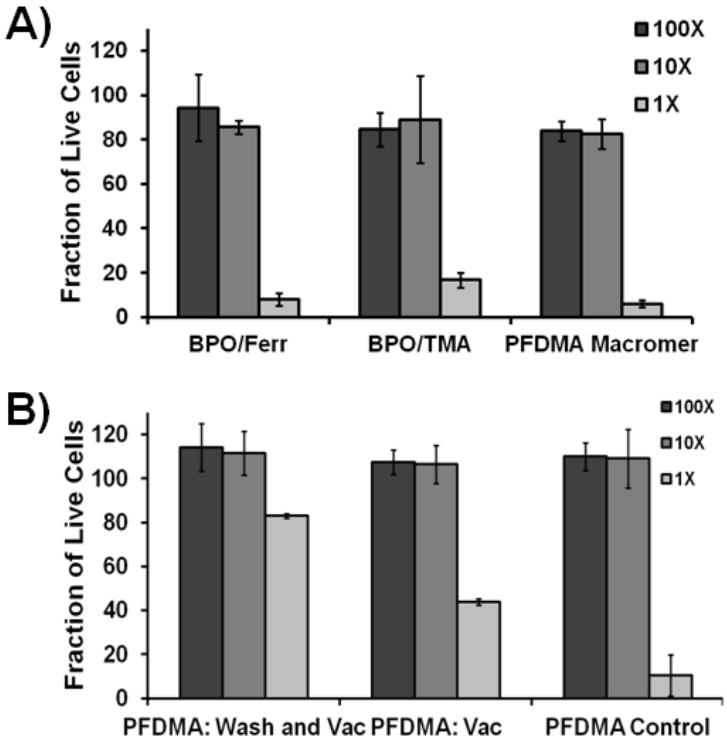

Figure 4.2. 10 minute extractions and dilutions based on ISO 10993-5 A) Percent viability on PFDMA macromer extractions with 0.5 wt% BPO/ 2.5 wt% ferrocene, 0.5 wt% BPO/ 2.5 wt% trimethylaniline, or no initiator B) Percent viability on PFDMA macromer extractions after further purification procedures

4.3.2 Indirect Cytocompatibility of PolyHIPEs

After testing and altering components and purification protocols to ensure all HIPE components were cytocompatible, indirect culture methods were utilized to decouple the effects of hMSC adhesion from the effect of possible diffusion of

macromer and radicals from uncured HIPE and leachables from polyHIPE sections. First, a Transwell® culture system with polycarbonate membrane inserts was employed to determine any cytotoxicity during cure. hMSCs were seeded on the polystyrene wells and uncrosslinked PFDMA HIPEs with varying ratios of BPO/TMA or BPO/Ferrocene were injected into the inserts and covered with growth media. Cell viability after exposure to any diffused macromer or radicals from the HIPE compositions was assessed using the Live/Dead stains as seen in **Figure 4.3.** These indirect contact studies of hMSCs with injectable polyHIPEs with different initiators and ratios resulted in spread cells and good viability (~80-85%) comparable to empty Transwell® inserts at 3 hours. These results indicated cytocompatibility of any diffusible components that encapsulated cells could experience during cure. Additionally, cytocompatibility of any

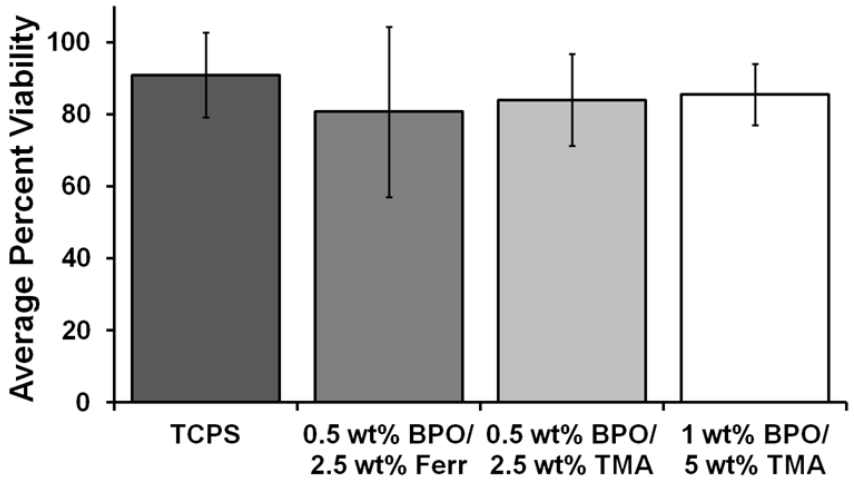

Figure 4.3. Transwell® study investigating the cytocompatibility of any diffusible mac**romer and radicals during cure of polyHIPEs with either BPO/Ferrocene or BPO/TMA initiator systems**

polyHIPE leachables was done using the same Transwell® culture system with polycarbonate membrane inserts. PFDMA polyHIPEs fabricated with either 5 wt% AIBN or BPO were placed in inserts after subjecting to sterilization and a wetting ladder. Viability through 72 hours illustrated good cytocompatibility of any leachables from the polyHIPE sections, **Figure 4.4**. This work allowed for future studies investigating cell behavior (adhesion, spreading, and morphology) when seeded directly on monoliths.

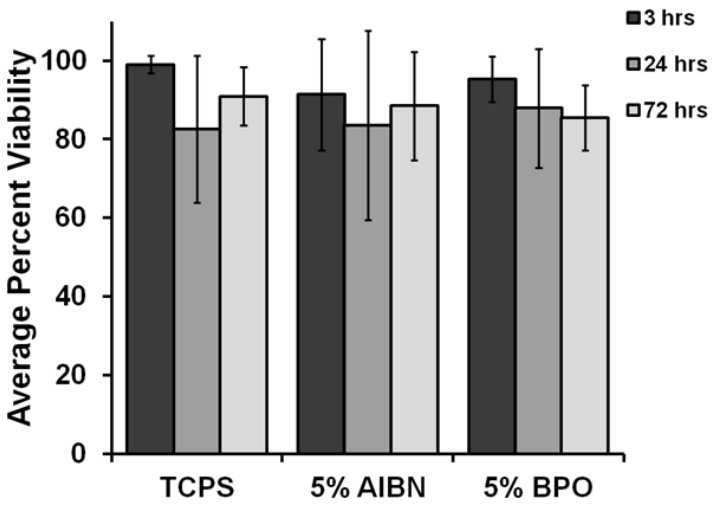

Figure 4.4. Transwell® study investigating the cytocompatibility of any leachables from cured PFDMA polyHIPE monoliths

4.3.3 Direct Cytocompatibility of PolyHIPEs

4.3.3.1 Effect of Serum Concentration and Seeding Density on Morphology

Culturing and assessing cell behavior on 3D scaffolds is more difficult than 2D

substrates (e.g. tissue culture polystyrene) because this is a new avenue of cell culture research. To this end, multiple culturing parameters must be determined for each new 3D culture system. The effect of hSMC seeding density and overnight serum incubation concentration on qualitative cell adhesion and morphology were determined. FBS concentration on hMSC adhesion and morphology was determined after 6 hours of cure. Cells were seeded on polyHIPE sections that had incubated in 10, 40, or 70 wt% FBS overnight as seen in **Figure 4.5**. hMSCs seeded onto monoliths with 40 wt% serum exhibited the largest relative amount of adhesion and spreading. From this study, 40 wt% FBS was chosen as the concentration to continue with in all future work. **Figure 4.6** displays hMSC morphology in response to a range of seeding densities from 2,000 – 250,000 cells/scaffold. As the number of cells seeded onto the polyHIPEs increased, the

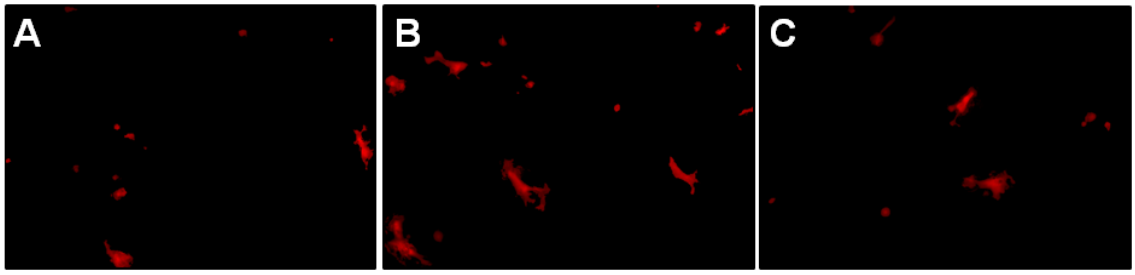

Figure 4.5. Qualitative effect of overnight fetal bovine serum concentration on hMSC adhesion and morphology at 6 hours A) 10 wt% FBS B) 40 wt% FBS C) 70 wt% FBS

increase in cell spreading and overall cell number increased. Kim *et al.* elucidated the effect of seeding density on hMSC viability, proliferation, alkaline phosphatase activity, and amount of mineralization and saw the highest seeding density group resulted in enhanced ALP activity and calcium deposition.[191] Thus, the seeding density is important in future studies in which hMSC ALP activity and calcium deposition is measured in response to bioactive agents.

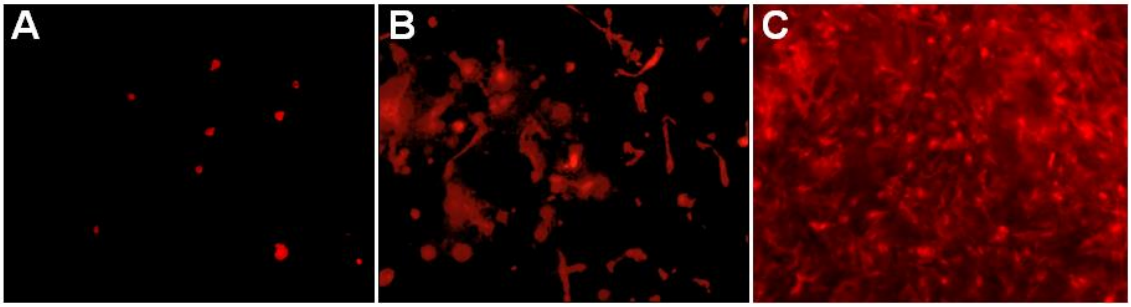

Figure 4.6. Effect of initial hMSC seeding density on cell morphology after 72 hours of culture A) 2,000 cells/scaffold B) 10,000 cells/scaffold C) 250,000 cells/scaffold. Cells were stained with Cell Tracker Orange™

4.3.3.2 Effect of Initiator on Morphology after Direct Seeding

Early work conducted with hMSC culture on PFDMA polyHIPEs was done with 5 wt% AIBN. Recent work in the lab progressed to utilizing redox initiation systems to produce quick-curing HIPEs with enhanced compressive properties at 24 hours. In these compositions, BPO was utilized as the oxidizing agent. The cell morphologies of

polyHIPEs fabricated with either AIBN or BPO are illustrated in **Figure 4.7**. hMSCs seeded on AIBN polyHIPEs exhibit increased spreading and interaction with proteins

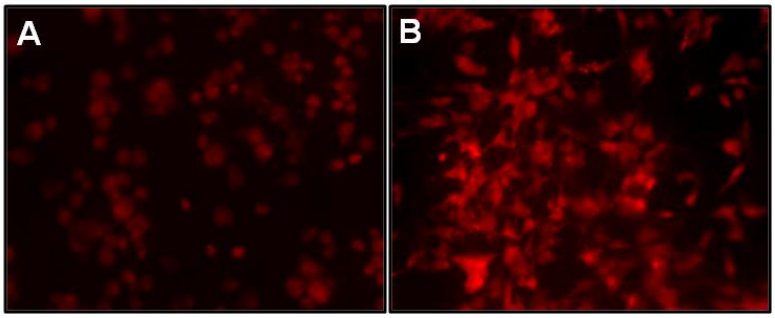

Figure 4.7. Effect of organic phase initiator on hMSC morphology at 3 hrs on PFDMA polyHIPEs. Cells were seeded at 25,000 cells/scaffold. A) 5 wt% BPO B) 5 wt % AIBN

on the scaffold compared to that on BPO polyHIPE sections which resulted in balled up cells. This observation can be further explained by the lack of cell adhesion on tissue culture polystyrene when BPO was dissolved and added to the media for direct analysis. Cell-cell signaling studies in 2D by Nelson *et al.* demonstrated the importance of cell spreading and the resulting cell-cell communication on proliferation highlighting the importance of cell morphology on polyHIPE sections.[192] Although AIBN-initiated polyHIPEs elicit better hMSC interactions, AIBN is a poor oxidizing agent limiting its use in producing quick-curing monoliths. Therefore, additional studies in this chapter probe the ability to decrease initiator concentration while maintaining quick work and set times, comparable compressive properties, and interconnected pore architecture.

4.3.3.3 Effect of Increased Gel Fraction on Cell Viability

Viability of hMSCs directly seeded onto redox-initiated polyHIPEs was first assessed with PFDMA and BDMA with 1 wt% BPO and TMA. **Figure 4.8** illustrates a decrease in viability at 72 hours of hMSCs on PFDMA to 47% compared to 87% on BDMA polyHIPEs with the same amount of surfactant and initiator.

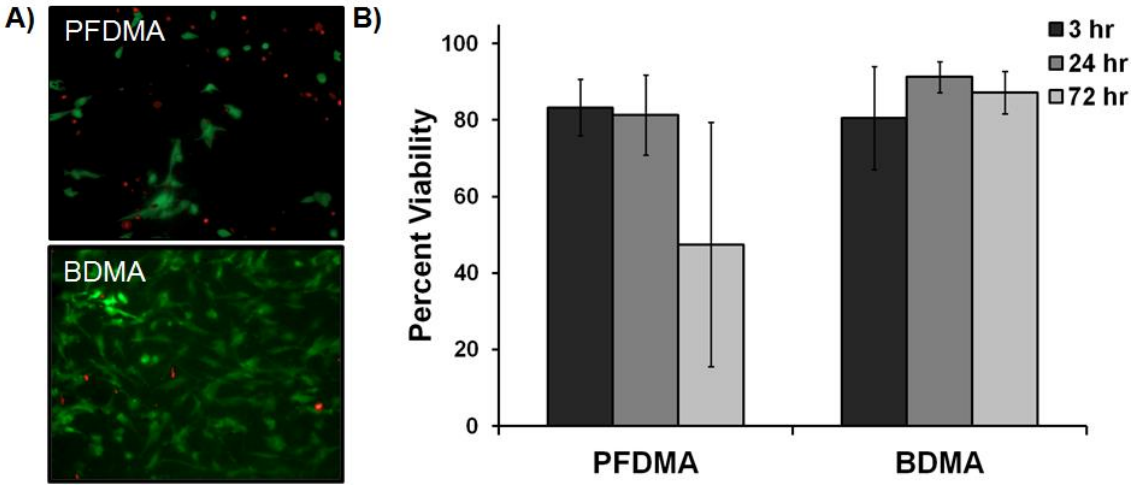

Figure 4.8. hMSC viability after 3, 24, and 72 hrs directly seeded on PFDMA and BDMA 1% redox polyHIPE sections. A) Micrographs illustrating live (green) and dead (red) cells on the respective polyHIPE sections at 72 hrs B) Viability of cells at each timepoint (n=20)

Earlier Transwell™ extraction and extraction dilution viability studies showed that the initiator radicals were cytocompatible during cure. Therefore, the effect of uncrosslinked macromer was investigated. Initial work on the redox-initiated PFDMA polyHIPE system indicated a decrease in crosslinking efficiency compared to BDMA polyHIPEs

crosslinked with the same initiator concentration.[180] It was hypothesized that this was due to the increased viscosity of the PFDMA organic phase relative to BDMA because of larger molecular weight. Increased viscosity can reduce radical diffusion and increase steric hindrance thereby decreasing crosslinking efficiency leaving unreacted macromer in the polyHIPE. Therefore, the effect of any unreacted macromer was determined by decreasing HIPE organic phase viscosity with BDMA at molar ratios of 70:30 and 50:50 and determining the gel fraction and hMSC viability. **Figure 4.9** displays the increase in crosslinking efficiency with an increase in BDMA due to an overall decrease in organic

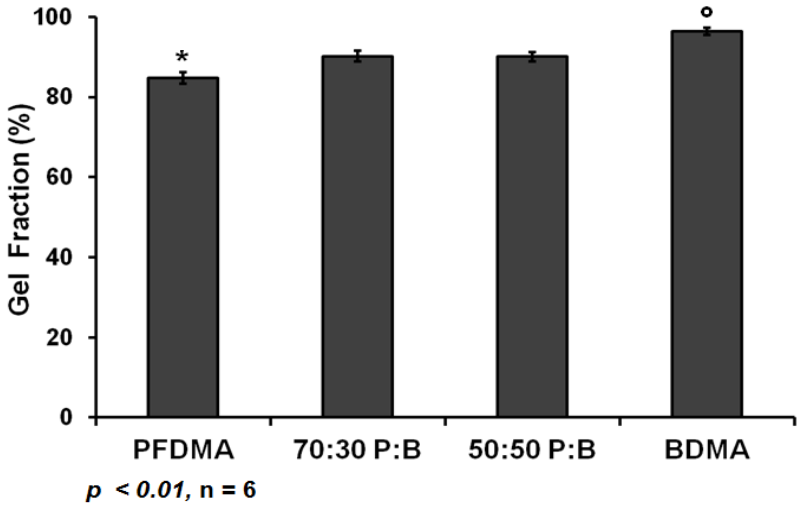

Figure 4.9. Effect of BDMA concentration on crosslinking efficiency assessed by gel fraction

phase viscosity. All BDMA polyHIPEs exhibited gel fractions significantly higher than that of the PFDMA control polyHIPE. Thus, decreasing organic phase viscosity is a method to increase crosslinking efficiency in 1 wt% redox polyHIPEs. Solvent extraction solutions from the gel fraction procedure contained unreacted macromer as shown by fourier transform infrared analysis (data not shown). The effect of the increase in crosslinking efficiency and potential decrease in unreacted macromer on hMSC viability was assessed. As hypothesized, increasing gel fraction increased hMSC viability as seen in **Figure 4.10.** The effect of unreacted unsaturated bonds may be a cause of decreasing viability. Klouda *et al*. illustrated a decrease in fibroblast viability with increased concentration of unreacted acrylated and methacrylated macromers and the time in which cells were exposed to these solutions before the network was formed.[193] This worked established the time of exposure in which cells are tolerable to reactive acrylates and methacrylates in this particular system. In the future, a similar systematic study should be done to determine what concentrations of macromers and initiators and durations of exposure are tolerable by hMSCs. This information will be vital in maintaining viability of encapsulated cells in the polyHIPE.

4.3.4 Cytocompatibility of PFDMA/Tetrathiol PolyHIPEs

A tetrathiol macromer was incorporated into PFDMA polyHIPEs to tune the hydrolytic degradation rate for future modulation to match a range of *in vivo* bone healing rates. The effect of tetrathiol on hMSC viability was first assessed in an extraction dilution viability assay. All concentrations of tetrathiol tested resulted in viable hMSCs shown in **Figure 4.11**. These results supported investigating one week

viability of hMSCs directly seeded on PFDMA/tetrathiol polyHIPE specimens. However, poor viability was observed on both the PFDMA control and 10 mol% tetrathiol PFDMA polyHIPEs after 72 hours of culture, **Figure 4.12**. However, specimens with 10% thiol promoted good cell adhesion and spreading and cells

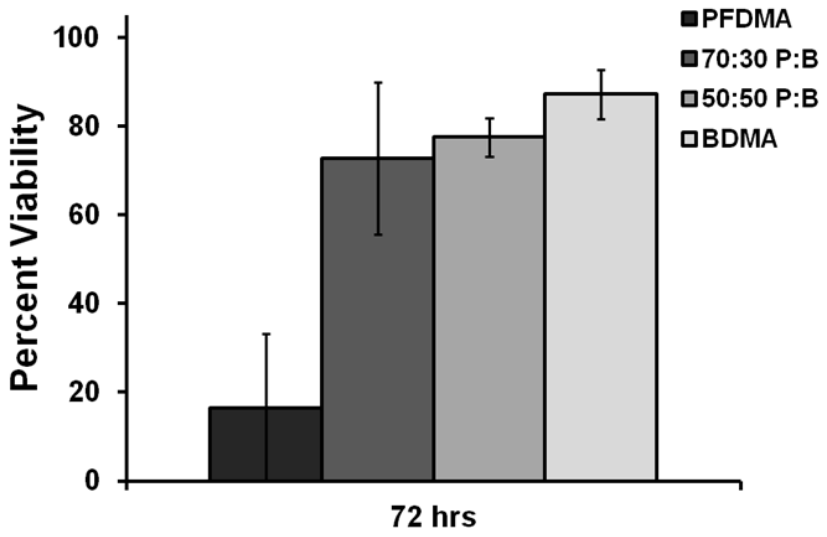

Figure 4.10. Effect of BDMA concentration and increased gel fraction on 72 hour hMSC viability

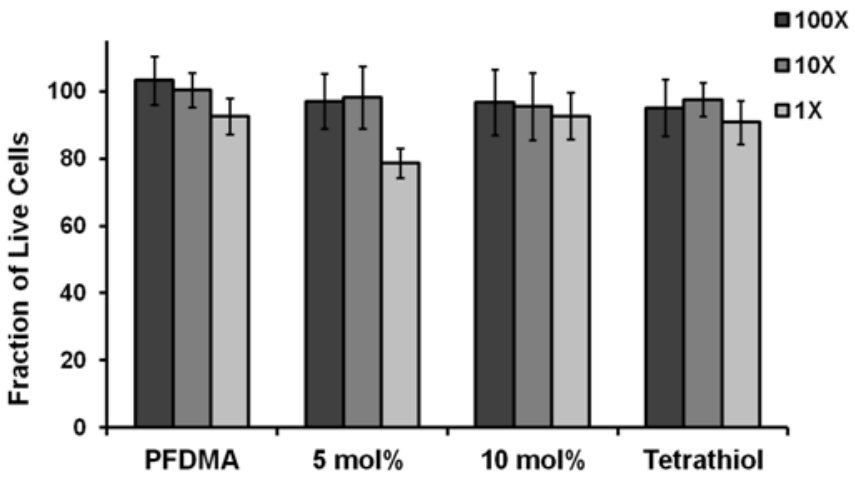

Figure 4.11. Effect of tetrathiol concentration on hMSC viability using a modified extraction dilution live/dead assay based on ISO 10993-5

remained at 1 week (42% viability) whereas a negligible amount of cells were adhered on PFDMA control specimens after 1 week. Brink *et al.* observed an increase in cell number and cell aggregate area in oligo(poly(ethylene glycol) fumarate) hydrogels with poly(ethylene glycol) dithiol compared to control OPF gels indicating a possible effect of thiol chemistry on cell adhesion and behavior.[194] As discussed previously, it was hypothesized that the viscosity of the PFDMA/thiol HIPE inhibited initiator and

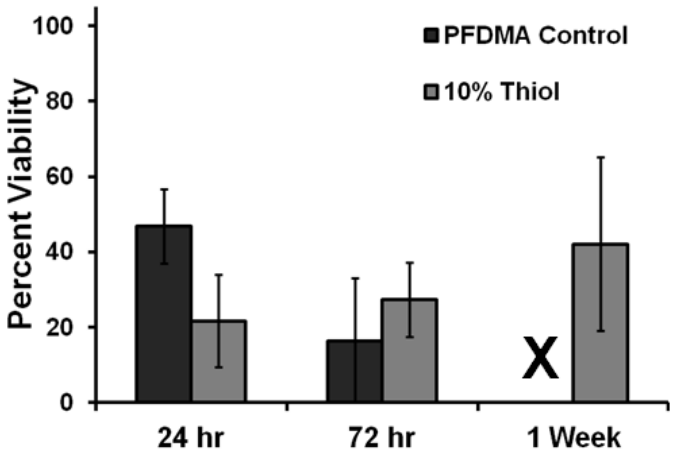

Figure 4.12. hMSC viability after direct seeding on PFDMA polyHIPEs with 10 mol% tetrathiol. No cells were remaining on PFDMA controls at 1 week.

macromer diffusion potentially resulting in pockets of uncured macromer and unreacted radicals. In response, lower viscosity HIPEs fabricated with a 50:50: molar ratio of PFDMA:BDMA were seeded with hMSCs to ascertain the effect of uncured macromer on cell adhesion and viability. Gel fraction results in **Figure 4.13** display an increase in percent of crosslinked material in the polyHIPE as the viscosity decreased giving evidence that in PFDMA/tetrathiol HIPEs the poor viability can be attributed to unreacted macromer. Thereby, the viscosity of PFDMA/tetrathiol HIPEs was decreased by incorporating BDMA at a 1:1 molar ratio. The resulting 1 week viability is shown in **Figure 4.14**. As hypothesized, increasing gel fraction by decreasing organic phase viscosity was seen in specimens without tetrathiol. Viability of both tetrathiol compositions (with and without BDMA) was comparable at each timepoint. The only differences between the PFDMA/BDMA and PFDMA/BDMA/tetrathiol polyHIPEs is

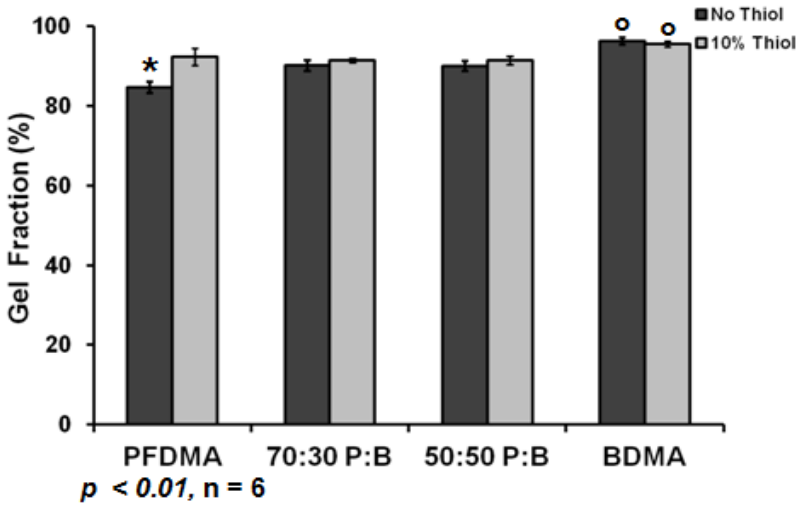

Figure 4.13. Effect of BDMA on gel fraction with and without 10 mol% tetrathiol

the incorporation of the thiol. A Transwell™ extraction study was conducted on 50:50 PFDMA:BDMA with and without 10 mol% thiol specimens to differentiate the effect of extractables compared to direct seeding on polyHIPEs. All values at 24 and 72 hours were greater than 80% and comparable between the control and thiol specimens indicating a negligible effect of the tetrathiol polyHIPE leachables on cell viability,

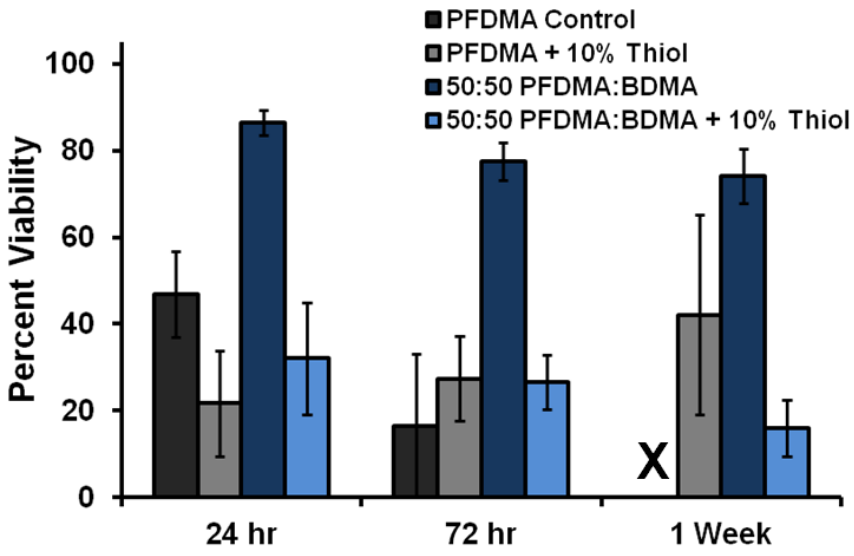

Figure 4.14. Effect of decreasing HIPE viscosity on hMSC viability directly on polyHIPEs with 10 mol% tetrathiol

Figure 4.15. Therefore, it is hypothesized that the change in chemistry with the addition of the thiol is altering cell behavior at the polyHIPE surface. The tetrathiol is more hydrophobic than PFDMA and BDMA (LogP values, increasing value indicates increase in hydrophobicity, Tetrathiol =1.0, BDMA = 3.0, PFDMA = 3.4). This microscopic increase in polyHIPE surface hydrophilicity may affect the amount and/or conformation of adsorbed proteins thereby altering integrin binding sites for hMSCs. Another theory is the addition of the thiol-methacrylate reaction and increase in rates of reaction may result in an increase in unreacted imitator or radicals. Although viability increased with the increase in polyHIPE gel fraction in control specimens, all polyHIPE systems with tetrathiol exhibit poor viability a mechanism which is currently being investigated.

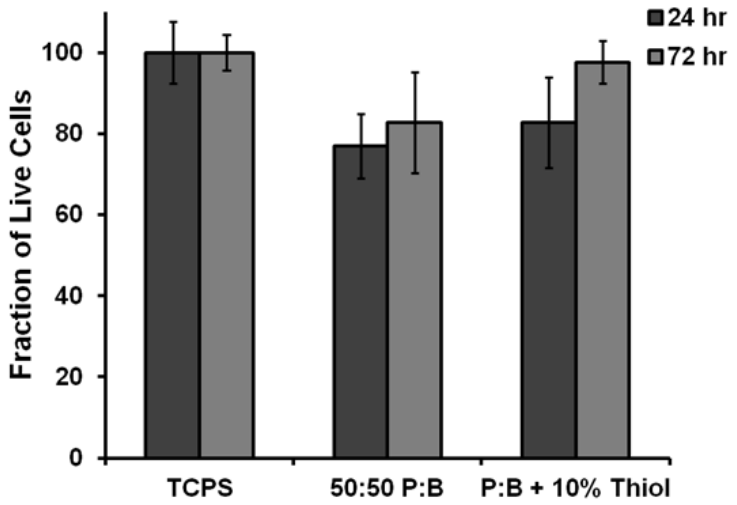

Figure 4.15. Transwell™ viability assay on 50:50 PFDMA:BDMA polyHIPEs with 10 mol% tetrathiol at 24 and 72 hours

4.3.5 Synthesis of Cell Adhesive Amphiphile

To increase hMSC adhesion and viability on PFDMA-based polyHIPEs, an amphiphile containing RGDS as an integrin binding site was synthesized. The chemistry was designed such that the macromolecule would self-assemble at the HIPE pore wall and anchor into the organic phase with the RGDS sequence available for cells seeded on top or encapsulated in the aqueous phase to recognize. Octadecyl isocyanate was reacted with the primary amines on a lysine-terminated RGDS at 40°C, anhydrous, for 24 hours. The removal of the isocyanate peak at 2270 cm^{-1} and the introduction of the carbonyl of the urea at 1618 cm^{-1} indicated successful coupling of the fatty acid chain to the adhesion peptide. FTIR results illustrated these molecular changes are displayed in **Figure 4.16.** Furthermore, a schematic of the reaction and the theoretical location of the amphiphile once incorporated are in **Figure 4.17**. The overall goal of incorporating this

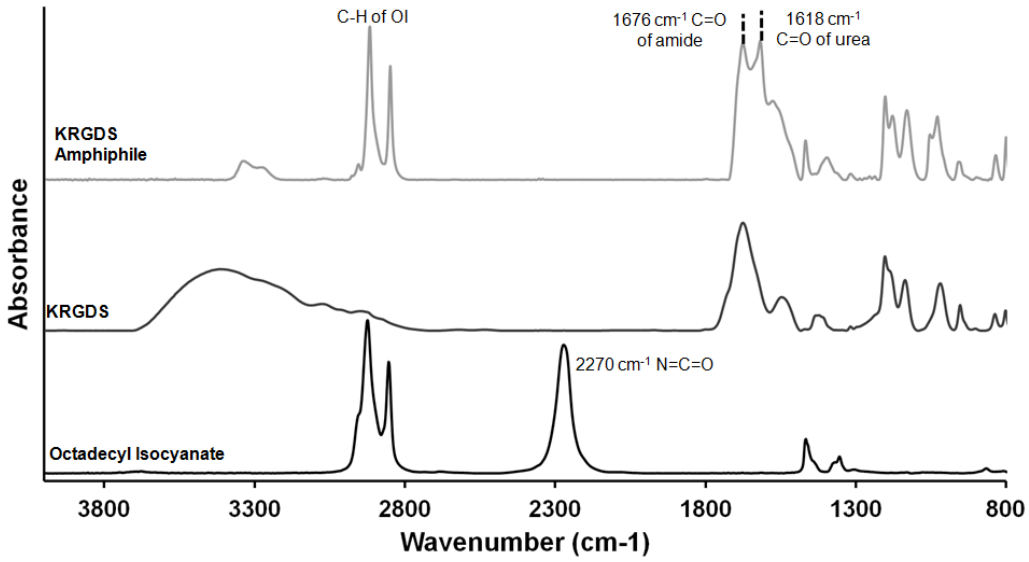

Figure 4.16 FTIR spectra illustrating the coupling of octadecyl isocyanate with lysine-terminated RGDS

amphiphile into the HIPE prior to cure is to increase cell adhesion and interaction with the polyHIPE without a post-fabrication processing to ensure injectability. An increase in spreading was observed of hMSCs seeded on polyHIPE sections with 3 mM RGDS amphiphile relative to the polyHIPE control. This knowledge may be further used to increase hMSC behavior once encapsulated.

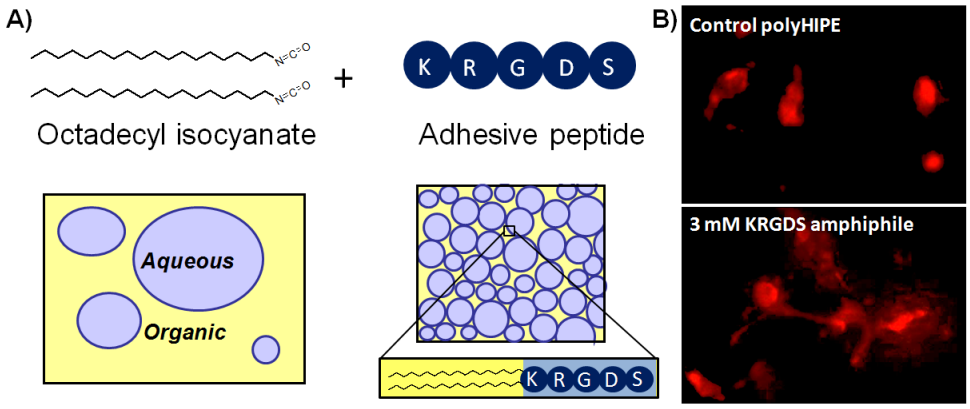

Figure 4.17. Schematic illustrating the reaction of octadecyl isocyanate with a lysine-terminated RGDS to fabricate an amphiphile that will self-assemble at the HIPE pore wall to promote hMSC adhesion and spreading. A) Reaction and location B) 24 hr analysis of CellTracker™ Orange-stained hMSCs seeded on either a control polyHIPE section or a polyHIPE section with 3 mM RGDS amphiphile

4.3.6 Cell Behavior Post Encapsulation in Rigid HIPE

Delivering viable, autologous hMSCs to the defect site would increase healing while reducing any rejection which may be caused from using allogeneic tissue. Encapsulating cells in a rigid, highly porous foam could address issues of mechanical weakness in typical hydrogel systems and provide a substrate that can withstand the physiological loading of bone. Two main parameters are currently being modulated to ensure encapsulation and viability maintenance with injectable PFDMA-based polyHIPEs: adequate viscosity to mix with cell suspension and quick cure time to reduce time for diffusion of unreacted macromer and radicals into the cell-laden aqueous phase. **Figure 4.18** illustrates the proposed injection set-up and the system used to run the *in vitro* studies. A BDMA HIPE with 0.5 wt% BPO and 2.5 wt% Ferrocene was fabricated

with basal media as the aqueous phase and loaded in the larger side of a 10:1 double barrel syringe. Cells at Passage 5 were trypsinized and loaded in the smaller side in a suspension to ensure a 10:1 ratio. This size double barrel syringe was utilized to ensure the HIPE could mix completely with the cell suspension. Decreasing organic phase viscosity more may allow the use of a 1:1 double barrel while maintaining successful mixing of the two phases. A representative micrograph of 3 hr hMSC viability is shown in **Figure 4.19** illustrating a majority of viable cells post encapsulation. hMSCs were visible throughout all sections illustrating the ability to adequately mix the cell suspension with the HIPE for increased distribution within the monolith.

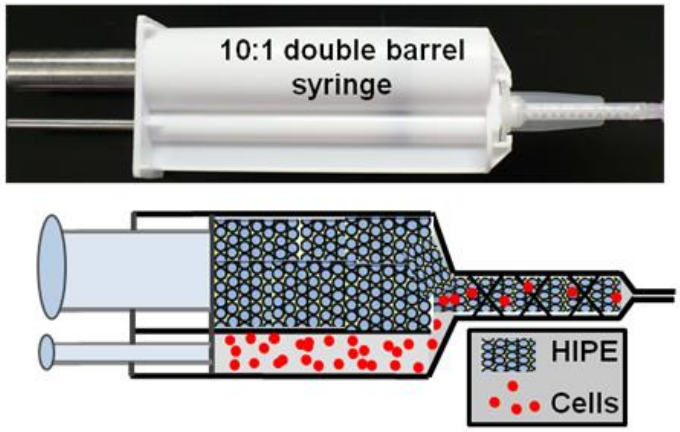

Figure 4.18. Schematic illustrating the potential to encapsulate hMSCs in the injectable HIPE within the surgical suite utilizing a double barrel syringe with mixing head setup

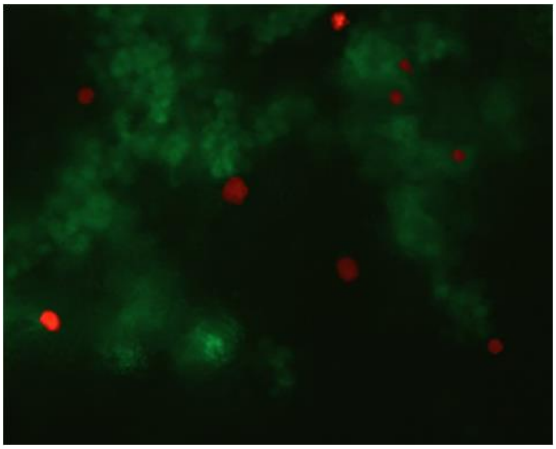

Figure 4.19. 3 hr hMSC viability post encapsulation in a BDMA HIPE initiated with 0.5 wt% BPO/ 2.5 wt% Ferrocene

The effect of encapsulated hMSCs on pore architecture is illustrated in **Figure 4.20.** In this study, the presence of cells during the cure process destabilized the emulsion and resulted in larger, homogenous pore sizes (20-100 μm) and interconnect sizes (5-10 μm). It is hypothesized that this effect could be modulated based on the HIPE composition, the number of cells encapsulated, and the media components. This effect could be utilized to increase interconnected polyHIPE pore size to increase nutrient and waste transport through the monolith. The average compressive modulus of this composition at 24 hour cure (no cells) was 22 MPa and strength of 1.5 MPa. These values are higher than typical hydrogel matrices and are comparable to similar scaffolds shown to be suitable for promoting healing validating the use of this composition for hMSC encapsulation and delivery.[53]

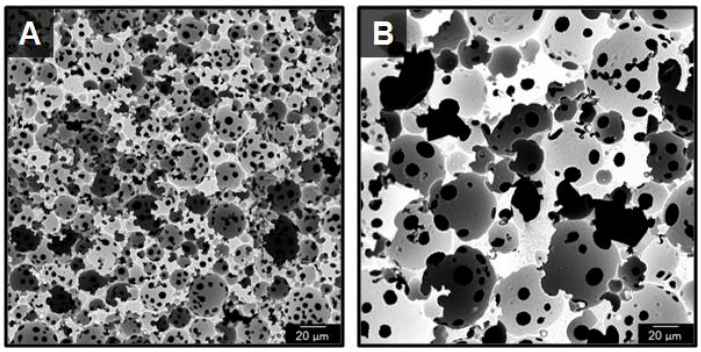

Figure 4.20. Effect of encapsulated hMSCs on pore architecture A) control BDMA polyHIPE B) BDMA polyHIPE with 0.3 million cells/ml HIPE encapsulated

The work time of this HIPE composition allowed for adequate time to load the double barrel syringe and inject multiple specimens for cure in a 48 well plate. The set time was also important as it is hypothesized that a short set time is ideal to reduce any unreacted macromer or radicals which could leach out into the media. This particular system exhibited a set time of 1.5 minutes which is much less than the 10 minute incubation period in which good viability was seen after the extraction of macromer and initiators. As discussed previously, the impact of organic phase chemistry, initiator concentrations, and cure time must be determined in a systematic extraction viability study to ascertain what conditions and durations are tolerable to encapsulated hMSCs. With this information, hMSC viability and ALP activity will be assessed post encapsulation in the predetermined HIPE composition utilizing the established protocols. Overall, performance of this study mimics a surgeon adding a bone marrow aspirate/concentrate to the double barrel syringe which has been pre-loaded with the

HIPE. This technique also precludes the significant cost and time associated with cell expansion while retaining the benefits of autologous cell delivery. The facile double barrel syringe method provides the proof of concept that an injectable HIPE can be combined with cells in the surgical suite without a costly or complex apparatus and illustrates the strong clinical translation potential.

4.3.7 PolyHIPE Injection and Integration with Bone

Injectable scaffolds that integrate with native tissue are expected to enhance bone healing with minimal inflammation and scarring. To this end, the ability of a PFDMA HIPE to integrate with native tissue in a porcine femur defect was evaluated. **Figure 4.21** illustrates the microscale integration of the HIPE in an *ex vivo* porcine femur defect evident as evidenced by the lack of gap between polyHIPE and cortical bone**.**

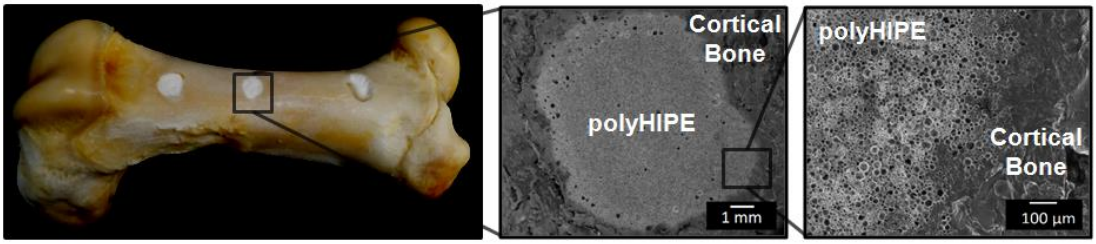

Figure 4.21. Injectable PFDMA HIPEs fill irregularly-shaped defects created in a porcine femur and integrate with bone without shrinkage upon cure at 37°C.

Furthermore, the ability of the HIPE to resist flow and remain at a defect site throughout cure was investigated. It was hypothesized that the viscosity of the HIPE will be

advantageous in preventing extravasation and result in maintenance of the scaffold at the defect. The viscosity of HIPE prior to cure was 11.0 ± 2.3 Pa·s, comparable to mayonnaise. **Figure 4.22** illustrates the ability of PFDMA HIPE to resist flow when inverted in a clear tube. Additionally, the HIPE remains at the defect site in the porcine femur during cure when inverted in an aqueous environment. SEM analysis indicated integration of HIPE into the bone with no evident gap after inversion in an aqueous environment overnight in all nine specimens evaluated.

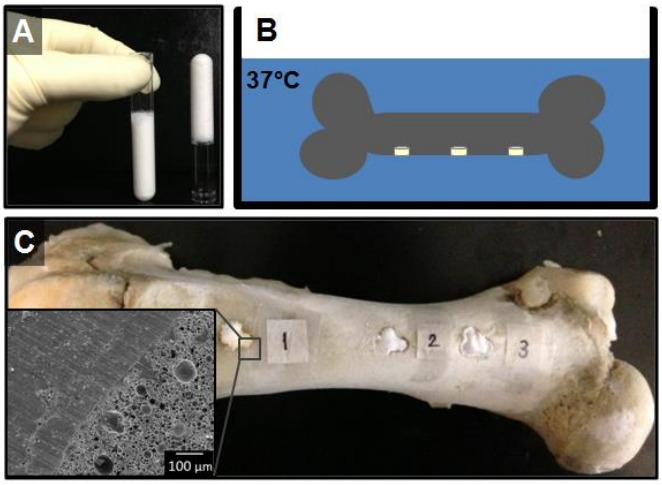

Figure 4.22 The viscosity of a PFDMA HIPE prior to cure results in retention of the scaffold at the defect site during cure in an aqueous environment. A) HIPE does not flow upon inversion in transparent tube. B) Schematic illustrating the inversion of porcine femur with HIPE injected in 1 X 1 X 0.5 cm defects in 37°C water bath. C) Digital and scanning electron micrographs showing good integration of HIPE with bone during inversion in water.

Initial studies illustrated the feasibility of using a quick-curing redox HIPE for non-load bearing studies in a rat cranial critical-size defect as seen in **Figure 4.23**. These feasibility studies established a platform protocol for future work to evaluate the *in vivo* HIPE integration with bone and the ability of these polyHIPEs to promote osteogenesis. Evaluation of the pullout strength will also be conducted to determine the extent to which the HIPE has integrated into the native bone.

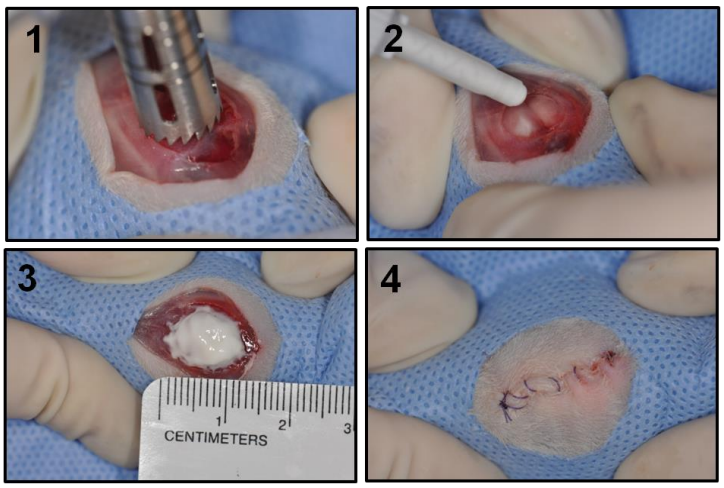

Figure 4.23. Preliminary studies in a rat cranial defect illustrate the feasibility of injecting HIPEs into non-load bearing defects to later evaluate integration and healing

4.4 Conclusions

The development of a new biomaterial system requires extensive investigation of scaffold components to ensure cytocompatibility. Specifically, injectable systems in which cells are encapsulated must be designed and processed so that cytocompatibility is

maintained prior, during, and post-cure. To this end, all HIPE components and concentrations were extensively analyzed to determine under what conditions encapsulated hMSCs could remain viable and primed for osteogenesis. Methods were first established to successfully assess effects of HIPE components on hMSC viability and polyHIPE microstructure and chemistry on cell morphology and behavior. A seeding density of 100,000 cells/cm^2 (of well plate) and a 40 wt% FBS overnight soak were determined to enhance cell adhesion and spreading. Techniques to purify macromer were established for use in future encapsulation work. Current investigation is focused on determining the maximum initiator concentrations which are tolerable by cells. These protocols are useful for *in vitro* culture of cells on 3D foams and will help advance the development of multiple HIPE compositions as tissue engineered scaffolds. Moreover, a double barrel syringe and mixing head setup was utilized to efficiently mix cells through the HIPE suspension illustrating the proof of concept that an injectable HIPE can be combined with cells in the surgical suite without a costly or complex apparatus and illustrates the strong clinical translation potential. Furthermore, these studies elucidated key structure-property relationships in emulsion templated scaffolds that can be used in future studies to modulate cell-material interactions.

CHAPTER V

MATERIAL-INDUCED OSTEOGENESIS IN POLYHIPES WITH CALCIUM PHOSPHATE AND DEMINERALIZED BONE MATRIX

5.1 Introduction

Tissue engineered bone grafts combine the healing potential of autografts with the availability of allografts. A major challenge in designing functional bone grafts is determining a material composition which promotes ingrowth of surrounding bone and proliferation of cells (osteoconduction), the differentiation of progenitor cells down an osteoblastic lineage (osteoinduction), and osseointegration with native bone. Osteogenesis encompasses all of these processes resulting in full tissue regeneration. Various scaffold chemistries and bioactive agents are currently studied to provide a matrix that provides cues to stimulate osteoblast differentiation of hMSCs and promote integration and healing.

The most effective approach in designing a 3D scaffold to stimulate osteogenesis is to mimic the extracellular matrix of bone. This encompasses the protein chemistries, inorganic mineral composition, topography, morphology, compressive properties, and degradation rate. Extensive research has focused on recombinant growth factors, such as bone morphogenetic proteins (BMPs), for effective osteoblastic differentiation of hMSCs. Unfortunately, these potent factors have resulted in undesired tissue growth and fatal inflammation. Utilizing inorganic minerals and matrix proteins for differentiation is advantageous over growth factors as the decrease in potency may reduce undesired

effects while encouraging natural repair based on *in vivo* cell signaling as a response to the material.

Calcium phosphates comprise the main mineral component of native bone and are commonly utilized in bone tissue engineering to promote osteogenesis. Based on Ca/P ratio, crystallinity, and degree of impurities, a range of bioactivities and degradation rates are achieved with calcium phosphates.[1] Hydroxyapatite (HA) has been utilized extensively in biomaterial research and illustrated the potential for calcium phosphates to promote osteogenesis *in vitro*. However, in physiological pH, highly crystalline HA exhibits poor solubility and hinders cell responses due to low concentrations of calcium and phosphate ions released.[195] Amorphous calcium phosphate lacks any crystal structure and is resorbed more readily than crystalline hydroxyapatite.[196] The relative ability of these calcium phosphate minerals to stimulate progenitor cell proliferation and differentiation are dependent on physiological environment and presentation in the scaffold.

A unique attribute of the HIPE system is the thermodynamics that can drive phase separation depending on hydrophobicities of the internal and continuous phase. This results in the ability to introduce small particles that can self-assemble at the pore surface due to their size and surface charge. Emulsions stabilized by solid particles which adsorb to the oil-water interface rather than a molecular surfactant are termed Pickering emulsions.[86] Multiple groups have successfully fabricated and characterized water-in-oil (w/o) Pickering polyHIPEs utilizing both titania and silica nanoparticles.[87-90, 197] The preferential location of self-assembled particles, including the ACP and HA

nanoparticles, at the pore wall in direct contact with encapsulated MSCs is beneficial for providing a bioactive component that could be utilized for osteoblast differentiation. Furthermore, this methodology promotes the ability to use less of the expensive bioactive particles and still achieve the desired cellular response due to the presentation of the particles in the polyHIPE pore walls with large surface area.

Demineralized bone matrix (DBM) is proposed to stimulate bone growth by providing an environment in which invading progenitor and inflammatory cells are stimulated to release trophic cytokines to recruit cells for repair.[119] Furthermore, the demineralization process exposes growth factors and other bioactive molecules which would otherwise remain inactive in the presence of minerals.[119, 198] Additional work by Pietrzak *et al.* explained that inorganic minerals reduced hydration of the organic matrix limiting the solubility and thereby bioactivity of growth factors such as BMPs.[199] Multiple studies have illustrated the ability for DBM to promote osteogenesis both *in vitro* and *in vivo*. Incorporating both calcium phosphate and demineralized bone matrix into injectable polyHIPEs may provide a rigid foam capable of promoting material-based osteogenesis for encapsulated hMSCs.

The use of polyHIPE monoliths as scaffolds to repair bone has been pursued by multiple groups but not widely studied. Bokhari and colleagues incorporated hydroxyapatite into styrene-divinylbenzene polyHIPEs and illustrated the ability to increase the production of bone matrix glycoprotein osteopontin and mineral deposition relative to control specimens.[104] These results are promising for use of this emulsion templating technique to fabricate rigid materials that promote enhanced behavior of bone

cells. However, all of this work was conducted with monoliths that were fabricated, extensively washed to purify, and then tested. The ability of an injectable polyHIPE fabricated without toxic solvent and cured at 37°C to promote hMSC adhesion and differentiation down an osteogenic lineage would increase the use of these materials in bone grafting applications.

In the earlier chapters of this work, polyHIPE compositional and processing parameters were utilized to modulate scaffold pore architecture, compressive properties, cure time, degradation rate, and interaction with hMSCs. In this chapter, we build upon our injectable polyHIPEs with tunable properties to fabricate monoliths with osteogenic potential. Amorphous calcium phosphate and hydroxyapatite nanoparticles, and demineralized bone matrix were added to the organic phase prior to fabrication to increase osteogenesis and hMSC proliferation. Redox-cured polyHIPEs allowed for incorporation of particles with a range of hydrophobicities and surface charge due to the quick set times which reduces time for phase separation. The ability to incorporate bioactive particles into the HIPE without affecting emulsion stability and resulting pore architecture was investigated using SEM. The effect of osteoinduction agent on the compressive properties of PFDMA/BDMA polyHIPEs was evaluated. Finally, the ability of these agents incorporated in the polyHIPE to promote hMSC differentiation *in vitro* was assessed by measuring alkaline phosphatase activity levels and observing hMSC calcium deposition with Alizarin red stain in response to ACP, HA, and DBM. The work in this chapter is the culmination of the work to develop an injectable polyHIPE for bone graft applications. The results from these studies will be utilized to determine injectable

HIPE compositions for future studies evaluating *in vivo* bone growth in a rabbit ulnar defect model.

5.2 Materials and Methods

5.2.1 Materials

Polyglycerol polyricinoleate (PGPR 4125) was donated by Palsgaard (Morris Plains, NJ). Human mesenchymal stem cells were provided by the Texas A&M Health Science Center College of Medicine Institute for Regenerative Medicine at Scott & White. All other chemicals were purchased and used as received from Sigma Aldrich (Milwaukee, WI) unless otherwise noted.

5.2.2 Demineralizing and Homogenizing Rat Long Bones

Euthanized Sprague Dawley rats were obtained from the tissue share program at the Laboratory Animal Research and Resources facility at Texas A&M University. The demineralization process was adapted from Figueiredo *et al.*[200] Long hind bones were extracted from the rats, rid of soft tissue using a scalpel and gauze, and the majority of marrow removed with water and compressed air. Bones were soaked in a 1:1 volume chloroform: methanol solution at 1g bone to 30 mL solution for 3 hours. After solvent treatment, bones were washed once with RO water and placed in a 0.6M HCl solution and stirred for 24 hours to decalcify. Residual HCl was then removed by rinsing with water, stirring DBM in freezing water, and placed under vacuum at 40°C overnight. DBM was then blended into smaller pieces and homogenized into particles using a handheld digital homogenizer (IKA T25 digital ULTRA-TURRAX). Scanning electron

microscopy was utilized to determine relative particles sizes as seen in **Figure 5.1**. Visual assessment determined particle sizes range from 50 – 200 μm.

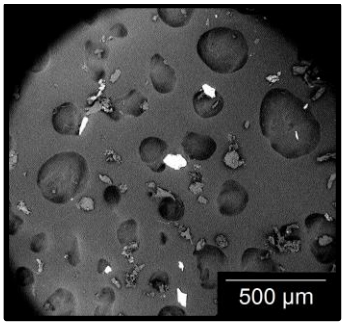

Figure 5.1. Demineralized bone matrix particles after homogenization procedure

5.2.3 BDMA Inhibitor Removal

Butanediol dimethacrylate (BDMA) was passed through a column containing alumina oxide using high air pressure to remove the monomethyl ether hydroquinone inhibitor and collected in a round bottom flask.

5.2.4 PolyHIPE Fabrication

Quick-curing redox polyHIPEs were fabricated using the method detailed in earlier chapters. A 70:30 molar ratio of PFDMA:BDMA was utilized to ensure an adequate viscosity to mix with a cell suspension for encapsulation. The organic phase was further comprised of 10 wt% PGPR, 1 wt% BPO or TMA and either 2 wt% amorphous calcium phosphate nanoparticles (ACP), 5 wt% hydroxyapatite

nanoparticles, or 15 wt% demineralized bone matrix (DBM). The concentrations reflect results from scoutings to determine the maximum concentration of osteoinductive components that promoted HIPE formation. The aqueous solution of calcium chloride (1 wt%) and deionized water was then added to the organic phase (75% v) in six additions and mixed at 500 rpm for 2.5 min each to promote emulsion formation. The two HIPEs (BPO and TMA) were mixed at 2500 rpm for 30 seconds in the Speedmixer to initiate crosslinking. HIPEs were transferred to either 2 mL microcentrifuge tubes or 15 mL centrifuge tubes and placed in a 37°C aluminum bead bath to facilitate crosslinking overnight.

5.2.5 Pore Size Characterization

SEM (Phenom Pro, Nanoscience Instruments) was utilized to image all polyHIPEs and determine any effect of the incorporation of osteogenic particles on polyHIPE pore sizes. PolyHIPEs were subjected to vacuum drying for 72 hours to remove water prior to pore architecture characterization. PolyHIPEs cured in 15 ml centrifuge tubes were sectioned into thirds, fractured at the center, coated with gold, and imaged in a rastor pattern yielding five images. Pore size measurements were completed on the first ten pores that crossed the median of each 4000X magnification micrograph. Average pore sizes for each polyHIPE composition are reported (n=150). A statistical correction was calculated to account for non-perfect spherical pores, $h^2 = R^2 - r^2$, where R is the void diameter's equatorial value, r is the diameter value measured from the micrograph, and h is the distance from the center. The average diameter values were

multiplied by this correction factor resulting in a more accurate description of pore diameter.[95]

5.2.6 Compressive Testing

The effect of each osteoinductive agent on polyHIPE compressive modulus and strength was investigated following ASTM D1621-04a. PolyHIPEs cured in 15 mL centrifuge tubes were sectioned into disks with a 3:1 diameter to height ratio using an Isomet saw (Buehler) and compressed using an Instron 3300 at a strain rate of 50 mm/s. The compressive modulus was calculated from the slope of the linear region and the compressive strength was identified, after correcting to zero strain, as the stress at the yield point or 10% strain, whichever point occurred first. Reported moduli and strength data were averages of the disks for each polyHIPE composition (n=3).

5.2.7 Alizarin Red Staining of ACP and HA in PolyHIPE

Alizarin red binds to calcium ions and was utilized to visually verify the incorporation of calcium phosphate particles. PolyHIPEs of each condition were sectioned to 1 mm width using an Isomet saw (Buehler). Specimens were first fixed with 3.7 vol% glutaraldehyde followed by a 5 minute incubation in 2 w/v% alizarin red in distilled water solution, pH 4.1-4.3. Stained specimens (n = 1) were washed with distilled water 5X to remove any unreacted dye. Digital micrographs were obtained.

5.2.8 Sirius Red Staining of Type I Collagen

Sirius red, which preferentially binds to Type I collagen, was used to both verify the matrix was collagen and illustrate the incorporation of DBM in the polyHIPEs. A 1 mg/ml solution of Sirius red was added to specimens and incubated at room temperature

for 30 minutes. Type I rat tail collagen (Sigma) was utilized as a positive control for the stain. Following staining, specimens (n = 3) were rinse with deionized water 5X and imaged with a digital camera.

5.2.9 Cytocompatibility of PolyHIPEs with ACP, HA, and DBM

Initial cytocompatibility verification of polyHIPEs with 2 wt% ACP, 5 wt% HA, and 15 wt% DBM was done following the protocol detailed in Chapter III. PolyHIPEs were cured in 2 ml microcentrifuge tubes and sectioned into 500 μm thick wafers using the Isomet® saw. Specimens were sterilized for 3 hours in 70% ethanol, washed 4 times with PBS, and incubated overnight in basal media supplemented with 40 w/v% FBS at 5% CO_2, 37°C. Cells were utilized at Passages 3 and seeded at a density of 10,000 cells/cm^2 onto the polyHIPE sections. Viability at 1 and 2 weeks was assessed utilizing the Live/Dead assay kit (Molecular Probes). Cells were washed with PBS, stained with 2 μM Calcein and 2 μM ethidium homodimer-1 for 30 minutes in 37°C, and replaced with PBS for imaging. Rastor imaging (5 images per specimen) was conducted on four specimens (n=20) utilizing a fluorescent microscope (Nikon Eclipse TE2000-S).

5.2.10 Osteoconductivity of PolyHIPEs

The ability of PFDMA/tetrathiol polyHIPEs to promote osteogenesis was accessed via alkaline phosphatase (ALP) activity and Alizarin red calcium staining. PolyHIPEs were sectioned and subjected to a wetting ladder and overnight serum incubation as stated previously. hMSCs were seeded at a density of 10^5 cells/scaffold (well). The ability of polyHIPEs to promote osteogenesis was assessed with ALP activity of cells seeded on polyHIPEs cultured in growth media. Cells were lysed at 1, 7,

and 14 days. Briefly, media was removed from wells and replaced with 300 μL phosphate buffered saline (PBS) and samples subjected to a thermal shock procedure in which specimens were placed in 37°C incubator followed by an 80°C freezer 3X to lyse the cells and release intracellular ALP. Alkaline phosphatase (ALP) activity was accessed using a fluorometric assay kit (Abcam, ab83371) in which ALP cleaves the phosphate of non-fluorescent 4-methylumbelliferyl phosphate disodium salt (MUP) substrate resulting in a fluorescent signal. A Quant-iT™ PicoGreen® dsDNA Assay Kit (Molecular Probes) was utilized to quantify dsDNA to report ALP activity per cell. Conversion of MUP substrate to a fluorescent signal by ALP was assessed using a plate reader (Tecan Infinite M200Pro) with excitation/emission wavelengths of 360/440 nm, respectively. Alizarin red staining was conducted on specimens utilized for viability analysis. After imaging for viability, cells on sections were fixed with 3.7% glutaraldehyde solution for 10 minutes, washed 1X with PBS, and stored in 300 μL distilled water. The staining procedure detailed previously was followed and digital micrographs obtained to ascertain relative amounts of calcium deposition across conditions.

5.2.11 Statistical Analysis

The data are displayed as mean ± standard deviation for each composition. A Student's t-test was performed on the compressive and viability data to determine any statistically significant differences between compositions. Tests were carried out at a 99% confidence interval ($P<0.01$) for all studies.

5.3 Results and Discussions

5.3.1 Fabrication and Characterization of Osteoinductive PolyHIPEs

The goal of incorporating osteogenic elements into PFDMA-based polyHIPEs was to confer an osteoinductive character to the grafts without negative impact on the desirable graft properties such as injectability, porosity, and mechanical properties. Incorporating components with a range of hydrophobicities and surface charges into HIPEs is often difficult as these changes in chemistries can drastically affect emulsion stability and resulting properties. Due to these differences in hydrophobicity, it was hypothesized that these particles will self-assemble at the pore wall. This is vital in ensuring encapsulated hMSCs will interact with the bioactive agents. Surface enrichment also allows for reduced concentrations and minimizes the impact on bulk properties. First, the effect of ACP and HA nanoparticles and DBM particles on pore architecture was assessed. All compositions formed stable monoliths. Initial scoutings utilizing EGDMA were done to determine the maxiumum concentration of each osteogenic element which promoted HIPE fabrication. Concentrations of 2 wt% ACP, 5 wt% HA, and 15 wt% DBM were the maxium that could be incorporated and were the relative amounts utilized for the remainder of studies. PolyHIPEs with a 70:30 molar ratio of PFDMA:BDMA were fabricated with the osteogenic components and resulting pore size was analyzed. Redox-cured polyHIPEs allow for incorporation of particles with a range of hydrophobicities and surface charge because quick set time reduces time for phase separation. **Figure 5.2** displays the effect of ACP, HA, and DBM on pore architecture. A quailitative assessment of polyHIPE pore size illustrated a negligible effect of ACP, HA, and DBM

on HIPE stability at concentrations analyzed. Quantitative analysis of pore size is displayed in **Table 5.1**.

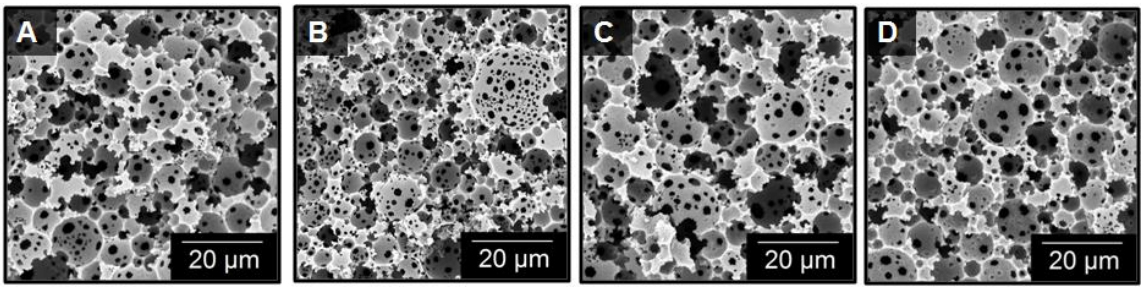

Figure 5.2. Scanning electron micrographs illustrating resulting polyHIPE pore architecture after the incorporation and cure of A) No agent B) 2 wt% ACP C) 5 wt% HA D) 15 wt% DBM

Table 5.1 Effect of osteogenic components on pore size and homogeneity

(n = 150)	**Pore Size (µm)**
70:30 P:B Control	8 ± 4
2 wt% ACP	8 ± 6
5 wt% HA	9 ± 6
15 wt% DBM	9 ± 4

The ability of the HIPE to fill and cure around the larger DBM particles with minimal gaps is demonstrated in **Figure 5.3.** These results illustrate the utility of this polyHIPE

stystem to incorporate a range of bioactive compenents without altering material properties.

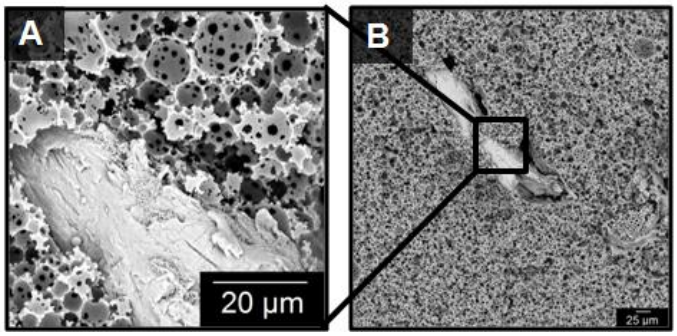

Figure 5.3. Scanning electron micrographs illustrating the pore architecture with the incorporation of DBM particles A) High magnification micrograph B) Low magnification micrograph

5.3.2 Compressive Properties of PolyHIPEs with ACP, HA, and DBM

A potential advantage of using PFDMA/BDMA polyHIPEs for bone grafts is their rigid compressive properties. Therefore, it was important to assess the effect of the bioactive agents on the graft compressive modulus and strength. **Figure 5.4** shows a slight decrease in compressive properties with the incorporation of ACP, HA, and DBM on polyHIPE. However, there was no significant difference among modulus values. This effect is further explained with the negligible change in pore architecture which greatly dictates monolith compressive properties. The ability to incorporate a variety of bioactive agents without affecting pore architecture and resulting compressive properties provides opportunity to design these polyHIPEs for a multitude of tissue engineering

applications. Furthermore, it may be possible to modulate cell response in a dose-dependent manner by incorporating a range of concentrations of proteins and inorganic minerals.

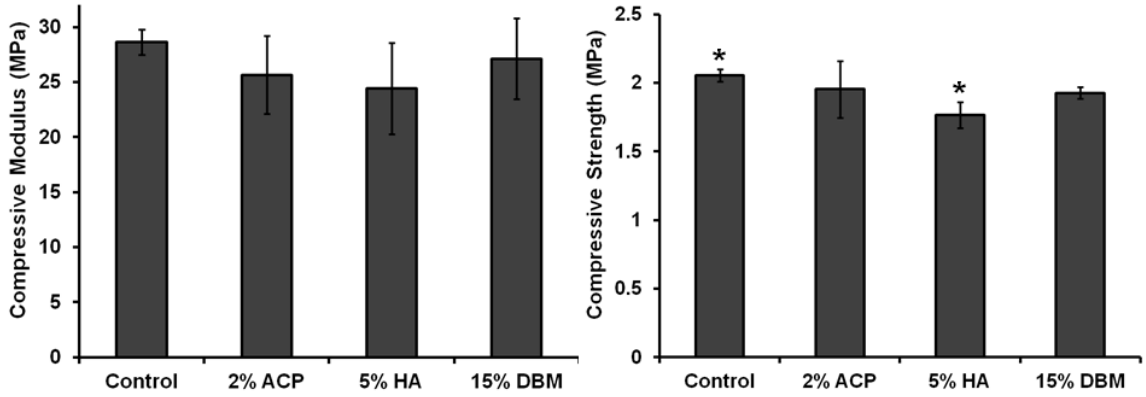

Figure 5.4. The effect of ACP, HA, and DBM on polyHIPE compressive properties when incorporated at indicated concentrations.

5.3.3 Calcium and Collagen Staining of PolyHIPEs

Staining assays were conducted to verify the presence of the particles at the surface of the polyHIPEs sections to ensure direct contact with encapsulated hMSCs. Alizarin red staining of calcium ions on polyHIPEs with ACP and HA illustrated the presence of these particles at the surface by a positive red stain as seen in **Figure 5.5**. PFDMA films with ACP and HA nanoparticles stained with alizarin red resulted in no staining as evidenced in **Figure 5.6**. It was hypothesized that the particles dissolved in the macromer lack any driving force to self-assemble at the film surface unlike the HIPE

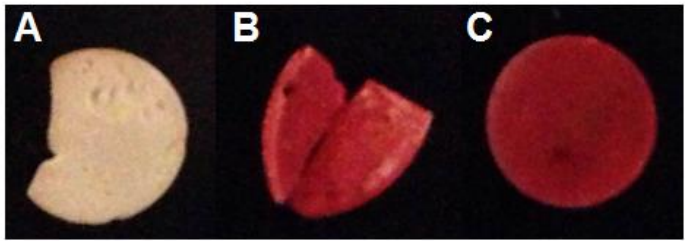

Figure 5.5. Alizarin red staining of calcium ions in polyHIPEs with A) no agent B) 2 wt% ACP and C) 5 wt% HA

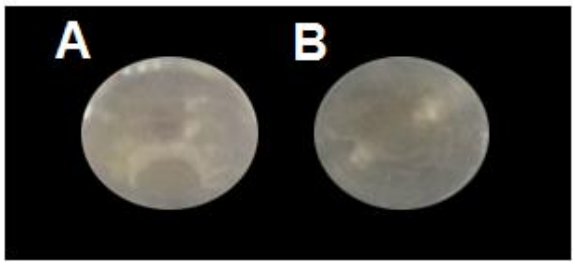

Figure 5.6. Alizarin red staining of PFDMA films A) no HA nanoparticles B) 5 wt% HA nanoparticles

system where the change in hydrophobicities at the pore wall promote this self-assembly. Therefore, the negative staining on the films compared to the positive staining on the polyHIPEs illustrates the surface enrichment of these particles in the polyHIPEs. The self-assembly of these particles at the pore wall indicates the ability to incorporate a lower concentration of bioactive particles while maintaining cellular response due to increased surface area of particles at the oil/water interface. Elemental analysis using energy dispersive x-ray technology (EDS) on HA specimens is currently underway to

further indicate the presence of these particles at the polyHIPE surface. Sirius red collagen staining was utilized to locate DBM particles within the polyHIPE. Because these particles were larger, visual inspection with the naked eye verified their incorporation. Positive staining of these particles within the polyHIPE indicated the DBM protocol maintained type 1 collagen-rich particles, **Figure 5.7**.

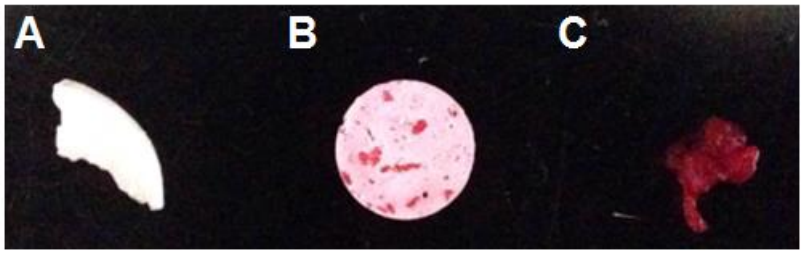

Figure 5.7. Sirius red staining of A) control polyHIPE B) 15 wt% DBM polyHIPE C) type I collagen from rat tail

5.3.4 hMSC Viability and ALP Activity on PolyHIPEs

Illustrating the ability of these injectable polyHIPEs to promote material-based differentiation of hMSCs down an osteoblastic pathway is one of the major goals of this research. As discussed in Chapter IV, initially determining the viability and morphology of hMSCs on polyHIPE sections is crucial to moving forward with additional cell behavior studies. Two week hMSC viability after direct culture on polyHIPEs with ACP, HA and DBM are shown in **Figure 5.8**. All conditions promoted good viability through two weeks. An increase in cell viability was seen with all bioactive agents compared to

the PFDMA/BDMA control at one week. PolyHIPEs with ACP, HA, and DBM resulted in greater than 85% viability. This may be attributed to increased cell-cell signaling with the calcium and phosphate ions and an enhanced frequency of integrin-binding sites from the collagen in the DBM.

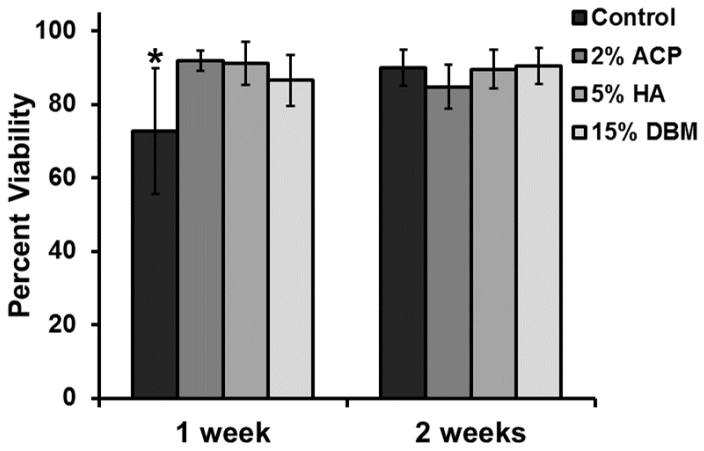

Figure 5.8. hMSC 1 and 2 week viability on 70:30 PFDMA:BDMA polyHIPEs with 2 wt% ACP, 5 wt% HA, and 15 wt% DBM

ALP activity was determined from hMSCs cultured on polyHIPE specimens cultured in growth media. Typically, researchers utilize osteogenic media supplemented with dexamethasone, ascorbic acid and β-glycerol phosphate to determine a material's osteoconductivity in *in vitro* studies. The results from these studies illustrate the osteoconductive nature of the material; however, it is difficult to conclude how the material would perform without the addition of potent osteoinductive agents. The work

presented here shows an elevation in ALP activity with each bioactive component in growth media lacking any additional components, **Figure 5.9**. Alizarin red staining of

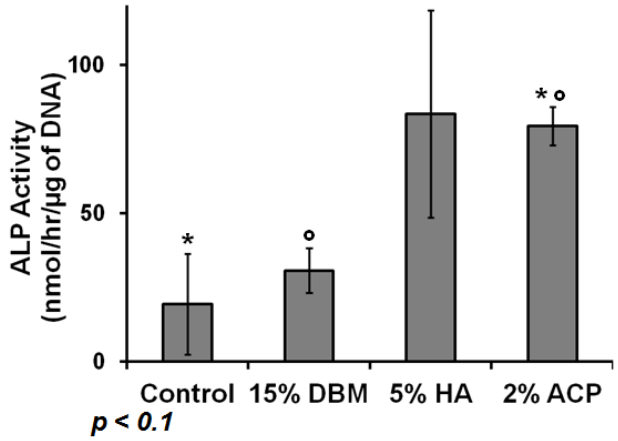

Figure 5.9. Effect of osteoinductive component on hMSC ALP activity at 1 week

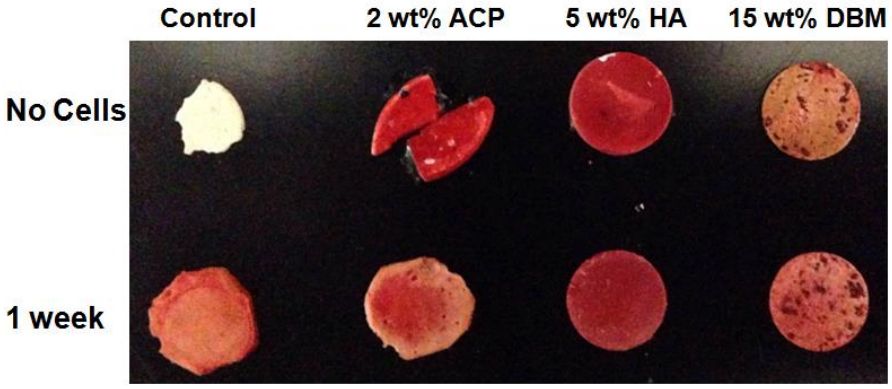

Figure 5.10. Calcium deposition of hMSCs on respective polyHIPE sections

one week polyHIPE specimens with cells yielded qualitative evidence that hMSCs are depositing calcium as seen in **Figure 5.10**. Comparing ACP and HA specimens before and after cell culture may suggest the increases resorption of ACP in media. The HA

staining post cell seeding may be convoluted by residual calcium in the crystalline HA particles that have not been utilized by the hMSCs.

Current work in the laboratory of Dr. Mariah Hahn is focused on determining the upregulation of RNA for bone specific proteins osteocalcin and osteopontin as additional early signs of these polyHIPEs promoting osteogenesis. Furthermore, stable EGDMA polyHIPEs with 2 wt% HA and 10 wt% DBM were fabricated illustrating the potential to incorporate multiple bioactive agents to further promote cell adhesion, proliferation, and differentiation. Future work will focus on the effect of polyHIPEs containing both ACP and DBM to elicit whether there is a synergistic or antagonistic effect. These results highlight the potential of these polyHIPEs to elucidate an osteoinductive effect *in vivo*.

5.4 Conclusions

ACP, HA, and DBM particles were added to PFDMA-based polyHIPEs to confer osteoinductive character and enhance bone regeneration. To this end, stable HIPEs with each of these bioactive agents were formed with a range of particle concentrations with negligible change in pore architecture and compressive properties. Initial hMSC viability testing indicated that the osteogenic agents enhanced cytocompatibility to greater than 85%. Furthermore, ACP, HA, and DBM particles all enhanced one week ALP activity of hMSCs directly seeding on specimens indicating the potential of these functionalized polyHIPEs as osteoinductive bone grafts. Overall, this work demonstrates the ability to incorporate a range of bioactive components (inorganic nanoparticles and protein matrices) into these injectable polyHIPEs to increase cellular interactions and direct

specific behavior without compromising scaffold architecture and resulting properties. These improved porosity, degradability, and bioactivity as compared to current bone cements as well as the improved mechanical properties as compared to bioactive bone grafts highlights the potential of these polyHIPE grafts as improved bone grafting materials.

CHAPTER VI

CONCLUSIONS

6.1 Summary

The work presented here details the fabrication of injectable polyHIPE scaffolds with tunable properties for use in delivery autologous mesenchymal stem cells to bone defects. These highly porous monoliths address current limitations of autologous and allogeneic bone grafts to provide a 3D scaffold which promotes osteogenesis and osseointegration.

PFDMA polyHIPE pore size, interconnected porosity, compressive properties, injection parameters, and degradation rate were modulated by altering compositional variables (e.g. macromer chemistry, surfactant concentration, initiator chemistry) and processing parameters (e.g. mixing speed, storage conditions, time of cure). This demonstrated ability to readily tune scaffold properties is expected to improve function in a wide range of pathologies. In particular, the rate of healing in bone differs widely due to physiology of the defect, health of the patient, and severity of injury. Therefore, understanding how to modulate polyHIPE chemistries and pore architecture to tune the degradation rate for the promotion of healing is advantageous in addressing large bone defects. To this end, a tetrathiol was then introduced into the PFDMA polyHIPEs to enhance the hydrolytic degradation rate without compromising the desirable graft properties.

Methods were then developed to characterize hMSC adhesion, spreading, viability, and proliferation on polyHIPE specimens. These specific protocols are useful

for *in vitro* culture of cells on 3D foams and will help advance the development of multiple HIPE compositions as tissue engineered scaffolds. A double barrel syringe and mixing head setup was then utilized to efficiently mix cells into the HIPE during injection and prior to cure. This illustrates the proof of concept that an injectable HIPE can be used as a cell carrier. Notably, special care was placed on a design that permitted isolation of cells and combination with the HIPE in the surgical suite without a costly or complex apparatus to ensure clinical translation potential. These studies also elucidated key cell-material interactions in emulsion templated scaffolds that can be used in future studies to modulate cell behavior.

Finally, these injectable polyHIPEs were fabricated with ACP, HA, and DBM particles to confer an osteoinductive character to the rigid polyHIPE grafts. The addition of these osteoinductive agents enhanced hMSC viability, ALP activity, and calcium deposition on the polyHIPEs. This work demonstrates the ability to incorporate a range of bioactive components (inorganic nanoparticles and protein matrices) into these injectable polyHIPEs to increase cellular interactions and direct specific behavior without compromising scaffold architecture and resulting properties. Furthermore, these injectable polyHIPEs which promote osteogenesis address currently limitations of calcium-phosphate based bone cements which exhibit limited porosity and a brittle compressive behavior.

Overall, this body of work highlights the potential of interconnected PFDMA-based polyHIPEs as injectable scaffolds for bone tissue engineering. Beyond this specific application, the structure-property relationships elucidated from this work can

be utilized to design functional 3D polyHIPE monoliths with enhanced cell-material interactions for a variety of tissue engineering applications.

6.2 Significance of Work

PolyHIPEs were fabricated without a toxic solvent, exhibited reaction kinetics that promoted cure at physiological temperature, and a viscosity that promoted injection and flow into a defect site. Injectable polyHIPEs that cure in situ can advance bone grafting procedures by 1) space-filling defect to promote tissue integration; 2) providing osteogenic cues to stimulate osteoblast differentiation; 3) and deliver hMSCs to stimulate bone growth.

In Chapter II, compositional and processing variables were altered to modulate injectable polyHIPE pore architecture. PolyHIPEs have been investigated for over three decades for applications in solid-phase synthesis, catalyst support, and filtration. The majority of this work has resulted from trial and error-based studies to achieve scaffold properties for the desired application. We focused to mechanistically determine the effect of compositional variables on polyHIPE architecture and resulting mechanical properties for future rationale design of scaffolds for many clinical applications. Current scaffold fabrication techniques focus on porosity *or* injectability. Achieving a highly porous and injectable scaffold with compressive strength and modulus able to withstand physiological load is a major challenge in orthopedic tissue engineering. Additionally, fabrication techniques that result in a scaffold with relatively high compressive properties require post-fabrication modifications before implantation. This work resulted

in an injectable, highly porous polyHIPE able to withstand physiological load post implantation.

Incorporation of a β-thioester to increase the hydrolytic degradation rate of PFDMA polyHIPEs was discussed in Chapter III. Previous biodegradable polyHIPE systems have the capacity to degrade over time; however, the rate at which this process occurs cannot match the wide range of bone healing rates which is dependent on the physiology of the defect, severity of injury, and health of the patient. Therefore, developing a polyHIPE system with a tunable degradation rate is crucial to utilizing this product for a range of patients and indications. Modulating the susceptibility of the ester carbonyl to hydrolysis via the concentration of the tetrathiol is a means to fabricate interconnected polyHIPEs with the same tunable pore architecture and a range of degradation rates.

In Chapter IV, hMSC adhesion, spreading, and viability on injectable PFDMA-based polyHIPEs were demonstrated. This research resulted in established working protocols for all future studies of hMSC behavior on polyHIPE foams. Additionally, these studies provided the platform for current work to encapsulate and maintain viable hMSCs for one week for autologous stem cells delivery in the surgical suite. This work not only elucidated the effects of biocompatible compositional components on the tunability of the PFDMA polyHIPE system for bone tissue engineering but also provided an understanding of these variables for scaffold fabrication in other clinical applications including wound dressings and soft tissue repair. Hydrogels have been a model system for encapsulating cells and maintaining their viability for delivery to injured tissue.[201]

However, hydrogel systems are not able to withstand the physiological load necessary for promoting osteogenesis. Cells encapsulated in a rigid foam which is capable of maintaining mechanical integrity during load is advantageous in ensuring robustness of the scaffold as well as providing the mechanotransductive cues necessary for differentiating hMSCs into osteoblasts. The innovation and advancement to the field lies in the ability to encapsulate hMSCs and maintain viability in a scaffold able to withstand physiological load for increased osteogenesis and healing of large, bone defects.

In Chapter V, bioactive components were incorporated into the polyHIPE during fabrication to confer an osteoinductive character to the scaffolds. PolyHIPE fabrication with reproducible pore architecture is a sensitive process as emulsion stability, which is affected by a multitude of factors, dictates pore architecture crucial for mechanical properties and cellular response. In this sense, incorporating additional bioactive components into the HIPE fabrication process is difficult as most methods alter phase hydrophobicities and change HIPE stability. Incorporating calcium phosphate nanoparticles which self-assemble at the oil-water interface circumvents many of the issues faced when adding bioactive components to the aqueous phase before HIPE fabrication. Furthermore, quick-curing polyHIPEs reduce the time for phase separation during cure thereby increasing the ability to incorporate a range of bioactive agents.

Overall, we have developed injectable polyHIPEs with tunable pore architectures, compressive properties, injectability parameters, and degradation rates for the use in healing large bone defects. Determining key mechanisms that control scaffold properties and resulting cell behavior will be instrumental in designing polyHIPEs for

use in delivering autologous cells to promote integration and healing in various tissue engineering applications.

6.3 Future Directions and Challenges

Detailed in this work is the development of injectable polyHIPE scaffolds with tunable properties and osteoinductive potential. Although we have illustrated monolith cytocompatibility and the ability to promote osteogenic differentiation *in vitro*, additional work must be done to ensure these grafts promote osteogenesis *in vivo.*

Multiple properties of the polyHIPE scaffold may need to be modulated to better promote cellular ingrowth and viability of encapsulated cells. It has been reported that pore sizes ranging from 50 – 400 μm are required to promote full bone healing.[46] We have a great understanding of how to control emulsion stability which dictates pore size. However, in this work we report a maximum pore size of ~ 30 μm for PFDMA polyHIPEs and indicate that it may be possible to use hydrophilic polymers (PEG) in EGDMA (lower viscosity) to drive osmosis and phase separation resulting in larger pores. Utilizing the reagents and techniques we have established with the work and previous HIPE work in our lab, we can further investigate using organic phase combinations with a higher concentration of lower viscosity macromer and longer set times to increase the time for phase separation. Preliminary work illustrated a homogenous increase in pore size after incorporating hMSCs into the HIPE system. Additional studies will determine the reproducibility of this effect and additional effects of cell number on emulsion stability. Furthermore, adding higher concentrations of

osteoinductive particles could result in decreased emulsion stability which could be controlled by the fast cure of redox HIPEs to reduce inhomogeneity of pore sizes.

Increasing blood flow into the polyHIPE constructs may be necessary to increase oxygen distribution to cells in the bulk of the scaffold. Adequate and timely vascularization of tissue engineered scaffolds is important to provide vital metabolites, inflammatory cells, and stem cells to signal healing. Researchers have engineered ways to pre-vascularize the scaffold prior to implantation by suturing the material to the periosteum. The delivery of growth factors such as VEGF and PDGF, which are potent inducers of angiogenesis and stable vasculature formation, has also been investigated for tissue engineered scaffolds. The co-delivery of BMP-2 and VEGF has been shown to enhance healing due to a signaling pathway and feedback loop between the two growth factors.[202] Our laboratory is currently fabricating and characterizing polyHIPE microspheres for the delivery of proteins. BMP-2 and VEGF could be incorporated into these delivery vehicles and mixed into the polyHIPE monoliths with the potential to increase vascularization in these injectable polyHIPEs. The HIPE system, with adequate viscosity to flow and remain around the defect site, is advantageous with the potential to cure around microvasculature within the defect providing an alternative method to promote angiogenesis within the bulk of the polyHIPE.

The native, hierarchical structure of bone results in great compressive strength and increased toughness and plasticity. An issue with traditional calcium phosphate bone cements is their brittle compressive properties. Therefore, one goal of the injectable polyHIPEs is to increase monolith toughness without sacrificing modulus and strength.

Initial work done in our lab illustrated the ability to increase polyHIPE toughness with the addition of 10 mol% tetrathiol. This effect was observed drastically with EGDMA polyHIPEs and less with BDMA and PFDMA networks. Therefore, polyHIPEs comprised of ratios of EGDMA and PFDMA with 10 mol% tetrathiol may result in an increase in toughness without a significant change in modulus and strength.

Further investigation on the preparation of the demineralized bone matrix particles may be done to elicit their maximum effect on osteoblastic differentiation. The degree of demineralization and particle size of DBM has been shown to alter *in vitro* and *in vivo* osteogenic differentiation.[121] DBM de-calcified to 2% residual calcium and particle sizes ranging from 500 – 710 μm resulted in the largest amount of calcium deposition and enhanced ALP activity. Thus, this effect should be pursued in the current 70:30 PFDMA:BDMA polyHIPE system to potentially increase the response of hMSCs. The larger particle sizes may also increase HIPE stability and result in larger pore sizes which remain homogenous.

Furthermore, it is probable that the hMSC-polyHIPE interactions should be enhanced to increase viability and proliferation and reduce the need for an excess of cells during encapsulation. The incorporation of the integrin-binding sequence, RGDS, was discussed in Chapter IV via the self-assembly of a conjugated amphiphile at the pore wall. While we illustrate the potential for this design to increase hMSC adhesion and spreading, an alternate method may need to be explored. A couple of research groups have illustrated the ability to fabricate polyHIPEs using natural polymers in the internal phase or functionalizing with peptides post-functionalization. While these

methods lacked injectability, the potential to utilize natural polymers within the HIPE system should be explored. Furthermore, functionalizing bioactive macromolecules and covalently attaching them into the network may provide binding sequences for cells at the pore wall. Adding acrylated gelatin into PFDMA polyHIPEs to increase hMSC interactions was attempted during the early part of this work without any effect on cell adhesion. With the understanding of HIPE properties in quick-curing HIPEs from Chapter II and the development of protocols that provide good viability and characterization of cell behavior on 3D monoliths in Chapter IV, it is possible that incorporating natural polymers now may result in more promising results. Also, Madl *et al.* incorporated a thiol-functionalized BMP2 mimicking peptide into a hydrogel for covalent binding into the network to increase osteogenic differentiation.[203] A similar chemistry functionalized with any bioactive peptide (e.g. RGDS) could be utilized within the thiol-ene polyHIPEs to potentially increase cellular interaction. The viability of hMSCs encapsulated in injectable polyHIPEs must be maintained for at least one week *in vitro* to illustrate the potential of these polyHIPEs to promote bone healing *in vivo*. To this end, a systematic, throughput study must be conducted to determine which organic phase composition (macromer combination, amount of unsaturated bonds after set time, and initiator concentration) combined with shorter set times promotes good viability of encapsulated hMSCs. Once the candidate composition is determined, hMSC viability, proliferation, and ALP activity will be investigated for two weeks. Illustrating good cell behavior *in vivo* will allow for translation of the technology into small animal models. Preliminary animal studies will provide information on any polyHIPE properties

that must be altered to best promote osseointegration and healing. Osseointegration and upregulation of bone markers will be evaluated in both a non-loaded (rat cranial) and a loaded (rabbit ulnar) defect model. The *in vivo* results may indicate the necessity to increase pore size, increase vascularization into the polyHIPE, and eventually increase matrix toughness. At this point, our understanding of the requisite tools to tune polyHIPE properties will be vital in future iterations of the design to address the needs of bone healing.

While additional work and challenges exist before these injectable polyHIPEs can be utilized as a clinical option for bone grafting procedures, a platform technology has been established that can readily be tuned and adjusted to address future results of *in vivo* studies. Protocols were established after determination of the driving mechanisms that affect pore architecture and resulting compressive properties. The alteration in organic phase chemistry to modulate degradation rate or promote osteogenic differentiation had a negligible effect on scaffold properties illustrating the ability to incorporate a range of chemistries and bioactive peptides to enhance *in vivo* behavior. Overall, these injectable polyHIPEs have the potential as autologous cell delivery vehicles which can degrade at a rate comparable to neotissue formation and promote osteogenesis upon injection.

REFERENCES

1. Bose, S. & Tarafder, S. Calcium phosphate ceramic systems in growth factor and drug delivery for bone tissue engineering: A review. *Acta Biomaterialia* **8**, 1401-1421 (2012).

2. Praemer, A., Furner, S. & Rice, D.P. in Musculoskeletal conditions in the United States 85-124 (American Academy of Orthopaedic Surgeons, Park Ridge, IL; 1992).

3. Hollinger, J.O. & Kleinschmidt, J.C. The critical size defect as an experimental model to test bone repair materials. *The Journal of Craniofacial Surgery* **1**, 60-68 (1990).

4. Toombs, J.P., Wallace, L.J., Bjorling, D.E. & Rowland, G.N. Evaluation of key's hypothesis in the feline tibia: an experimental model for augmented bone healing studies. *American Journal of Veterinary Research* **46**, 513-518 (1985).

5. Rodan, G.A. Introduction to bone biology. *Bone* **13**, S3-S6 (1992).

6. Yaszemski, M.J., Payne, R.G., Hayes, W.C., Langer, R. & Mikos, A.G. Evolution of bone transplantation: molecular, cellular and tissue strategies to engineer human bone. *Biomaterials* **17**, 175-185 (1996).

7. Coombes, A.G.A. & Meikle, M.C. Resorbable synthetic polymers s replacements for bone graft. *Clinical Materials* **17**, 35-67 (1994).

8. Kalfas, I.H. Principles of bone healing. *Neurosurgical Focus* **10**, 1-4 (2001).

9. Sommerfeldt, D.W. & Rubin, C.T. Biology of bone and how it orchestrates the form and function of the skeleton. *European Spine Journal* **10**, S86-S95 (2001).

10. Caplan, A.I. Review: mesenchymal stem cells: cell-based reconstructive therapy in orthopedics. *Tissue Engineering* **11**, 1198-1211 (2005).

11. Dimitriou, R., Tsiridis, E. & Giannoudis, P.V. Current concepts of molecular aspects of bone healing. *Injury* **36**, 1392-1404 (2005).

12. Bostrom, M.P.G. Expression of bone morphogenetic proteins in fracture healing. *Clinical Orthopaedics and Related Research*, S116-S123 (1998).

13. Lieberman, J.R., Daluiski, A. & Einhorn, T.A. The role of growth factors in the repair of bpme. *Journal of Bone & Joint Surgery, American Volume* **84-A**, 1032-1044 (2002).

14. Gerstenfeld, L.C., Cullinane, D.M., Barnes, G.L., Graves, D.T. & Einhorn, T.A. Fracture healing as a post-natal developmental process: Molecular, spatial, and temporal aspects of its regulation. *Journal of Cellular Biochemistry* **88**, 873-884 (2003).

15. Caplan, A. Why are MSCs therapeutic? New data: new insight. *Journal of Pathology* **217**, 318-324 (2009).

16. Caplan, A.I. Stem cell delivery vehicle. *Biomaterials* **11**, 44-46 (1990).

17. Chamay, A. & Tschantz, P. Mechanical influences in bone remodeling. Experimental research on Wolff's law. *Journal of Biomechanics* **5**, 173-180 (1972).

18. Bruder, S.P., Fink, D.J. & Caplan, A.I. Mesenchymal stem cells in bone development, bone repair, and skeletal regenaration therapy. *Journal of Cellular Biochemistry* **56**, 283-294 (1994).

19. Pittenger, M.F. et al. Multilineage potential of adult human mesenchymal stem cells. *Science* **284**, 143-147 (1999).

20. Caplan, A.I. & Dennis, J.E. Mesenchymal stem cells as trophic mediators. *Journal of Cellular Biochemistry* **98**, 1076-1084 (2006).

21. Caplan, Arnold I. & Correa, D. The msc: an injury drugstore. *Cell Stem Cell* **9**, 11-15 (2011).

22. Park, K.-S. et al. Trophic molecules derived from human mesenchymal stem cells enhance survival, function, and angiogenesis of isolated islets after transplantation. *Transplantation* **89**, 509-517 (2010).

23. Zhang, M. et al. SDF-1 expression by mesenchymal stem cells results in trophic support of cardiac myocytes after myocardial infarction. *Faseb Journal* **21**, 3197-3207 (2007).

24. Shabbir, A., Zisa, D., Suzuki, G. & Lee, T. Heart failure therapy mediated by the trophic activities of bone marrow mesenchymal stem cells: a noninvasive therapeutic regimen. *American Journal of Physiology: Heart and Circulatory Physiology* **296**, H1888-H1897 (2009).

25. Lai, R.C. et al. Exosome secreted by MSC reduces myocardial ischemia/reperfusion injury. *Stem Cell Research* **4**, 214-222 (2010).

26. Mahay, D., Terenghi, G. & Shawcross, S.G. Schwann cell mediated trophic effects by differentiated mesenchymal stem cells. *Experimental Cell Research* **314**, 2692-2701 (2008).

27. Wu, L., Prins, H.-J., Helder, M.N., van Blitterswijk, C.A. & Karperien, M. Trophic effects of mesenchymal stem cells in chondrocyte co-cultures are independent of culture conditions and cell sources. *Tissue Engineering: Part A* **18**, 1542-1551 (2012).

28. Leng, L. et al. Molecular imaging for assessment of mesenchymal stem cells mediated breast cancer therapy. *Biomaterials* **35**, 5162-5170 (2014).

29. Yaszemski, M.J., Oldham, J.B., Lu, L. & Currier, B.L. Bone Engineering, Edn. 1st. (eds Davies, J.E.) 541-547 (EM Squared Incorporated, Toronto; 2000).

30. LeGeros, R.Z. Calcium phosphate-based osteoinductive materials. *Chemical Reviews* **108**, 4742-4753 (2008).

31. Gutta, R. & Waite, P.D. Cranial bone grafting and simultaneous implants: a submental technique to reconstruct the atrophic mandible. *British Journal of Oral and Maxillofacial Surgery* **46**, 477-479 (2008).

32. Samartzis, D. et al. Comparison of allograft to autograft in multilevelanterior cervical discectomy and fusion with rigid plate fixation. *The Spine Journal* **3**, 451-459 (2003).

33. Chau, A. & Mobbs, R. Bone graft substitutes in anterior cervical discectomy and fusion. *European Spine Journal* **18**, 449-464 (2009).

34. Bauer, T.W. & Muschler, G.F. Bone graft materials - An overview of the basic science. *Clinical Orthopaedics and Related Research*, 10-27 (2000).

35. Kretlow, J.D., Young, S., Klouda, L., Wong, M. & Mikos, A.G. Injectable biomaterials for regenerating complex craniofacial tissues. *Advanced Materials* **21**, 3368-3393 (2009).

36. Dumas, J.E. et al. Synthesis and characterization of an injectable allograft bone/polymer composite bone void filler with tunable mechanical properties. *Tissue Engineering: Part A* **16**, 2505-2518 (2010).

37. Haas, S.S., Brauer, G.M. & Dickson, G. A characterization of polymethylmethacrylate bone cement. *Journal Article* **57**, 380-391 (1975).

38. DiMaio, F.R. The science of bone cement: a historical review. *Orthopedics* **25**, 1399-1407 (2002).

39. Jefferiss, C.D., Lee, A.J.C. & Ling, R.S.M. Therma aspects of self-curing polymethylmethacrylate. *Journal of Bone and Joint Surgery: British Volume* **57**, 511-518 (1975).

40. Van der Stok, J., Van Lieshout, E.M.M., El-Massoudi, Y., Van Kralingen, G.H. & Patka, P. Bone substitutes in the netherlands – a systematic literature review. *Acta Biomaterialia* **7**, 739-750 (2011).

41. Morgan, T.T. et al. Encapsulation of Organic Molecules in Calcium Phosphate Nanocomposite Particles for Intracellular Imaging and Drug Delivery. *Nano Letters* **8**, 4108-4115 (2008).

42. Zhang, J., Liu, W., Schnitzler, V., Tancret, F. & Bouler, J.-M. Calcium phosphate cements for bone substitution: Chemistry, handling and mechanical properties. *Acta Biomaterialia* **10**, 1035-1049 (2014).

43. Rose, F.R.A.J. & Oreffo, R.O.C. Bone tissue engineering: hope vs hype. *Biochemical and Biophysical Research Communications* **292**, 1-7 (2002).

44. Kenley, R. et al. Biotechnology and bone graft substitutes. *Pharmaceutical Research* **10**, 1393-1401 (1993).

45. Langer, R. & Vacanti, J.P. Tissue engineering. *Science* **260**, 920-926 (1993).

46. Karageorgiou, V. & Kaplan, D. Porosity of 3D biomaterial scaffolds and osteogenesis. *Biomaterials* **26**, 5474-5491 (2005).

47. Akay, G., Birch, M.A. & Bokhari, M.A. Microcellular polyHIPE polymer supports osteoblast growth and bone formation in vitro. *Biomaterials* **25**, 3991-4000 (2004).

48. Ishaug-Riley, S.L., Crane-Kruger, G.M., Yaszemski, M.J. & Mikos, A.G. Three-dimensional culture of rat calvarial osteoblasts in porous biodegradable polymers. *Biomaterials* **19**, 1405-1412 (1998).

49. Madden, L.R. et al. Proangiogenic scaffolds as functional templates for cardiac tissue engineering. *Proceedings of the National Academy of Sciences* **107**, 15211-15216 (2010).

50. Marcacci, M. et al. Stem cells associated with macroporous bioceramics for long bone repair: 6-to 7-year outcome of a pilot clinical study. *Tissue Engineering* **13**, 947-955 (2007).

51. Taylor, D. Fatigue of bone and bones: An analysis based on stressed volume. *Journal of Orthopaedic Research* **16**, 163-169 (1998).

52. Muggli, D.S., Burkoth, A.K. & Anseth, K.S. Crosslinked polyanhydrides for use in orthopedic applications: Degradation behavior and mechanics. *Journal of Biomedical Materials Research* **46**, 271-278 (1999).

53. Temenoff, J.S. & Mikos, A.G. Injectable biodegradable materials for orthopedic tissue engineering. *Biomaterials* **21**, 2405-2412 (2000).

54. Dumas, J. et al. Balancing the rates of new bone formation and polymer degradation enhances healing of weight-bearing allograft/polyurethane composites in rabbit femoral defects. *Tissue Engineering: Part A* **20**, 115-129 (2014).

55. Pham, Q.P., Sharma, U. & Mikos, A.G. Electrospinning of polymeric nanofibers for tissue engineering applications: a review. *Tissue Engineering* **12**, 1197-1211 (2006).

56. Stankus, J.J., Guan, J. & Wagner, W. Fabrication of biodegradable elastomeric scaffolds with sub-micron morphologies. *Journal of Biomedical Materials Research* **70A**, 603-614 (2004).

57. Nezarati, R.M., Eifert, M.B. & Cosgriff-Hernandez, E. Effects of humidity and solution viscosity on electrospun fiber morphology. *Tissue Engineering: Part C: Methods* **19**, 810-819 (2013).

58. Harris, L.D., Kim, B.-S. & Mooney, D.J. Open pore biodegradable matrices formed with gas foaming. *Journal of Biomedical Materials Research* **42**, 396-402 (1998).

59. Kim, T.K., Yoon, J.J., Lee, D.S. & Park, T.G. Gas foamed open porous biodegradable polymeric microspheres. *Biomaterials* **27**, 152-159 (2006).

60. Hacker, M. et al. Solid lipid templating of macroporous tissue engineering scaffolds. *Biomaterials* **28**, 3497-3507 (2007).

61. Mistry, A.S. et al. Fabrication and in vitro degradation of porous fumarate-based polymer/alumoxane nanocomposite scaffolds for bone tissue engineering. *Journal of Biomedical Materials Research: Part A* **89A**, 68-79 (2009).

62. Zhang, D., Petersen, K.M. & Grunlan, M.A. Inorganic-organic shape memory polymer (SMP) foams with highly tunable properties. *ACS Applied Materials & Interfaces* **5**, 186-191 (2013).

63. Marshall, A.J. & Ratner, B.D. Quantitative characterization of sphere-templated porous biomaterials. *AIChE Journal* **51**, 1221-1232 (2005).

64. Barralet, J.E., Grover, L., Gaunt, T., Wright, A.J. & Gibson, I.R. Preparation of macroporous calcium phosphate cement tissue engineering scaffold. *Biomaterials* **23**, 3063-3072 (2002).

65. Jabbari, E. et al. Synthesis, material properties, and biocompatibility of a novel self-cross-linkable poly(caprolactone fumarate) as an injectable tissue engineering scaffold. *Biomacromolecules* **6**, 2503-2511 (2005).

66. Pêgo, A.P., Poot, A.A., Grijpma, D.W. & Feijen, J. Biodegradable elastomeric scaffolds for soft tissue engineering. *Journal of Controlled Release* **87**, 69-79 (2003).

67. Lin-Gibson, S., Cooper, J.A., Landis, F.A. & Cicerone, M.T. Systematic investigation of porogen size and content on scaffold morphometric parameters and properties. *Biomacromolecules* **8**, 1511-1518 (2007).

68. Shi, X. et al. Fabrication of porous ultra-short single-walled carbon nanotube nanocomposite scaffolds for bone tissue engineering. *Biomaterials* **28**, 4078-4090 (2007).

69. Guan, J., Fujimoto, K.L., Sacks, M.S. & Wagner, W.R. Preparation and characterization of highly porous, biodegradable polyurethane scaffolds for soft tissue applications. *Biomaterials* **26**, 3961-3971 (2005).

70. Day, R.M. et al. In vivo characterisation of a novel bioresorbable poly(lactide-co-glycolide) tubular foam scaffold for tissue engineering applications. *Journal of Materials Science: Materials in Medicine* **15**, 729-734 (2004).

71. Hearon, K. et al. Porous shape-memory polymers. *Polymer Reviews* **53**, 41-75 (2013).

72. Singhal, P. et al. Ultra low density and highly crosslinked biocompatible shape memory polyurethane foams. *Journal of Polymer Science: Part B: Polymer Physics* **50**, 724-737 (2012).

73. Singhal, P., Small, W., Cosgriff-Hernandez, E., Maitland, D.J. & Wilson, T.S. Low density biodegradable shape memory polyurethane foams for embolic biomedical applications. *Acta Biomaterialia* **10**, 67-76 (2014).

74. Singhal, P. et al. Controlling the actuation rate of low-density shape-memory polymer foams in water. *Macromolecular Chemistry and Physics* **214**, 1204-1214 (2013).

75. Zhang, D., Giese, M., Prukop, S. & Grunlan, M. Poly(ε-caprolactone)-based shape memory polymers with variable polydimethylsiloxane soft segment lengths. *Journal of Polymer Science: Part A: Polymer Chemistry* **49**, 754-761 (2011).

76. Gurevitch, I. & Silverstein, M. Shape memory polymer foams from emulsion templating. *Soft Matter* **8**, 10378-10387 (2012).

77. Schmedlen, R.H., Masters, K.S. & West, J.L. Photocrosslinkable polyvinyl alcohol hydrogels that can be modified with cell adhesion peptides for use in tissue engineering. *Biomaterials* **23**, 4325-4332 (2002).

78. Gunn, J.W., Turner, S.D. & Mann, B.K. Adhesive and mechanical properties of hydrogels influence neurite extension. *Journal of Biomedical Materials Research: Part A* **72A**, 91-97 (2005).

79. Hahn, M.S. et al. Photolithographic patterning of polyethylene glycol hydrogels. *Biomaterials* **27**, 2519-2524 (2006).

80. Kretlow, J.D. & Mikos, A.G. From material to tissue: Biomaterial development, scaffold fabrication, and tissue engineering. *AIChE Journal* **54**, 3048-3067 (2008).

81. Park, S., Lee, S. & Kim, W. Fabrication of hydrogel scaffolds using rapid prototyping for soft tissue engineering. *Macromolecular Research* **19**, 694-698 (2011).

82. Miller, T., Goude, M.C., McDevitt, T.C. & Temenoff, J.S. Molecular engineering of glycosaminoglycan chemistry for biomolecule delivery. *Acta Biomaterialia* **10**, 1705-1719 (2014).

83. Nicodemus, G.D. & Bryant, S.J. Cell encapsulation in biodegradable hydrogels for tissue engineering applications. *Tissue Engineering: Part B: Reviews* **14**, 149-165 (2008).

84. Burdick, J.A. & Anseth, K.S. Photoencapsulation of osteoblasts in injectable RGD-modified PEG hydrogels for bone tissue engineering. *Biomaterials* **23**, 4315-4323 (2002).

85. Ritchie, R.O., Buehler, M.J. & Hansma, P. Plasticity and toughness in bone. *Physics Today* **62**, 41-47 (2009).

86. Pickering, S.U. Emulsions. *Journal of the Chemical Society* **91**, 2001-2021 (1907).

87. Gurevitch, I. & Silverstein, M.S. Polymerized pickering HIPEs: effects of synthesis parameters on porous structure. *Journal of Polymer Science: Part A: Polymer Chemistry* **48**, 1516-1525 (2010).

88. Ikem, V.O., Menner, A. & Bismarck, A. High internal phase emulsions stabilized solely by functionalized silica particles. *Angewandte Chemie: International Edition* **47**, 8277-8279 (2008).

89. Ikem, V.O., Menner, A., Horozov, T.S. & Bismarck, A. Highly permeable macroporous polymers synthesized from pickering medium and high internal phase emulsion templates. *Advanced Materials* **22**, 3588-3592 (2010).

90. Maeda, H., Okada, M., Fujii, S., Nakamura, Y. & Furuzono, T. Pickering-type water-in-oil-in-water multiple emulsions toward multihollow nanocomposite microspheres. *Langmuir* **26**, 13727-13731 (2010).

91. Bokhari, M., Carnachan, R.J., A., P.S. & Cameron, N.R. Emulsion-templated porous polymers as scaffolds for three dimensional cell culture: effect of synthesis parameters on scaffold formation and homogeneity. *Journal of Materials Chemistry* **17**, 4088–4094 (2007).

92. Lumelsky, Y. & Silverstein, M. Biodegradable porous polymers through emulsion templating. *Macromolecules* **42**, 1627-1633 (2009).

93. Williams, J.M., Gray, A.J. & Wilkerson, M.H. Emulsion stability and rigid foams from styrene or divinylbenzene water-in-oil emulsions. *Langmuir* **6**, 437-444 (1990).

94. Hayman, M.W., Smith, K.H., Cameron, N.R. & Przyborskia, S.A. Growth of human stem cell-derived neurons on solid three-dimensional polymers. *Journal of Biochemical and Biophysical Methods* **62**, 231-240 (2005).

95. Carnachan, R.J., Bokhari, M., Przyborski, S.A. & Cameron, N.R. Tailoring the morphology of emulsion-templated porous polymers. *Soft Matter* **2**, 608-616 (2006).

96. Hainey, P., Huxham, I.M., Rowatt, B. & Sherrington, D.C. Synthesis and ultrastructural studies of styrene-divinylbenzene polyHIPE polymers. *Macromolecules* **24**, 117-121 (1991).

97. Mercier, A., Deleuze, H. & Mondain-Monval, O. Preparation and functionalization of (vinyl)polystyrene polyHIPEs. Short routes to binding functional groups through a dimethylene spacer. *Reactive and Functional Polymers* **46**, 67–79 (2000).

98. Busby, W., Cameron, N.R. & Jahoda, C.A.B. Tissue engineering matrixes by emulsion templating. *Polymer International* **51**, 871-881 (2002).

99. Busby, W., Cameron, N.R. & Jahoda, C.A.B. Emulsion-derived foams (polyHIPEs) containing poly(ε-caprolactone) as matrixes for tissue engineering. *Biomacromolecules* **2**, 154-164 (2001).

100. Lumelsky, Y., Lalush-Michael, I., Levenberg, S. & Silverstein, M. A degradable, porous, emulsion-templated polyacrylate. *Journal of Polymer Science Part A: Polymer Chemistry* **47**, 7043-7053 (2009).

101. David, D. & Silverstein, M. Porous polyurethanes synthesized within high internal phase emulsions (HIPEs). *Journal of Polymer Science: Part A: Polymer Chemistry* **47**, 9 (2009).

102. Umez-Eronini, N.O., Collins, A. & Neal, D.E. Optimisation of bladder stromal culture on polyHIPE *European Cells and Materials* **4**, 77-78 (2002).

103. Christenson, E.M., Soofi, W., Holm, J.L., Cameron, N.R. & Mikos, A.G. Biodegradable fumarate-based polyHIPEs as tissue engineering scaffolds. *Biomacromolecules* **8**, 3806-3814 (2007).

104. Bokhari, M.A., Akay, G., Zhang, S. & Birch, M.A. The enhancement of osteoblast growth and differentiation in vitro on a peptide hydrogel—polyHIPE polymer hybrid material. *Biomaterials* **26**, 5198-5208 (2005).

105. Knight, E., Murray, B., Carnachan, R. & Przyborski, S. in 3D Cell Culture, Vol. 695. (ed. J.W. Haycock) 323-340 (Humana Press, Clifton, New Jersey; 2011).

106. Williams, J.M. & Wrobleski, D.A. Spatial distribution of the phases in water-in-oil emulsions. Open and closed microcellular foams from cross-linked polystryene. *Langmuir* **4**, 656-662 (1988).

107. Cameron, N.R. & Sherrington, D.C. Non-aqueous high internal phase emulsions. Preparation and stability. *Journal of the Chemical Society: Faraday Transactions* **92**, 1543-1547 (1996).

108. Robinson, J., Moglia, R., Stuebben, M., McEnery, M.A.P. & Cosgriff-Hernandez, E. Achieving Interconnected Pore Architecture in Injectable PolyHIPEs for Bone Tissue Engineering. *Tissue Engineering: Part A* **20**, 1103-1112 (2014).

109. Livshin, S. & Silverstein, M.S. Crystallinity and Cross-Linking in Porous Polymers Synthesized from Long Side Chain Monomers through Emulsion Templating. *Macromolecules* **41**, 3930-3938 (2008).

110. Gitli, T. & Silverstein, M.S. Bicontinuous hydrogel-hydrophobic polymer systems through emulsion templated simultaneous polymerizations. *Soft Matter* **4**, 2475-2485 (2008).

111. Lovelady, E., Kimmins, S.D., Wu, J. & Cameron, N.R. Preparation of emulsion-templated porous polymers using thiol-ene and thiol-yne chemistry. *Polymer Chemistry* **2**, 559-562 (2011).

112. Sergent, B., Birot, M. & Deleuze, H. Preparation of thiol–ene porous polymers by emulsion templating. *Reactive and Functional Polymers* **72**, 962-966 (2012).

113. Caldwell, S. et al. Degradable emulsion-templated scaffolds for tissue engineering from thiol-ene photopolymerisation. *Soft Matter* **8**, 10344-10351 (2012).

114. Barbetta, A. et al. Scaffolds based on biopolymeric foams. *Advanced Functional Materials* **15**, 118-124 (2005).

115. Audouin, F., Larragy, R., Fox, M., O'Connor, B. & Heise, A. Protein immobilization onto poly(acrylic acid) functional macroporous polyHIPE obtained by surface-initiated ARGET ATRP. *Biomacromolecules* **13**, 3787-3794 (2012).

116. Bohner, M. Calcium othophosphates in medicine: from ceramics to calcium phosphate cements. *Injury* **31**, SD37-SD48 (2000).

117. Kon, E. et al. Autologous bone marrow stromal cells loaded onto porous hydroxyapatite ceramic accelerate bone repair in critical-size defects of sheep long bones. *Journal of Biomedical Materials Research* **49**, 328-337 (2000).

118. Davison, N.L. et al. Liposomal clodronate inhibition of osteoclastogenesis and osteoinduction by submicrostructured beta-tricalcium phosphate. *Biomaterials* **35**, 5088-5097 (2014).

119. Urist, M.R. Bone - Formation by autoinduction. *Science* **150**, 893-& (1965).

120. Harakas, N.K. Demineralized bone-matrix-induced osteogenesis. *Clinical Orthopaedics and Related Research*, 239-251 (1984).

121. Zhang, M., Powers, R.M. & Wolfinbarger, L. Effect(s) of the demineralization process on the osteoinductivity of demineralized bone matrix. *Journal of Periodontology* **68**, 1085-1092 (1997).

122. Mauney, J.R., Volloch, V. & Kaplan, D.L. Role of adult mesenchymal stem cells in bone tissue engineering applications: current status and future prospects. *Tissue Engineering* **11**, 787-802 (2005).

123. Petite, H. et al. Tissue-engineered bone regeneration. *Nature Biotechnology* **18**, 959-963 (2000).

124. Terella, A., Mariner, P., Brown, N., Anseth, K. & Streubel, S.-O. Repair of a calvarial defect with biofactor and stem cell-embedded polyethylene glycol scaffold. *Archives of Facial Plastic Surgery* **12**, 166-171 (2010).

125. Zeitouni, S. et al. Human mesenchymal stem cell-derived matrices for enhanced osteoregeneration. *Science Translational Medicine* **4** (2012).

126. Yang, W.-Z. et al. Safety evaluation of allogeneic umbilical cord blood mononuclear cell therapy for degenerative conditions. *Journal of Translational Medicine* **8**, 1-6 (2010).

127. Prasad, V.K. & Kurtzberg, J. Umbilical cord blood transplantation for non-malignant diseases. *Bone Marrow Transplantation* **44**, 643-651 (2009).

128. Gerecht, S. et al. A porous photocurable elastomer for cell encapsulation and culture. *Biomaterials* **28**, 4826-4835 (2007).

129. Cameron, N.R., Sherrington, D.C., Albiston, L. & Gregory, D.P. Study of the formation of the open-cellular morphology of poly(styrene/divinylbenzene) polyHIPE materials by cryo-SEM. *Colloid and Polymer Science* **274**, 592-595 (1996).

130. Hayman, M.W., Smith, K.H., Cameron, N.R. & Przyborski, S.A. Enhanced neurite outgrowth by human neurons grown on solid three-dimensional scaffolds. *Biochemical and Biophysical Research Communications* **314**, 483-488 (2004).

131. Barbetta, A., Dentini, M., Zannoni, E.M. & De Stefano, M.E. Tailoring the Porosity and Morphology of Gelatin-Methacrylate PolyHIPE Scaffolds for Tissue Engineering Applications. *Langmuir* **21**, 12333-12341 (2005).

132. Cameron, N.R., Barbetta, A. & Cooper, S.J. High internal phase emulsions (HIPEs) containing divinylbenzene and 4-vinylbenzyl chloride and the morphology of the resulting PolyHIPE materials. *Chemical Communications*, 221–222 (2000).

133. Bokhari, M.A., Birch, M.A. & Akay, G. Polyhipe polymer: a novel scaffold for in vitro bone tissue engineering. *Experimental Medical Biology: Tissue Engineering, Stem Cells, and Gene Therapies* **534**, 247-254 (2003).

134. Cameron, N.R. & Sherrington, D.C. Synthesis and characterisation of poly(aryl ether sulfone) polyHIPE materials. *Macromolecules* **30**, 5860-5869 (1997).

135. Youssef, C., Backov, R., Treguer, M., Birot, M. & Deleuze, H. Preparation of amazingly hard polyHIPE material from a direct emulsion. *Materials Research Society Symposium* **1269**, 1-6 (2010).

136. Lepine, O. Preparation of macrocellular PU–PS interpenetrating networks. *Polymer* **46**, 9653–9663 (2005).

137. Kovačič, S., Štefanec, D. & Krajnc, P. Highly porous open-cellular monoliths from 2-hydroxyethyl methacrylate based high internal phase emulsions (HIPEs): preparation and void size tuning. *Macromolecules* **40**, 8056-8060 (2007).

138. Jabbari, E. et al. Synthesis, material properties, and biocompatibility of a novel self-cross-linkable poly(caprolactone fumarate) as an injectable tissue engineering scaffold. *Biomacromolecules* **6**, 2503-2511 (2005).

139. Hayman, M.W., Smith, K.H., Cameron, N.R. & Przyborskia, S.A. Growth of human stem cell-derived neurons on solid three-dimensional polymers. *Journal of Biochemical and Biophysical Methods* **62**, 231-240 (2005).

140. Busby, W., Cameron, N.R. & Jahoda, C.A.B. Tissue engineering matrixes by emulsion templating. *Polymer International* **51**, 871-881 (2002).

141. David, D. & Silverstein, M. Porous polyurethanes synthesized within high internal phase emulsions (HIPEs). *Journal of Polymer Science: Part A: Polymer Chemistry* **47**, 5806-5814 (2009).

142. Moglia, R.S. et al. Injectable polyHIPEs as high-porosity bone grafts. *Biomacromolecules* **12**, 3621-3628 (2011).

143. Marcacci, M. et al. Stem cells associated with macroporous bioceramics for long bone repair: 6-to 7-year outcome of a pilot clinical study. *Tissue Engineering* **13**, 947-955 (2007).

144. Cameron, N.R., Sherrington, D.C., Albiston, L. & Gregory, D.P. Study of the formation of the open-cellular morphology of poly(styrene/divinylbenzene) polyHIPE materials by cryo-SEM. *Colloid and Polymer Science* **274**, 592-595 (1996).

145. Gurevitch, I. & Silverstein, M.S. Nanoparticle-based and organic-phase-based AGET ATRP polyHIPE synthesis within pickering HIPEs and surfactant-stabilized HIPEs. *Macromolecules* **44**, 3398-3409 (2011).

146. Mistry, A. et al. *In vivo* bone biocompatibility and degradation of porous fumarate-based polymer/alumoxane nanocomposites for bone tissue engineering. *Journal of Biomedical Materials Research: Part A* **92A**, 451-462 (2010).

147. Peter, S.J., Kim, P., Yasko, A.W., Yaszemski, M.J. & Mikos, A.G. Crosslinking characteristics of an injectable poly(propylene fumarate)/β-tricalcium phosphate paste and mechanical properties of the crosslinked composite for use as a biodegradable bone cement. *Journal of Biomedical Materials Research* **44**, 314-321 (1999).

148. Peter, S.J., Lu, L., Kim, D.J. & Mikos, A.G. Marrow stromal osteoblast function on a poly(propylene fumarate)/β-tricalcium phosphate biodegradable orthopaedic composite. *Biomaterials* **21**, 1207-1213 (2000).

149. Timmer, M.D., Horch, A.R., Ambrose, C.G. & Mikos, A.G. Effect of physiological temperature on the mechanical properties and network structure of biodegradable poly(propylene fumarate)-based networks. *Journal of Biomaterial Science: Polymer Edition* **14**, 369-382 (2003).

150. ASTM Standards Committee D20 on Plastics. Standard Test Method for Compressive Properties of Rigid Cellular Plastics (D 1621-04a) (2004).

151. Williams, J.M. High internal phase water-in-oil emulsions: influence of surfactants and cosurfactants on emulsion stability and foam quality. *Langmuir* **7**, 1370-1377 (1991).

152. Coombes, A.G.A. & Meikle, M.C. Resorbable synthetic polymers as replacements for bone graft. *Clinical Materials* **17**, 35-67 (1994).

153. Svaldi-Muggli, D., Burkoth, A.K. & Anseth, K.S. Crosslinked polyanhydrides for use in orthopaedic applications: degradation behavior and mechanics. *Journal of Biomedical Materials Research* **46**, 271-278 (1999).

154. Muggli, D.S., Burkoth, A.K. & Anseth, K.S. Crosslinked polyanhydrides for use in orthopedic applications: Degradation behavior and mechanics. *Journal of Biomedical Materials Research* **46**, 271-278 (1999).

155. International Organization for Standardization. ISO5833: Implants for Surgery: Acrylic Resin Cements (2002).

156. Rai, B. et al. Combination of platelet-rich plasma with polycaprolactone-tricalcium phosphate scaffolds for segmental bone defect repair. *Journal of Biomedical Materials Research: Part A* **81A**, 888-899 (2007).

157. International Organization for Standardization. ISO9917: Dentistry: Water-based Cements (1994).

158. Dumas, J.E. et al. Synthesis and characterization of an injectable allograft bone/polymer composite bone void filler with tunable mechanical properties. *Tissue Engineering: Part A* **16**, 2505-2518 (2010).

159. Winter, H.H. Can the gel point of a cross-linking polymer be detected by the G′ – G″ crossover? *Polymer Engineering and Science* **27**, 1698-1702 (1987).

160. Hulbert, S.F. et al. Potential of ceramic materials as permanently implantable skeletal prostheses. *Journal of Biomedical Materials Research* **4**, 433-456 (1970).

161. Tsuruga, E., Takita, H., Itoh, H., Wakisaka, Y. & Kuboki, Y. Pore size of porous hydroxyapatite as the cell-substratum controls BMP-induced osteogenesis. *Journal of Biochemistry* **121**, 317-324 (1997).

162. Cestro, H.J., Salyer, K.E. & Toranto, I.R. Bone growth into porous carbon, polyethylene, and polypropylene prostheses. *Journal of Biomedical and Materials Research* **9**, 1-7 (1975).

163. Schoenmakers, R.G., van de Wetering, P., Elbert, D.L. & Hubbell, J.A. The effect of the linker on the hydrolysis rate of drug-linked ester bonds. *Journal of Controlled Release* **95**, 291-300 (2004).

164. Elbert, D.L. & Hubbell, J.A. Conjugate addition reactions combined with free-radical cross-linking for the design of materials for tissue engineering. *Biomacromolecules* **2**, 430-441 (2001).

165. Reddy, S.K., Cramer, N.B., Cross, T., Raj, R. & Bowman, C.N. Polymer-derived ceramic materials from thiol-ene photopolymerizations. *Chemistry of Materials* **15**, 4257-4261 (2003).

166. Cramer, N.B. & Bowman, C.N. Kinetics of thiol–ene and thiol–acrylate photopolymerizations with real-time fourier transform infrared. *Journal of Polymer Science Part A: Polymer Chemistry* **39**, 3311-3319 (2001).

167. Hoyle, C.E. & Bowman, C.N. Thiol–ene click chemistry. *Angewandte Chemie International Edition* **49**, 1540-1573 (2010).

168. Jacobine, A.F. in Radiation Curing in Polymer Science and Technology III, Polymerisation Mechanisms, Vol. 3. (eds. J.D. Fouassier & J.F. Rabek) 219 (Elsevier Applied Science, London; 1993).

169. Rydholm, A.E., Bowman, C.N. & Anseth, K.S. Degradable thiol-acrylate photopolymers: polymerization and degradation behavior of an in situ forming biomaterial. *Biomaterials* **26**, 4495-4506 (2005).

170. Huber, H.F. in Radiation Curing in Polymer Science and Technology, Vol. IV. (eds. J.P. Fouassier & J.F. Rabek) 58 (Elsevier Applied Science, Essex, England; 1993).

171. Cramer, N.B. & Bowman, C.N. Kinetics of thiol-ene and thiol-acrylate photopolymerizations with real-time Fourier transform infrared. *Journal of Polymer Science: Part A: Polymer Chemistry* **39**, 3311-3319 (2001).

172. Cramer, N.B., Reddy, S.K., O'Brien, A.K. & Bowman, C.N. Thiol-ene photopolymerization mechanism and rate limiting step changes for various vinyl functional group chemistries. *Macromolecules* **36**, 7964-7969 (2003).

173. Reddy, S.K., Anseth, K.S. & Bowman, C.N. Modeling of network degradation in mixed step-chain growth polymerizations. *Polymer* **46**, 4212-4222 (2005).

174. Reddy, S.K., Cramer, N.B. & Bowman, C.N. Thiol-vinyl mechanisms. 1. termination and propagation kinetics in thiol-ene photopolymerizations. *Macromolecules* **39**, 3673-3680 (2006).

175. Rydholm, A.E., Held, N.L., Bowman, C.N. & Anseth, K.S. Gel permeation chromatography characterization of the chain length distributions in thiol-acrylate photopolymer networks. *Macromolecules* **39**, 7882-7888 (2006).

176. Rydholm, A.E., Reddy, S.K., Anseth, K.S. & Bowman, C.N. Controlling Network Structure in Degradable Thiol−Acrylate Biomaterials to Tune Mass Loss Behavior. *Biomacromolecules* **7**, 2827-2836 (2006).

177. McCall, J.D. & Anseth, K.S. Thiol–ene photopolymerizations provide a facile method To encapsulate proteins and maintain their bioactivity. *Biomacromolecules* **13**, 2410-2417 (2012).

178. Kircher, L., Theato, P. & Cameron, N.R. Reactive thiol-ene emulsion-templated porous polymers incorporating pentafluorophenyl acrylate. *Polymer* **54**, 1755-1761 (2013).

179. Cook, W.D., Chen, F., Pattison, D.W., Hopson, P. & Beaujon, M. Thermal polymerization of thiol–ene network-forming systems. *Polymer International* **56**, 1572-1579 (2007).

180. Moglia, R. et al. Injectable polyHIPEs with rapid in situ curing. *Biomacromolecules* (2014).

181. Foudazi, R., Gokun, P., Feke, D.L., Rowan, S.J. & Manas-Zloczower, I. Chemorheology of Poly(high internal phase emulsions). *Macromolecules* **46**, 5393-5396 (2013).

182. Li, W.H., Hamielec, A.E. & Crowe, C.M. Kinetics of the free-radical copolymerization of methyl-methacrylate ethylene-glycol dimethacrylate 1. experimental investigation. *Polymer* **30**, 1513-1517 (1989).

183. O'Brien, J.L. & Gornick, F. Chain transfer in the polymerization of methyl methacrylate. I. transfer with monomer and thiols. The mechanism of the termination reaction at 60 *Journal of the American Chemical Society* **77**, 4757-4763 (1955).

184. Plessis, C. et al. Seeded semibatch emulsion polymerization of butyl acrylate: Effect of the chain-transfer agent on the kinetics and structural properties. *Journal of Polymer Science: Part A: Polymer Chemistry* **39**, 1106-1119 (2001).

185. Graham, N.B. & Cameron, A. Nanogels and microgels: The new polymeric materials playground. *Pure and Applied Chemistry* **70**, 1271-1275 (1998).

186. Yaszemski, M.J. et al. The ingrowth of new bone tissue and initial mechanical properties of a degrading polymeric composite scaffold. *Tissue Engineering* **1**, 41-52 (1995).

187. Peter, S.J., Miller, S.T., Zhu, G., Yasko, A.W. & Mikos, A.G. In vivo degradation of a poly(propylene fumarate)/β-tricalcium phosphate injectable composite scaffold. *Journal of Biomedical Materials Research* **41**, 1-7 (1998).

188. Hayward, A.S. et al. Galactose-functionalized polyHIPE scaffolds for use in routine three dimensional culture of mammalian hepatocytes. *Biomacromolecules* **14**, 4271-4277 (2013).

189. Viswanathan, P., Chirasatitsin, S., Ngamkham, K., Engler, A.J. & Battaglia, G. Cell instructive microporous scaffolds through interface engineering. *Journal of the American Chemical Society* **134**, 20103-20109 (2012).

190. Bryant, S.J., Nuttleman, C.R. & Anseth, K.S. Cytocompatibility of UV and visible light photoinitiating systems on cultured NIH/3T3 fibroblasts in vitro. *Journal of Biomaterial Science: Polymer Edition* **11**, 439-457 (2000).

191. Kim, K., Dean, D., Mikos, A.G. & Fisher, J.P. Effect of initial cell seeding density on early osteogenic signal expression of rat bone marrow stromal cells cultured on cross-Linked poly(propylene fumarate) disks. *Biomacromolecules* **10**, 1810-1817 (2009).

192. Nelson, C.M. & Chen, C.S. Cell-cell signaling by direct contact increases cell proliferation via a PI3K-dependent signal. *FEBS Letters* **514**, 238-242 (2002).

193. Klouda, L., Hacker, M.C., Kretlow, J.D. & Mikos, A.G. Cytocompatibility evaluation of amphiphilic, thermally responsive and chemically crosslinkable macromers for in situ forming hydrogels. *Biomaterials* **30**, 4558-4566 (2009).

194. Brink, K.S., Yang, P.J. & Temenoff, J.S. Degradative properties and cytocompatibility of a mixed-mode hydrogel containing oligo[poly(ethylene glycol)fumarate] and poly(ethylene glycol)dithiol. *Acta Biomaterialia* **5**, 570-579 (2009).

195. Osborn, J.F. & Newesely, H. The material science of calcium phosphate ceramics. *Biomaterials* **1**, 108-111 (1980).

196. Popp, J.R., Laflin, K.E., Love, B.J. & Goldstein, A.S. Fabrication and characterization of poly(lactic-co-glycolic acid) microsphere/amorphous calcium phosphate scaffolds. *Journal of Tissue Engineering and Regenerative Medicine* **6**, 12-20 (2012).

197. Gurevitch, I. & Silverstein, M.S. Polymerized pickering HIPEs: effects of synthesis parameters on porous structure. *Journal of Polymer Science Part a-Polymer Chemistry* **48**, 1516-1525 (2010).

198. Tuli, S. & Singh, A. The osteoninductive property of decalcified bone matrix. An experimental study. *Journal of Bone and Joint Surgery: British Volume* **60**, 116-123 (1978).

199. Pietrzak, W.S. The hydration characteristics of demineralized and nondemineralized allograft bone: scientific perspectives on graft function. *Journal of Craniofacial Surgery* **17**, 120-130 (2006).

200. Figueiredo, M. et al. Influence of hydrochloric acid concentration on the demineralization of cortical bone. *Chemical Engineering Research and Design* **89**, 116-124 (2011).

201. Cruise, G.M., Hegre, O.D., Scharp, D.S. & Hubbell, J.A. A sensitivity study of the key parameters in the interfacial photopolymerization of poly(ethylene glycol) diacrylate upon porcine islets. *Biotechnology and Bioengineering* **57**, 655-665 (1998).

202. Krishnan, L., Willett, N.J. & Guldberg, R.E. Vascularization strategies for bone regeneration. *Annals of Biomedical Engineering* **42**, 432-444 (2014).

203. Madl, C.M., Mehta, M., Duda, G.N., Heilshorn, S.C. & Mooney, D.J. Presentation of BMP-2 mimicking peptides in 3D hydrogels directs cell fate

commitment in osteoblasts and mesenchymal stem cells. *Biomacromolecules* **15**, 445-455 (2014).